Kleyde Delsy Delgado Ramos

Licenciada em Ciências Biomédicas

Development of wound healing biomaterials based on bacterial exopolysaccharides

Dissertação para obtenção do Grau de Mestre em Bioquímica

Orientadora: Professora Doutora Maria Filomena Andrade de Freitas, UCIBIO-Requimte, FCT-UNL

Co-orientadora: Doutora Ana Teresa Serra, Food & Health Division, iBET

FACULDADE DE CIÊNCIAS E TECNOLOGIA
UNIVERSIDADE NOVA DE LISBOA

Setembro, 2021

Development of wound healing biomaterials based in bacterials exopolysacharides

Kleyde Ramos

2021

Kleyde Delsy Delgado Ramos

Licenciada em Ciências Biomédicas

Development of wound healing biomaterials based on bacterial exopolysaccharides

Dissertação para obtenção do Grau de Mestre em Bioquímica

Orientadora: Professora Doutora Maria Filomena Andrade de Freitas, UCIBIO-Requimte, FCT-UNL

Co-orientadora: Doutora Ana Teresa Serra, Food & Health Division, iBET

Setembro, 2021

Development of wound healing biomaterials based on bacterial exopolysaccharides

Agradecimentos

Queria agradecer primeiramente a Deus, pela força, coragem e por me ajudar, por meio da minha fé, a ultrapassar todos os obstáculos encontrados ao longo desta caminhada.

Um especial agradecimento a minha orientadora Dra. Filomena Freitas, pelos ensinamentos, pela paciência, atenção, por estar presente e me estender a mão sempre que precisei, e principalmente pelo incentivo e por me fazer acreditar na concretização deste projeto.

Queria agradecer também a minha co-orientadora, Dra. Teresa Serra, pela experiência compartilhada, pela disponibilidade e ajuda de sempre.

A toda a equipa Bioeng, em especial ao pessoal do 407, pela boa energia, por proporcionarem um ambiente de trabalho descontraído e por toda a ajuda dispensada.

Um especial agradecimento a Patrícia Reís, por compartilhar os conhecimentos comigo, pela paciência, pela disponibilidade, pelos conselhos e dicas e por toda ajuda, pois foi tudo indispensável, a ti, minha imensa gratidão.

Também queria agradecer a Ana Catarina Macedo do iBET, por toda a ajuda disponibilizada, pela dedicação na realização dos ensaios biológicos e pelo empenho em partilhar os resultados da forma mais clara possível.

Um muitíssimo obrigado ao Prof. Jean Guezennec (IFREMER, França) e à Pacific Biotech (Polinésia Francesa), pela produção e envio dos EPSs, e também ao Prof. Christian Grandfils (ULiège, Bélgica) pelas análises de potencial Zeta e DLS.

Aos meus colegas de mestrado, em especial ao Thomas, a Marta e a Cristiana pela amizade e pela interajuda e aos meus amigos pelo carinho e incentivo nos momentos de desânimo.

Por fim, gostaria de expressar a minha gratidão, aos meus pais e irmãos por me apoiarem sempre nas minhas escolhas e projetos, por acreditarem em mim e principalmente, por nunca me deixarem sentir só, por estarem sempre presentes, apesar dos km de distância que nos separa, sem vocês nada disso seria possível.

Resumo

Atualmente, os biopolímeros têm despertado grande interesse principalmente na área alimentar, farmacêutica, cosmética e também na área biomédica, devido às propriedades inteligentes e versáteis que apresentam, nomeadamente, biocompatibilidade, biodegradabilidade e não toxicidade. Além dessas propriedades, muitos polímeros possuem características vitais que ajudam em processos de cicatrização de feridas e quando incorporados com nanopartículas de elementos como a prata (Ag), ouro (Au) e selénio (Se), aumentam ainda mais a eficácia desses polímeros.

Assim sendo, o principal objetivo deste estudo foi determinar as melhores condições de preparação de biocompósitos para aplicação em tratamento de feridas, utilizando diferentes polissacáridos bacterianos extracelulares (EPSs) (EPS1, EPS2, EPS3, EPS4 e FucoPol) como agentes redutores e estabilizadores para a síntese de nanopartículas de prata (AgNP), ouro (AuNP) e selénio (SeNP). Os EPSs foram caracterizados quanto à composição em açúcares e grupos substituintes, pois, dependendo da composição, podem interferir de certa forma nas propriedades apresentadas por cada um. O EPS1 é composto principalmente por manose (56.1 %mol), o EPS2 e o EPS3 são compostos principalmente por glucose, 67 %mol e 39.1 %mol respectivamente, o EPS4 é composto maioritariamente por ácido glucurónico (55.9 %mol) e o FucoPol por fucose (34.9 %mol). Os biocompósitos também foram caracterizados por espectroscopia UV-vis, FTIR, TGA, XRD, DLS, potencial Zeta e por ICP.

A citotoxicidade e o efeito de cicatrização de feridas dos EPS e dos biocompósitos EPSs/NPs foram analisados em células de queratinócitos humanos (linha celular HaCaT). As amostras foram testadas usando uma concentração de polímero de 62.5-1000 mg/L e nenhuma amostra apresentou citotoxicidade, excepto para o biocompósito EPS3/Ag^{+} quando testado em uma concentração de polímero acima de 125 mg/L, com um teor de Ag^{+} acima de 6.9 mg/L (diminuição da viabilidade cellular em ~ 91.9%). Por outro lado, entre todos os EPSs e seus materiais funcionalizados, o FucoPol e o biocompósito FucoPol/AgNP exibiram uma maior capacidade de promover a migração *in vitro* dos queratinócitos. Embora o EPS1 não tenha apresentado efeito cicatrizante, os biocompósitos EPS1/AgNP (100 mg/L) e EPS1/AuNP (500 mg/L) mostraram promover a migração de células HaCaT. Os resultados obtidos sugerem que tanto o FucoPol e o biocompósito FucoPol/AgNP, bem como os biocompósitos EPS1/AgNP e EPS1/AuNP podem ter potencial aplicação na dermocosmética, sobretudo nos mecanismos de cicatrização de feridas.

Palavras - chave

Exopolissacáridos, nanopartículas, citotoxicidade, cicatrização de feridas, biopolímero, síntese de biocompósitos.

Abstract

Currently, biopolymers have aroused great interest mainly in the food, pharmaceutical, cosmetic, and also in the biomedical fields, due to the intelligent and versatile properties that present, namely, biocompatibility, biodegradability, and non-toxicity. In addition to these properties, many polymers have vital characteristics that assist in wound healing processes and, when incorporated into nanoparticles of elements such as silver (Ag), gold (Au), and selenium (Se), further increase the effectiveness of these polymers.

Therefore, the main objective of this study was to determine the best conditions for the preparation of biocomposites for application in the treatment of wounds, using different extracellular bacterial polysaccharides (EPSs) (EPS1, EPS2, EPS3, EPS4, and FucoPol) as reducing and stabilizing agents for the synthesis of silver nanoparticles (AgNP), gold (AuNP) and selenium (SeNP). EPSs were characterized as to the composition in sugars and substituting groups, because, depending on the composition, they can interfere in some way in the properties of each one. EPS1 is composed mainly of mannose (56.1% mol), EPS2 and EPS3 are composed mainly of glucose, 67% mol and 39.1% mol, respectively, EPS4 is composed mainly of glucuronic acid (55.9% mol) and FucoPol by fucose (34.9 mol%). Biocomposites were also characterized by UV-vis spectroscopy, FTIR, TGA, XRD, DLS, Zeta potential and ICP.

Cytotoxicity and wound healing effect of EPSs and EPS/NPs biocomposites were analyzed in human keratinocyte cells (HaCaT cell line). The samples were tested using a polymer concentration of 62.5 - 1000 mg/L and none of the samples showed cytotoxicity, except for the EPS3/Ag^{+} biocomposite when tested at a polymer concentration above 125 mg/L, with a content Ag^{+} above 6.9 mg/L (decreased cell viability by ~91.9%). On the other hand, among all EPSs and their functionalized materials, FucoPol and the biocomposite FucoPol/AgNP exhibited a greater capacity to promote keratinocyte migration *in vitro*. Although EPS1 did not present wound healing effect, the biocomposites EPS1/AgNP (100 mg/L) and EPS1/AuNP (500 mg/L) showed to promote the migration of HaCaT cells. The results obtained suggest that both FucoPol and the biocomposite FucoPol/AgNP, as well as the biocomposites EPS1/AgNP and EPS1/AuNP, may have potential application in dermo-cosmetics, mainly in wound healing mechanisms.

Keywords

Exopolysaccharides, nanoparticles, cytotoxicity, wound healing, biopolymer, biocomposites synthesis.

List of contents

List of Figures

List of tables

Acronyms

AgNPs	Silver Nanoparticles
AuNPs	Gold Nanoparticles
DMEM	Dulbecco's Modified Eagle's Medium
DMF	N,N-dimethylformamide (DMF)
DLS	Dynamic Ligth Scrattering
EPS	Exopolysaccharide
FBS	Fetal Bovine Serum
FTIR	Fourier transform infrared spectroscopy
HPLC	High performance liquid chromatography
ICP	Inductivity Coupled Plasma
LB	Luria broth
OD_{450nm}	Optical density
PS	Penicillin-Streptomycin
rpm	Rotation per minute
RSM	Response surface method
SeNPs	Selenium Nanoparticles
SLPM	Standard litres per minute
SPR	Surface plasmon resonance
TFA	Trifluoroacetic acid
TGA	Thermogravimetric Analysis
UV-vis	Visible ultraviolet
XRD	X-Ray Diffration

Variables

A_{max}	Maximum absorbance
CDW	Cell dry weight (g/L)
dP	Variation of concentration of product (g/L)
dt	Variation of time (days)
FWHM	Full width at half maximum at the SPR band
rP	Volumetric productivity (g/(L.d))
Yp/S	Product yield on substrate (g/g)
Δp	Product produced (g_{EPS})
ΔS	Substrate consumed ($g_{glycerol}$)
λ_{max}	Maximum wavelength
Ψ	Experience design answer

1. Introduction

1.1. Wound healing

The skin is the largest organ in the body, with a surface that varies from 1.8 to 2 m^2 and weighs approximately 9 kg. It is composed of the epidermis, dermis, layers of subcutaneous tissue, as well as skin appendages, such as hairs and glands, which expand from the depth of the dermis to the superficial epidermal layers (Değim, 2008; Ho et al., 2017; Figure 1).

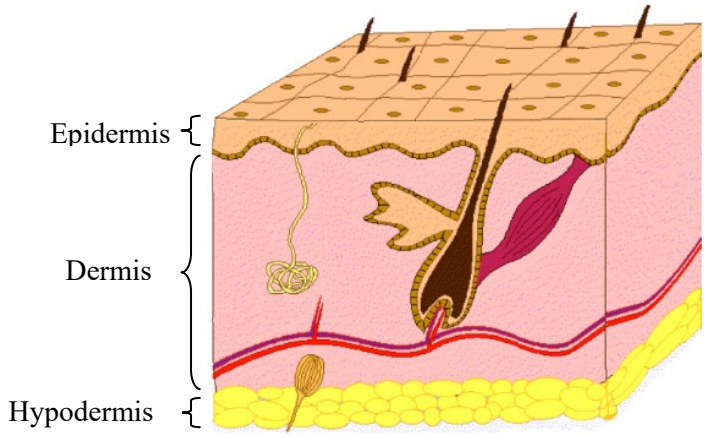

Figure 1. Simplified representation of healthy skin layers (adapted from (Değim, 2008)).

It forms a barrier between our internal and external environment, and has the flexibility to resist permanent movement distortions, and is also thin enough to allow a perception of stimuli, in addition to many other auxiliary functions (e.g. metabolism and sweat production, temperature control, and waste excretion, also functioning as a protective barrier against chemical agents and pathogens) (Değim, 2008; Ho et al., 2017).

A wound is generally characterized as a cellular and anatomical rupture of the structure and function of the tissue (Belachew et al., 2020). It can be caused by chemical, physical, microbial, thermal, or immunological damage to tissues (Velnar et al., 2009). Wound healing is a biological process of repair after an injury to the skin or other soft tissues and generally comprises four distinct phases: coagulation; inflammation, migration and proliferation; re-epithelialization, and, finally, restoration (Belachew et al., 2020; Negut et al., 2018; Figure 2).

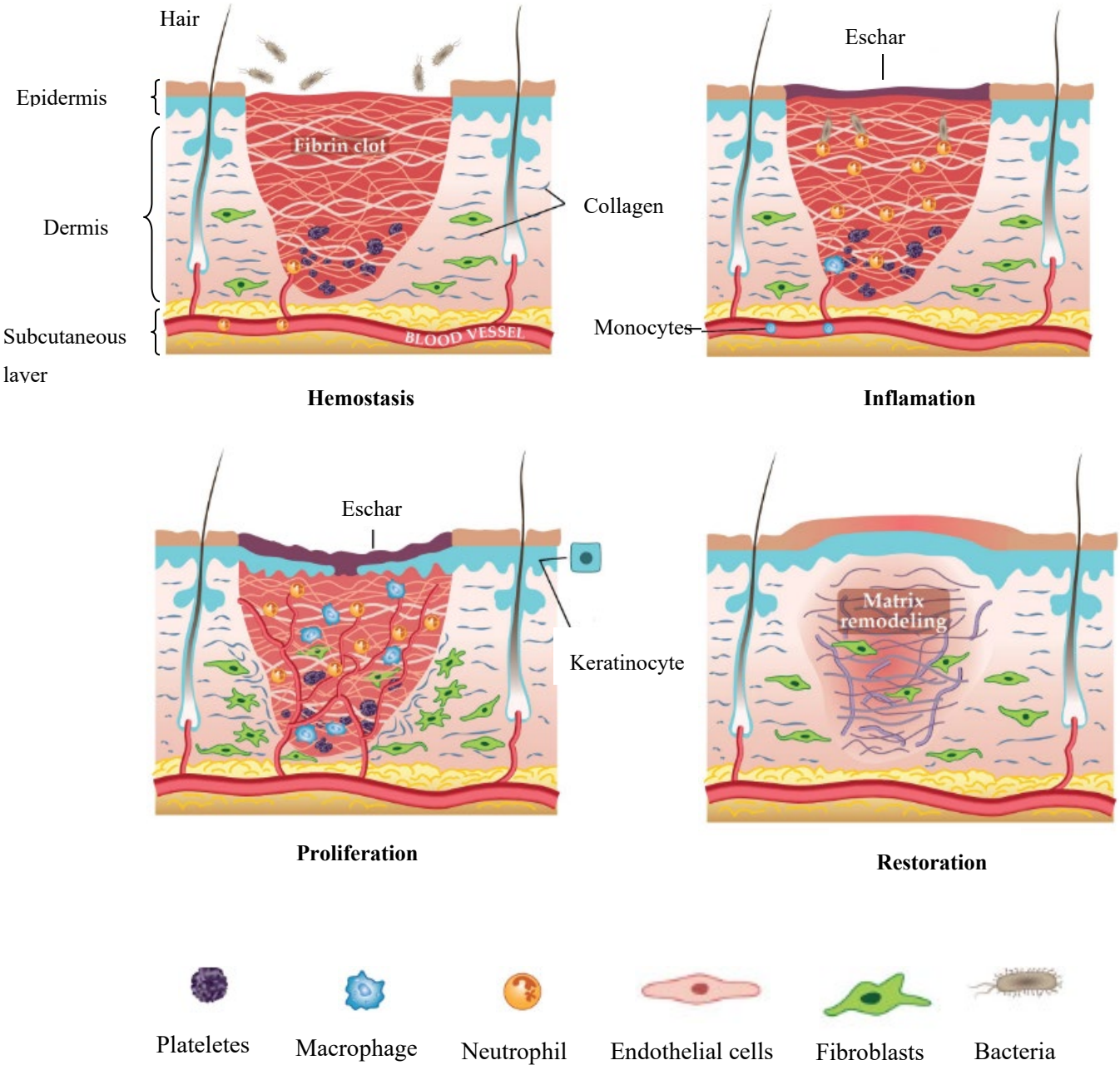

Figure 2. Schematic representation of the four stages of wound repair (adapted from (Negut et al., 2018)).

Each stage is influenced by a set of mediators, such as cytokines and platelets, inflammatory cells, cellular and extracellular matrix, proteinases, growth factors, and inhibitors (Belachew et al., 2020; Değim, 2008). In this healing process, the hemostatic and inflammatory phases usually occur immediately after the damage; however, the inflammatory phase can last for 6 days (Sorg et al., 2017). In turn, the proliferation phase is considered the beginning of angiogenesis and the development of the extracellular matrix (Xue & Jackson, 2015). The proliferation phase overlaps the inflammatory phase and lasts up to 4 weeks (Naderi et al.,

2018). Finally, remodeling occurs, which normally lasts for a year or more and involves the rearrangement and organization of collagen fibers, as well as the replacement of type III collagen by type I, which is a delicate balance between the inflammatory phases, proliferative and remodeling that results in satisfactory wound healing (Naderi et al., 2018).

Wounds are classified taking into account some criteria, time being one of them, as it is a significant factor in the assessment of wound behaviour (Velnar et al., 2009). Therefore, according to the wound healing time, it is usually differentiated into acute and chronic. For acute wounds, the normal wound healing process usually occurs within 5 to 10 days, while chronic wounds need more time to heal, and the healing process is often incomplete and disturbed by several factors including amplified levels of inflammatory mediators, wound infection, hypoxia, and malnutrition (Belachew et al., 2020; Demidova-Rice et al., 2012). In addition to these factors, others such as patient age and underlying comorbidities, for example, diabetes may be associated with long healing time (Boateng et al., 2008). Therefore, one of the main goals of wound healing is to reduce infection and pain, as well as tissue repair (Beam, 2009). Thus, materials and combinations, both synthetic and natural, are used, with numerous formulations, such as hydrogels (Koehler et al., 2018), films (Dutra et al., 2017), between others. When in contact with the wound, dressings must present properties that make them suitable for the treatment of a specific wound, such as providing a moist environment, maintaining the appropriate tissue temperature, must be biocompatible, among others (Dhivya et al., 2015; Ousey et al., 2016; Qiu et al., 2016).

In recent decades, new materials have been developed using natural polymers to improve wound healing activity, due to their biocompatibility and biodegradable nature, (Jayakumar et al., 2011). These natural polymers studied for dressing applications, which include examples of polysaccharides and proteins, are summarized (Table 1). However, these materials do not prevent microbial infections, requiring the addition of antimicrobial agents such as, for example, metallic nanoparticles.

Table 1. Examples of some polymers used in the wound healing process.

Polymers	Characteristics
Chitin	They play a notable role in biomaterials development and tissue engineering applications due to their versatile properties, including high biocompatibility, excellent biodegradability rate, antimicrobial activity, among others (Anitha et al., 2014; Kumar et al., 2018).
Chitosan	
Dextrans	Known for stimulating wound healing in several experimental models *in vivo*, it controls the proliferation of the *S. aureus* biofilm and affects the proliferation and metabolism of tumor cells (Logeart-Avramoglou & Jozefonvicz, 1999).
Cellulose	It has a distinct nanofibrillar structure that can make a perfect matrix as an ideal environment for wound healing (Czaja et al., 2006).
Alginates	Alginate-based dressings are generally used as they have hemostatic properties on oozing/bleeding wounds and burns(Ghadi et al., 2016).
Collagen	The use of collagen dressings has numerous benefits in wound care, including increased fibroblast production, fibronectin bioavailability, support to preserve leukocytes, macrophages, fibroblasts, and epithelial cells, as well as maintaining the chemical and thermostatic wound microenvironment to accelerate the healing process (Kumar et al., 2018).
Gelatine	It is a biopolymer with the potential to be used in wound dressings. It is a partially hydrolyzed collagen product and has excellent biocompatibility, biodegradability, and bioaffinity (Kumar et al., 2018).

1.2. Metal nanoparticles

The increase in multi-drug resistant pathogens has led to an increase in the use of nanoparticle-based (NPs) antimicrobials (Naderi et al., 2018). Currently, metallic NPs have drawn the attention of researchers and are carefully studied and analyzed, as antimicrobial and antibacterial potentials, in addition to the possibility of accelerating the wound healing process (Naderi et al., 2018; Rajendran et al., 2018). Due to the appearance of a high number of antibiotic-resistant bacteria, resulting in a serious health problem, it aroused the interest and

desire of researchers, leading them to explore new methods of preventing infections without the need for the use of antibiotics (Navarro Gallón et al., 2019). Metal NPs are created from the matter at the nanoscale, which typically ranges from 1-100 nm (Narayan et al., 2019). NPs can be incorporated into biomaterials and scaffolding to create smart nanocomposite materials that can aid wound healing through their selective and pro-angiogenic antimicrobial, anti-inflammatory, and pro-inflammatory properties (X. Liu et al., 2014; Lu et al., 2012; Nethi et al., 2014).

As for the synthesis, these NPs are synthesized through different approaches, namely, physical synthesis, chemical synthesis, and green synthesis. The main components of chemical synthesis are metal precursors, stabilizers, and reducers, for which reducing agents are used, such as sodium citrate, ascorbate, sodium borohydride, elemental hydrogen, among others (Zhang et al., 2016). In physical synthesis, material size is reduced by various physical methods, such as ultrasound, microwave irradiation, and the electrochemical method (Gour & Jain, 2019). The physicochemical approaches for the synthesis of NPs exert some pressure on the environment, since, in most cases, their metabolites are toxic, harmful to the environment and health, as there may be an increase in the toxicity and reactivity of the particles, causing unwanted adverse effects (Gour & Jain, 2019). For example, the synthesis of AgNPs by chemical reduction using hydrazine hydrate, sodium borohydride, DMF (N,N-dimethylformamide), and ethylene glycol can lead to the absorption of chemicals on the surfaces of NPs, thus leading to the problem of toxicity (Iravani, 2011). Therefore, researches have shown that ecological methods are more effective in the generation of metallic NPs, because, in addition to presenting advantages such as low failure probability, low cost, and ease of characterization, the green method still has great reduction potential of toxicity of metallic nanoparticles (Gour & Jain, 2019). An ecological example is the solution of AgNPs and AuNPs of anisotropic and spherical forms, which were basic by adjusting the needs of metal ions and extract of hibiscus leaves (*Hibiscus rosa Sinensis*) under environmental conditions, (Philip, 2010), treating them in this way in a simple, economical and stable method. This method is attractive because it is an intelligent technique with exceptional properties, making popular the use of vitamins, amino acids, plant extracts, among others, to synthesize metallic NPs (Gour & Jain, 2019).

1.2.1. Silver nanoparticles

AgNPs have aroused great interest for presenting special properties, with application in biosensors, cosmetic products, dental materials, lotions for sunscreens, and in the treatment of burns (Abbasi et al., 2014; Navarro Gallón et al., 2019), have also gained prominence for

having bacterial properties, which have been explored in several biomedical applications (Navarro Gallón et al., 2019). Topical silver-based creams have already been proven to be an effective antimicrobial regimen against pathological infections in wound healing (Firdhouse & Lalitha, 2015). Furthermore, it is documented that nanometric silvers exhibit unique physical and chemical properties, and are considered to be more effective in topical applications than in their macroscale form (Nowack et al., 2011). This is due to the exposure of microorganisms to their larger surface area (Kumar et al., 2018). Ashokkumar et al., (2015) as reported the synthesis of AgNPs using *Abutilon indicum* leaf extract, which exhibited highly potent antibacterial activity on *Staphylococcus aureus*, *Bacillus subtilis*, *Salmonella typhi*, and *Escherichia coli*. Also, *in vitro* studies of AgNPs-based dressings, Acticoat Flex 3 applied to a 3D fibroblast culture and, a patient with a true partial-thickness burn showed that AgNPs greatly reduce mitochondrial activity, and cell staining techniques revealed nuclear integrity with no signs of cell death (Rigo et al., 2013). In addition, AgNPs drive the differentiation of fibroblasts into myofibroblasts and promote wound contraction, thus increasing the effectiveness of wound healing (Gunasekaran et al., 2011).

1.2.2. Gold nanoparticles

Gold nanoparticles (AuNP) are considered one of the most attractive elements of the metal family, due to their potential applications (Aswathy Aromal & Philip, 2012). Depending on the optical properties, AuNP offers considerable promise in the field of biomedicine (Seo et al., 2008). They have been applied in biomedical areas, including drug administration, tissue/tumor imaging, photothermal therapy, and immunochromatographic identification of pathogens in clinical specimens (Philip, 2010). In addition, AuNPs have potent antioxidant effects on free radical extinction (Leu et al., 2012). These NPs have a large surface area, which results in a high tendency to accept electrons and interact with ROS (reactive oxygen spicies) to eliminate or deactivate them (Lau et al., 2017) and as a result, AuNPs become a strong antioxidant agent and play an important role in wound healing (Muthuvel et al., 2014). AuNPs not only have antioxidant properties but are also biocompatible, have high surface reactivity, and are non-toxic (Lau et al., 2017). According to Li et al., (2015) and Volkova et al., (2016), AuNPs are endowed with anti-inflammatory, antioxidant, antimicrobial, and non-antiangiogenic properties to increase fibroblast proliferation and decrease cell apoptosis in the wound healing process.

1.2.3. Selenium nanoparticles

Selenium (Se) exists in two forms, differentiated into organic and inorganic Se (Zhu et al., 2020). Organic Se has less toxicity and greater availability when compared to inorganic (Zhu et al., 2020). It is considered an essential mineral, which offers a wide range of biological functions and plays an extremely important role in human and animal health (Cai et al., 2018; Chaudhary et al., 2016; Cheng et al., 2017). When selenium is found in insufficient quantities, a reduction in selenoenzyme activity occurs, causing severe oxidative stress (Cheng et al., 2017). When analyzing health characteristics, in the presence and absence of Se, several clinical and epidemiological studies have demonstrated the existence of several diseases when Se is not present (Cai et al., 2018; Chaudhary et al., 2016). However, Se has a narrow boundary between functionality and toxicity, so it is important to find an appropriate form of Se (Cheng et al., 2017). Therefore, with the development of biological techniques for the synthesis of NPs, several ecological techniques have been put into practice (Cai et al., 2018).

1.3. Exopolysaccharides

Microbial polysaccharides can be divided into three main groups: intracellular, extracellular, and structural polysaccharides (Torres et al., 2011). Extracellular polysaccharides (EPS) have a wide range of physicochemical properties, being considered promising polymers with several applications in the industrial sector (for example, in pharmaceutical, food, and cosmetic products) (Freitas et al., 2011a). EPSs are generally composed of sugar monomers, including neutral, acidic and/or amino-sugars, but non-carbohydrate substituents, such as acyl groups, (acetate, pyruvate, succinate), and inorganic compounds (e.g. sulphate, phosphate) might also be present (Escárcega-González et al., 2018; Torres et al., 2011). Polysaccharide are produced and secreted by a variety of microorganisms, including bacteria, cyanobacteria, fungi, microalgae, and this family also includes plants (e.g. starch and pectins), algae (e.g. alginate and agar), and sources animals (e.g. chitosan) (Alves et al., 2010; Escárcega-González et al., 2018). They are an alternative and promising choice to replace materials from the fossil fuel industry since they present no risk of pollution to the environment, are light, and also represent the most abundant organic matter in the world (Martin-Pastor et al., 2019). Despite the wide variety of fonts that synthesize EPSs, they have advantages over each other. For example, polysaccharides synthesized by plants, to obtain a biopolymer with its respective characteristics, depends on the season and climatic conditions (Alves et al., 2010). On the other hand, when it is synthesized by bacterial/microbial fermentation, it has the advantage of not being influenced by climate change (Cruz et al., 2011). Also, bacterial EPS might have rare sugars in their composition that

represent a relevant source for its isolation and production. EPS synthesis is extremely important for microbial cells, since EPS exhibits biological properties crucial to their survival, highlighting cell protection, fixation on solid surfaces, cell aggregation, and cell-cell interactions (Escárcega-González et al., 2018). Also, EPSs from natural sources have attracted attention due to their applications in pharmacological and medical activities, such as anti-tumor, anti-inflammatory, and antioxidant effects (Yu et al., 2018). Among the EPSs produced by these microorganisms, some of the most known and studied are xanthan, cellulose, dextran, curdlan, gellan, levan, among others (Escárcega-González et al., 2018).

1.3.1. FucoPol

FucoPol is an extracellular heteropolysaccharide rich in fucose, synthesized by the gram-negative bacterium *Enterobacter* A47 (Alves et al., 2010; Freitas et al., 2014). It is a high molecular weight EPS (in the order of $5x10^6$ Da), with a low polydispersity index, composed of fucose (30-36 mol%), glucose (25-34 mol%), galactose (22-29 mol%), and glucuronic acid (9-10% mol); and acyl groups, such as succinyl (2-3% by weight), pyruvil (13-14% by weight) and acetyl (3-5% by weight) (Freitas et al., 2014; Torres et al., 2012, 2015). As for structure, fucoPol has a hexamer as a repeating unit, which has two fucose residues, two galactose, one glucose, and one glucuronic acid, the main chain being composed of two fucose residues linked to α-(1,4) and a β-linked glucose residue, one of the fucose residues being branched at position 3 and the branches are composed of 2 galactose and a glucuronic acid residue, with the terminal galactose residue pyruvate at positions 4 and 6 (Concórdio-Reis et al., 2020b; Concórdio-Reis et al., 2020a). The presence of glucuronic acid, as well the acyl substituents, makes FucoPol have a polyelectrolyte character (Torres et al., 2015). FucoPol has numerous valuable properties, including film formation, flocculation activities, in addition to having rheological, flocculating, and emulsifying properties (Freitas et al., 2014; Torres et al., 2014). That potentiates its utilization in areas like food, cosmetic and pharmaceutical products. In addition, FucoPol still can form gels (Fialho et al., 2021), and biological properties such as biocompatibility and application in wound healing (Concórdio-Reis et al., 2020b).

1.3.2. Exopolysaccharides from marine bacteria

Bacteria were one of the first life forms to appear on Earth and can still be found almost everywhere, from terrestrial to marine environments, as well as oceans and seas (Hamidi et al., 2019). Marine bacteria inhabit surface waters, from coastal areas to offshore areas, including oceanic areas in general, such as blue waters and areas with special conditions, such as hot

springs (Hamidi et al., 2019). To survive, marine bacteria have to adapt to the environmental conditions to which they are exposed in their marine habitats, thus reflecting on their physiological and biochemical characteristics (de Carvalho & Fernandes, 2010). These adaptations are responsible for their needs under conditions where nutrients are depleted (eg, nitrogen, sulfur, phosphorus, and potassium) and also during long periods of hunger (Wai et al., 1999). One of the most important survival strategies is the secretion of several products, one of them being the secretion of EPSs, which in turn play important roles in adhesion and colonization of surfaces, in protecting cells from extreme temperatures, salinity, and osmotic pressure, and also help detect quorum and biochemical interactions (Casillo et al., 2018; Nwodo et al., 2012).

EPSs make up a considerable part of the dissolved carbon in the marine environment and are involved in biofilm growth (Hamidi et al., 2019). This EPSs are produced by different marine bacteria, taking into account their ecological niche and physiological needs (Hamidi et al., 2019). It is also important to emphasize that EPSs are extremely important for the environment from a biotechnological point of view since they constitute the largest fraction of the organic matter reservoir dissolved in the marine environment (Gutierrez et al., 2013; Jensen & Fenical, 1994). Several marine bacteria are known to produce EPSs, such as *Halomonas* sp., *Bacillus* sp., *Pseudomonas* sp., *Pseudoalteromonas* sp., *Marinobacte* sp., *Alteromonas* sp., *Alcanivorax* sp. and *Rhodococcus* sp.,(Chakraborty et al., 2016), however, *Pseudomonas* sp*., Vibrio* sp*., Achromobacter* sp., *Flavobacterium* sp., *Flavobacterium* sp. and *Micrococcus* sp. are considered the main bacteria found in seawater (Baharum et al., 2010). Most EPSs produced by marine bacteria are heteropolysaccharides which generally consist of 3 or 4 different monosaccharides, which can be pentoses, hexoses, amino sugars, or uronic acid (Nichols et al., 2005).

In this study, a group of polymers synthesized by marine bacteria from microbial mats on atolls in French Polynesia was used. Microbial mats are the name given to laminated communities composed mainly of phototrophic and chemotrophic prokaryotes (Guézennec, et al., 2011). Application of nitrogen correction in microbial mats ecosystems of developing nitrogen-fixing cyanobacteria (Stal et al., 1984). The structure of microbial communities on the mat is dominated by some suitable groups of microorganisms, including cyanobacteria, the predominant genera being Phormidium and Scytonema, sulfurous and non-sulfuric photosynthetic bacteria, sulfate-reducing bacteria in the deeper layers, and Desulfo *vibrio* and Desulfobacter species (Guézennec, et al., 2011). In addition to these, other microorganisms stand out, namely *Chromatium* sp., *Thiocapsa, Thiocystis* spp., *Blastochloris* spp., *Rhodobacter* spp. and *Rhodospirillum* spp., together with heterotrophic bacteria belonging to the genera

Pseudomonas, *Alteromonas*, *Paracoccus* and *Vibrio* (Guézennec, et al., 2011). Typically, the most common components found in marine EPSs are monosaccharides such as pentoses (e.g., D-arabinose, D-Ribose, D-Xylose) and, hexoses (e.g., D-glucose, D-Galactose, D-Mannose, D-Alose, L-Ramnose, L-fucose), but uronic acids (D-glucuronic and D-Galacturonic) are also frequently found (Poli et al., 2010). In addition to these monosaccharides, organic or inorganic substituents can also be part of the composition of marine EPSs, such as sulfate, phosphate, acetic acid, succinic acid, and pyruvic acid (Poli et al., 2010).

1.4. Polysaccharides-metal bionanocomposites

Nanocomposites are generally known to be composed of various materials at the nanoscale or else incorporated into a bulk materiall (Zheng et al., 2014). Therefore, nanocomposites assume the properties of the materials present, as well as their size scale. Thus, the main challenges encountered in preparing nanocomposites include controlling their synthesis, ensuring the compatibility of their different components, and obtaining unique and desirable properties (Zheng et al., 2014). In the past few years, a wide variety of polysaccharides has been extensively explored for the synthesis and stabilization of metal nanoparticles.

1.4.1. Polysaccharide-AgNP biocomposite

EPS-AgNP biocomposites have inhibitory and bactericidal effects (Abbasi et al., 2014), therefore, they are of great interest in scientific studies. Several physical and chemical methods have been put into practice to synthesize and stabilize AgNPs (Nanda & Saravanan, 2009). In the chemical approach, several reducing agents are used, which can be organic or inorganic, electrochemical techniques, and also physicochemical reduction. However, lately, there has been a growing interest in NP synthesis using ecologically sound methods, i.e. green chemistry, which in turn has advantages over highly toxic conventional methods (Abbasi et al., 2014). In green synthesis, the reduction of Ag^{+} to obtain NPs is done in the presence of polysaccharides obtained from plants, bacteria, and algae (Abbasi et al., 2014). Polysaccharides not only allow the synthesis of NPs but also satisfy the need for green and safe synthesis routes (Navarro Gallón et al., 2019). In the synthesis of AgNP with polysaccharides forming an EPS/AgNP biocomposite, NPs are prepared using water as a solvent, which is a benign and ecologically correct solvent, and the polysaccharide is used as a protective agent and, in some cases, as a reducing agent, causing the reduction of Ag^{+}, leading to the formation of elemental silver (Ag^{0}) (Sharma et al., 2009). Chen et al., (2016) reported the synthesis of AgNPs, using a fungal EPS

(Cs-HK1 fungus), in which the formation and properties of AgNPs were evaluated at various temperatures, periods, and concentrations of $AgNO_3$ and EPSs, whose suitable conditions were 100°C, 60 min, 10 mM $AgNO_3$, and 1.0 mg/mL EPS. AgNPs synthesized in EPS solution demonstrated concentration-dependent inhibition of Gram-negative and positive bacteria, but very low cytotoxicity in RAW264.7 murine macrophage cells. Therefore, the results demonstrated the feasibility for the green synthesis of AgNPs as potential antibacterial agents using natural polysaccharides (Chen et al., 2016). AgNP biocomposites can be applied in various sectors, for example, as antimicrobial agents in the healthcare industry, in the food industry, in the cosmetics industry (Abbasi et al., 2014) and also Ag^+ has been used in dressing formulations of some topics to treat wounds and reduce the risk of infection (Değim, 2008). In addition, AgNPs are explored in medicine as dental materials, sunscreens and in the treatment of burns (Abbasi et al., 2014; Navarro Gallón et al., 2019).

1.4.2. Polysaccharide-AuNP biocomposite

The synthesis of AuNPs can be processed by chemical and physical methods; however, sometimes the chemicals used in these syntheses have some toxicity (Gopinath et al., 2013). To avoid these chemical substances, biological synthesis is used, an alternative to conventional methods and with an important antifungal role (Jayaseelan et al., 2013). Some studies report the synthesis of gold nanoparticles using plant extracts such as *Nacardium occidentale* (Sheny et al., 2011), *Cassia auriculata*, and, *Centella asiatica* (P. Kumar et al., 2011) among several other examples. Chitosan is an example of a polysaccharide used in the synthesis of gold nanoparticles, where a solution of chloroauric acid ($HAuCl_4$) at a certain concentration is mixed with the chitosan solution and heated to a specific temperature (Huang & Yang, 2004). The reduction in $AuCl^-_4$ is evident by the slow color change until a solution with a stable purple color is obtained (Smitha et al., 2009). Punuri et al., (2012), reported the synthesis of AuNPs using ethanolic extract of Piper betle leaf extract, which cytotoxicity was tested on cancer cell lines HeLa and MCF-7, and they were found to be non-toxic, indicating their biocompatibility, thus demonstrating the potential of AuNPs in various biomedical applications.

1.4.3. Polysaccharide-SeNP biocomposite

Several efforts have been made to prepare uniform selenium nanoparticles (SeNPs) using various dispersers or stabilizers (Cai et al., 2018). Currently, there are several methods to acquire Se polysaccharide compounds. In the last decade, the preparation of chemical synthesis of Se polysaccharides has received more attention from researchers, as the

operation is low-cost and relatively easy (de Araújo et al., 2011). However, this method has some disadvantages (eg, low Se transformation efficiency and slow reaction kinetics) (Zhu et al., 2020). Thus, the combination of Se with opportune macromolecules, such as proteins, polysaccharides, among others, has been an important tool to add Se functionalities (Xia et al., 2018). This means that in the food, cosmetics, and pharmaceutical industry, Se polysaccharide research has become a major area of interest (Zhu et al., 2020). Guo et al., (2013) and Cheng et al., (2017) reported the synthesis of SeNPs in the presence of *Lactococcus lactis* subsp. *lactis* and *Bacillus paralicheniformis* SR14, respectively, which demonstrate that SeNPs have been shown to have great antioxidant properties.

1.5. Motivation

Currently, there is a growing need to develop nanoparticle synthesis processes that are environmentally benign, that do not use toxic chemicals in the synthesis protocols (Gupta et al., 2016). Even if some nanoparticles are considered biocompatible, for example, Au, chemical synthesis methods can still lead to the presence of some toxic chemical species adsorbed on the surface that can have adverse effects in medical applications. Thus, it is necessary to develop ecologically correct experimental processes in the synthesis of nanoparticles. On the other hand, wound healing is a subject that has been extensively studied, to develop a technique that allows achieving a quick recovery and that results in a minimal scar (Adrian et al., 2019). Antibiotic resistance has become a serious global problem, leading the pharmaceutical and biomedical sectors to face challenges of continuous increase in multidrug-resistant human pathogens (MDR) (Rai et al., 2012). The treatment of wound infection by multi-resistant bacteria is a huge challenge, due to the inability of conventional antibiotics to treat these infections against multi-resistant bacteria (Yang et al., 2017). Therefore, the development of dressings for the treatment of wounds, in particular, for multi-resistant bacteria is a major challenge (Yang et al., 2017). Therefore, metallic nanoparticles (for example, gold, silver), have been increasingly used in dermo-cosmetics, due to their positive effects in accelerating wound healing, as well as in the treatment and prevention of bacterial infections (Adrian et al., 2019). In this work, different types of EPS (EPS1, EPS2, EPS3, EPS4, and FucoPol) were used to prepare and stabilize NPs of Ag, Au, and Se. The NPs were characterized in terms of sugar composition, UV-vis spectroscopy, FTIR, TGA, XRD, DLS, Zeta potential and ICP, in order to evaluate their potential for application in wound healing.

2. Experimental section

2.1. Exopolysaccharides

2.1.1. EPS from marine bacteria

The EPSs used in this study belonged to the genus *Alteromonas* (gram-negative bacteria) and *Vibrio*, as presented (Table 2). These bacteria were isolated from microbial mats in French Polynesia atolls. Assuming that EPSs were previously extracted and purified, no purification was performed (for example, ultrafiltration) before using them for testing. The freeze-dried EPS were kindly supplied by Jean Guezennec from the Institut Français de Recherche pour l'Exploitation de la Mer (IFREMER, France),and Pacific Biotech (French Polynesia).

Table 2. EPSs and respetive producing bactéria.

EPS	Bacteria
EPS1	*Alteromonas* sp. strain 169
EPS2	*Alteromonas* sp. strain 278
EPS3	*Alteromonas* sp. strain 1576
EPS4	*Vibrio* sp. strain MO 245
FucoPol	*Enterobacter* A47

2.1.2. FucoPol

2.1.2.1. Microorganism and media

The production of FucoPol was similar to that described in the literature, with minor changes (Antunes et al., 2017; Freitas et al., 2014). *Enterobacter* A47 bacterium (DSM 23139) was used for the production of FucoPol. Before being reactivated, *Enterobacter* A47 was preserved in glycerol (20%, v/v) at -80 ºC. Bacterial reactivation was carried out by cultivation in Petri dishes containing solidified agar (CHROMagar™ Orientation), at 30 ºC for 24 h. Pre-inoculum

was prepared in two 250 mL conical flasks, each containing 50 mL of Luria Broth (LB) medium, with the following composition (per liter): 10 g peptone; 5 g yeast extract and 10 g sodium chloride. A colony isolated from the Petri dish was inoculated in this medium and incubated in an orbital shaker (New Brunswick Scientific), at 200 rpm, 30 ºC for 24h.

After 24 hours, the inoculum was prepared by incubating 20 mL of pre-inocula in four 500 mL conical flasks, each containing 200 mL of slightly modified medium E* (to give a total inoculum volume of 800 mL), prepared with the following composition (per liter): 5.8 g K_2HPO_4; 3.7 g KH_2PO_4 and 3.3 g $(NH_4)_2HPO_4$; 10 mL of a $MgSO_4$ solution (100 mM) and 10 mL of a mineral solution (dil 1:10), with the following composition (per liter of 1 N HCl): 2.78 g $FeSO_4.7H_2O$; 1.98 g $MnCl_2.4H_2O$; 2.81 g $CoSO_4.7H_2O$; 1.67 g $CaCl_2.2H_2O$; 0.17 g $CuCl_2.2H_2O$ and 0.29 g $ZnSO_4.7H_2O$. Medium E* was supplemented with ~ 40 g/L of, glycerol. Inoculum was obtained after incubation in an orbital shaker at 30 ºC, 200 rpm for approximately 72 hours.

All the solutions used were previously autoclaved (20 min, 120 ºC, 1 bar) for sterilization and the handling of the microorganism was carried out in a laminar flow chamber, thus ensuring that there was no contamination by the external environment.

2.1.2.2. Bioreator operation

For the production of FucoPol, a 10-liter bioreactor (BioStat Bplus, Sartorius) was used, containing 7200 mL of medium E* supplemented with glycerol (40 g/L) and inoculated with 800 mL of the previously prepared inoculum. The cultivation of the bioreactor was carried out at controlled temperature (30.0 ± 0.1 ºC), and the pH was automatically controlled at 6.98 ± 0.05 by the addition of HCl (2 M) or NaOH (5 M). In addition, aeration was established at a flow rate of 1.6 standard liters per min (SLPM), and the dissolved oxygen concentration (DO) was controlled at 10% of the air saturation by automatically varying the stirrer speed (200-800 rpm). Finally, anti-foam (Sigma-Aldrich) was added automatically to prevent foam formation during the process.

Cultivation was performed in a batch mode for 8 hours, followed by a feed-batch mode, where a feeding solution (medium E* supplemented with approximately 1000 g/L glycerol), was supplied to the bioreactor at a constant rate of 5 mL per hour. Throughout the cultivation, broth samples (~24 mL) were collected from the bioreactor to quantify cell growth, nutrient consumption, and EPS production.

2.1.2.3. Analytical techniques

Cell growth was determined by measuring the optical density at 450 nm (VWR V-1200 spectrophotometer) of the samples that were taken from the bioreactor. All measurements of the optical density were made in duplicate. The cell dry weight (CDW) was calculated assuming that one OD450 unit corresponds to 0.26 g/L of CDW, as described by (Antunes et al., 2017). Afterwards, the broth samples recovered were centrifuged at 12000 g, for 15 min, at 4 ºC (Sigma 4-16 KS). The samples that showed higher viscosity were diluted with deionized water before being centrifuged (dilution 1:7 and 1:10, v/v). The cell-free supernatant was stored at -20 ºC for the quantification of FucoPol, as well as for the determination of glycerol and ammonia concentrations.

The determination of the glycerol concentration in the cell-free supernatant was performed as described by (Concórdio-Reis et al., 2018). In this analysis, high-performance liquid chromatography (HPLC) was used, with a Metacarb 87H column (Varian) coupled to a differential refractometer RI-71 detector (Merck). The analysis was carried out at a temperature of 50 ºC, using H_2SO_4 (0.01 N) as the eluent at a flow rate of 0.6 mL/min. The samples were diluted (1:50) and then filtered with Vectra Spin Micro Polysulfone filters (Whatman), which had a pore of 0.2 μm, at 3000 g for 10 min. Glycerol (99% w/w, Sigma-Aldrich) was used as a standard (1.0 g/L, 0.5 g/L, 0.25 g/L, 0.125 g/L and 0.0625 g/L). In this analysis, the samples were prepared in duplicate.

For the determination of ammonia concentration, cell-free supernatant was diluted indeionized water (1:200 dilution), and the ammonia content was determined by colorimetry using a segmented flow analyzer (Skalar 5100, Skalar Analytical, Netherlands). Ammoniaum chloride (NH_4Cl) was used as standard, at a concentration range of 4 to 20 ppm. The analysis was done in duplicate.

2.1.2.4. Exopolysaccharides quantification

EPS quantification was performed as described by (Concórdio-Reis et al., 2018). The cell-free supernatant, which contained the polymer, was dialyzed using a 12000 Da nominal molecular weight cut-off (MWCO) membrane (Zellutrans, Roth Carl) against deionized water, with constant stirring. Dialysis was controlled with frequent changes of water and measurement of conductivity over time, until equilibrium was reached, usually below 10 μS/cm. To prevent polymer degradation, a concentration of 10 mg/L of sodium azide was added to each water change until the dialysis process was completed. Finally, the pure polymer was lyophilized

(Scanvac, CoolSafe) for a period of 48 hours and weighed, to determine the polysaccharide content during cultivation.

2.1.2.5. Calculus

Product yield was determined by the following equation:

$$Y_{p/s} = \frac{\Delta P}{\Delta S} \quad (1)$$

Where ΔP (g/L) is the EPS produced, and ΔS (g/L) is the substrate consumed during the cultivation run.

To determine the volumetric productivity EPS (r_p, g/(L.d)) the following equation was used:

$$r_p = \frac{\Delta P}{\Delta T} \quad (2)$$

Where ΔP corresponds to the variation of concentration of product (EPS, g/L) in a interval (days), that corresponded to the duration of the production assay.

2.1.2.6. FucoPol extraction

FucoPol extraction was performed according to the protocol described by (Antunes et al., 2017), with some modifications. The final broth of the reactor was diluted with deionized water using a dilution factor (1:10, v/v), to decrease the viscosity. Subsequently, it was centrifuged at 8,000 g for 45 min at 4 ºC. After centrifugation, it was submitted to a thermal treatment at 70 ºC, for 1 h, in order to inactivate bacteria and enzymes that might cause degradation of the polymer during the extraction process. Then, the solution was centrifuged again at 8000 g for another 45 min, as this would remove any cell residue that might still be present, as well as the corresponding denatured proteins. Afterwards, the centrifugation and heat treatment process, the solution was subjected to a diaultrafiltration procedure, the main objective was to remove any low molecular weight unwanted components (salts, glycerol, proteins), thus resulting in a pure polymer. In this procedure a cross-flow module (Sartocon Slide Holder) was used, equipped with a membrane, with a molecular weight of 100 kDa nominal molecular weight cut-off (MWCO) having and a surface area of 100 cm^2 (Hydrosart® Ultrafiltration Cassette, Sartorius), operateding at a transmembrane pressure below 1.5 bar, thereby eliminating possible low

molecular weight contaminants. Throughout the diaultrafiltration process, the conductivity of the FucoPol solution was measured and when it reached a value below 150 µs/cm, the module was switched to ultrafiltration mode, without water addition, when volume reduction occurred, until a concentrated solution was obtained. Finally, after ultrafiltration, the FucoPol solution was lyophilized and stored at room temperature.

2.1.3. Exopolysaccharides characterization

2.1.3.1. Sugar and acyl groups

The analysis to determine the composition of the sugars and acyl groups of FucoPol and the other EPSs (EPS1, EPS2, EPS3, and EPS4) was performed as described by (Concórdio-Reis et al., 2020b). To analyze the sugar composition of the polymers, ~ 5 mg previously lyophilized samples were dissolved in 5 mL of deionized water and then hydrolyzed with trifluoroacetic acid (100 µL of 99% TFA) at 120 ºC for 2 hours. After hydrolysis and cooling, the samples were used to identify and quantify the constituent sugars by liquid chromatography (HPLC) with a CarboPacPA10 column (Thermo Scientific™ Dionex™, Sunnyvale, CA, USA), equipped with an amperometric detector. The analysis was carried out at 30 ºC, with 4 mM NaOH as eluent, at a flow rate of 0.9 mL/min. For the identification and quantification of sugar monomers, fucose, rhamnose, arabinose, glucosamine, galactose, glucose, ribose, glucuronic acid and galacturonic acid (Sigma-Aldrich) were used as internal standards (20 ppm) and as standards (1 to 100 ppm) To determine the acyl groups, the acid hydrolyzates were analysed by HPLC with an Aminex HPX-87H column 300 x 7.8 mm (Biorad, Hercules, CA, USA), coupled to an infrared (IR) detector, using 0.01 N H_2SO_4 as eluent, a flow rate of 0.6 mL/min and a temperature of 30 ºC. Acetate, pyruvate and succinate (Sigma-Aldrich) were used as standards at concentrations between 0.015 and 1.0 g/L.

2.1.3.2. Inorganic contents

To quantify the inorganic content, the polymers were submitted to pyrolysis at a temperature of 550 ºC, for 24 hours. The samples were weighed before and after pyrolysis, to determine the total inorganic content, as described by Freitas et al., 2014. The analysis was done in duplicate.

2.1.3.3. Protein content

The determination of protein content was done as described by Freitas et al., 2014. Aqueous EPSs solutions (4.5 g/L, 5.5 mL) were prepared, mixed with 1 mL of 20% NaOH and placed at 100 ºC for 5 min. After cooling on ice, 170 µL of $CuSO_4.5H_2O$ (25% w/v) were mixed. The samples were centrifuged (3500 × g, for 5 min) and the absorbance at 560 nm was measured. For the standards, albumin (Sigma-Aldrich) solutions (0.05 - 1.0 g/L) were prepared. The analysis was performed in duplicate.

2.2. Preparation of bionanocomposites

2.2.1. Biosynthesis of nanoparticles

In the initial phase of NP synthesis, several preliminary tests were carried out, including four different elements (Ag^+, Au^{3+}, Zn^{2+} Se^{4+}). Based on the literature (Concórdio-Reis et al., 2020b; Khademi-Azandehi & Moghaddam, 2015; Zhang et al., 2004) , different protocols have been tested to synthesize the biocomposites by combining these metals with different EPSs. The objective was to evaluate under what conditions (pH, temperature, time, and metal concentration) the NP formation occurred with results that were satisfactory. In the first phase, the evaluation was made by visual inspection, that is, if there was a color change in the prepared suspensions and also the formation of NPs was confirmed by UV-vis spectra, through a spectrophotometer (Amersham Biosciences Ultrospec 3100 pro), with different wavelength intervals, according to the metal in question. However, it is worth mentioning that it was not possible to proceed with the Zn-based tests, because even in the first phase of the tests it was not possible to obtain satisfactory results or to make sense.

2.2.1.1. Silver

For the synthesis of AgNP, the protocol described by Concórdio-Reis et al., (2020b) was followed, with some changes. A solution of silver nitrate ($AgNO_3$) (Sigma-Aldrich) was prepared with an Ag^+ concentration of 100 mM. For each polymer (EPS1, ESP2, ESP2I, EPS4, and FucoPol), ~ 5 mg was dissolved in 5 mL of deionized water (the only solvent used). In the first phase of the tests, the samples were tested with two different concentrations of Ag^+ (1 mM and 10 mM). As for pH, the EPS solution was maintained. The samples were incubated at room temperature under constant lighting by fluorescent light (4000 K, 12.17 ± 0.06 $W.m^{-2}$). The color change, which indicates the formation of NPs, was monitored by visual inspection and confirmed by UV-vis spectra measured from 300 to 700 nm. After carrying out these first tests,

it was possible to get an idea of how Ag^+ behaved with each EPS. However, more experiments were continued, expanding the range of factors to be tested and their respective values. The pH of the solutions was adjusted to obtain different values (5, 7, and 9), the $AgNO_3$ solution was mixed with the EPS solution, obtaining solutions with different concentrations of Ag^+, adding an average value (1 mM; 5.5 mM and 10 mM) and producing a final volume of 5 mL. Subsequently, the samples were incubated at different temperatures (20 ºC, 50 ºC, and 80 ºC) for some time (5 min, 182.5 min, and 360 min). At the end of each experiment, the formation of AgNP was monitored by visual inspection, and confirmed by UV-vis spectra. Control samples were run under the same conditions with deionized water without adding EPS. Table 3 shows a summary of the values used for each factor.

Table 3. Preliminary values used of each factor in the synthesis of AgNP.

	Factors			
Experiment	**Temperature (ºC)**	**pH**	**Time (min)**	**[Ag^+] (mM)**
1	80	~5.4	5	5
2	50	~5.4	120	1
3	80	9	300	11
4	Room temperature	9	360	10

With the monitoring by visual inspection and subsequent confirmation by UV-vis, it was possible to notice that better results were obtained when the AgNPs were prepared at pH ~ 9, with an Ag^+ concentration of ~ 10 mM, incubated at ~ 80 ºC for approximately 360 min. Then the EPSs were dissolved in deionized water, followed by adjusting the pH values, being for EPS1, EPS2, EPS3, EPS4, and FucoPol, equal to 8.81, 9.16, 9.2, 9.38, and 8.96, respectively. That done, the $AgNO_3$ solution was added to each EPS sample to obtain an Ag^+ concentration of 11 mM in both, with a final volume of 5 mL. Then, the samples were incubated in a digester (DryBlockHeater, Ohaus), both 380 min, with different incubation temperatures. For the EPS1/AgNP and EPS2/AgNP biocomposite, the incubation temperature was 80 ºC and for EPS3/AgNP, EPS4/AgNP and FucoPol/AgNP the incubation temperature was 85 ºC. After that, the samples were measured with the aid of the UV-vis spectrum, using a wavelength of 200-700 nm. Finally, to obtain purified biocomposites,

eliminating the excess of unreacted ions, the samples were subjected to a dialysis process (MWCO 12 kDa), against distilled water, with constant stirring at room temperature. After the dialysis process, part of the samples was stored in the refrigerator (~ -4 ºC), and others were freeze-dried for future analysis.

2.2.1.2. Gold

The synthesis of AuNP was performed as described by (Khademi-Azandehi & Moghaddam, 2015) with some modifications. Initially, a stock solution (20 mM) of chloroauric acid ($HAuCl_4$) (Sigma-Aldrich) was prepared. Then, approximately 3 mg of EPS was dissolved in 3 mL of deionized water, and after the EPS had completely dissolved, the $HAuCl_4$ solution (5 mL) was added, making a final Au concentration of 1 mM. The pH of the EPS solution was maintained and the solution was incubated at 80 °C. After some time (360 min aproximatly) it was possible to detect a color change in the solution, which was confirmed by the UV-vis spectrum. After that, a range of values was chosen for the different factors to evaluate the formation of AuNP. The pH values of the solutions varied between 5, 7, and 9, prepared in different Au concentrations (0.1 mM, 0.55 mM, and 1 mM), and finally incubated at different temperatures (80 ºC, 100 ºC, and 120 ºC) for different times (5 min, 182.5 min or 360 min). In the same conditions, control samples were prepared, using deionized water without EPS. Table 4 summarizes the conditions used to test $HAuCl_4$ with different EPSs. Finally, after incubation, the formation of AuNP was monitored by the color change of the sample and also by the UV-vis spectra, using a wavelength in the range of 300-800 nm.

Table 4. Tested values (maximum, average, and minimum) of each factor in the synthesis of AuNP.

Factors	Lowest value	Average value	Highest value
Temperature (ºC)	80	100	120
Times (min)	5	182.5	360
pH	5	7	9
[Au] (mM)	0.1	0.55	1

2.1.2.3. Selenium

For the synthesis of SeNP, the protocol described by (Zhang et al., 2004) was followed, with some modifications. Stock solutions of sodium selenite (Na_2SeO_3, 100mM) (Sigma-Aldrich), ascorbic acid (200 mM) (Sigma-Aldrich), and the EPSs under study were used. In this experiment, the EPS was dissolved in deionized water, at a concentration of 2 g/L. Initially, two different concentrations of Se (2 mM and 10 mM) were tested, and two different concentrations of ascorbic acid (2 and 5 mM), maintaining the pH of the EPS solution and incubated at room temperature. After evaluation by UV-vis spectra, the scale of values to be used for each factor was increased. Therefore, after the complete dissolution of the EPS, the pH of the solution was adjusted (6, 8, and 10). To obtain homogeneous solutions, sample tubes were prepared in which the EPS solution and the Na_2SeO_3 solution (2 mM, 6 mM, and 10 mM) were mixed, for approximately 2 min, and added to the ascorbic acid solution (5 mM), forming a final volume of 5 mL. Finally, the pH of the solutions was adjusted, varying between 6, 8, and 10. The samples were incubated at different temperatures (20 ºC, 35 ºC, and 50 ºC), for different times (5 min, 122.5 min, and 240 min). Control samples were prepared under the same conditions with deionized water without EPS. Table 5 shows a summary of the different conditions used in the synthesis of the SeNP. In addition to monitoring by visual inspection, which allowed a color change to be observed, the formation of SeNP was also evaluated by UV-vis spectra, with a wavelength between 200-700 nm.

Table 5. Tested values (maximum, average, and minimum) of each factor in the synthesis of SeNP.

Factors	Lowest value	Average value	Highest value
Temperature (ºC)	20	35	50
Times (min)	5	122.5	240
pH	6	8	10
[Se] (mM)	2	6	10

Note: For the different metals the same set of EPSs were used (EPS1, ESP2, ESP2I, EPS4, and FucoPol). Each metal, in addition to the standard samples, control samples were prepared, applying the same conditions, using deionized water, but without adding any type of solution containing polymer. The surface (SPR) for both nanoparticles was monitored by a UV-vis spectrophotometer.

2.2.2. Experimental design

For the preparation of AuNPs and SeNPs, a design of experiments was performed. In order to evaluate the ideal conditions for the synthesis of Au and Se biocomposites with different EPSs, the response surface methodology (RSM) was applied to evaluate the combined effect of different factors in the synthesis of biocomposites. A two-level fractional factorial design with four independent variables (pH, temperature, time, and metal concentration) was used, in which each variable was evaluated at two levels coded as +1 (the highest value) and -1 (the lowest value) plus the central value (0). An RSM is a robust technique used for the optimization of analytical procedures through the construction of mathematical models in factorial experiments to represent the role of various factors in a univariate or multivariate response (Ertürk, 2019). A fractional factorial design is a first-order response surface model, the best known of which has two layers (Núñez et al., 2018). These experiments consist of model $2^{(k-p)}$, where k is the number of factors, in this case, four (pH, temperature, metal concentration, and time), and p is the number of generators for the project (Núñez et al., 2018). To generate the matrix of experiments to be carried out in the laboratory, the program Statisca8 (StatSoft) was used, which generated a matrix (resolution IV), composed of 24 experiments, 8 of which are central points, in order to evaluate the linear effects and the curvature of the variables. The formation of NPs was monitored by visual inspection and accompanied by the formation of the surface plasmon resonance (SPR) band assessed by the following equation:

$$\psi = \frac{\text{Amax}}{\lambda\text{max FWHM}} \qquad \textbf{(3)}$$

Where, A_{max}, $\lambda_{max,}$ and FWHM are the maximum absorbance, the maximum wavelength and full width at half maximum at the SPR band, respectively, and ψ is the calculated answer.

The evaluation of the results of fractional factorial design, as well as the significance of each factor, was carried out through statistical analysis (ANOVA) at the 95% confidence level.

2.2.3. Validation experiments

After completing the data analysis with the RSM, it was possible to determine the optimal conditions for the synthesis of each biocomposite. That done, the next step was to validate the experiments, to see if the conditions considered optimal by the model worked, that is, if they provided satisfactory results that made sense. For each factor, a random value was chosen within the range of ideal values. For the synthesis of EPSs/AuNP biocomposites, a stock

solution of $HAuCl_4$ with an Au concentration of 20 mM and EPS solutions (1 g/L) was prepared. Each EPS was dissolved in distilled water and the pH value of each EPS solution was continued. For EPS1, ESP2, ESP3, EPS4, and FucoPol the pH values were 5.21, 5.19, 4.68, 4.92, and 5.08, respectively. The $HAuCl_4$ solution was added to the EPS solutions to obtain a solution with 1.2 mM Au in each of the samples, making a final volume of 5 mL. Then, samples of the EPS1/AuNP, and ESP2/AuNP biocomposites were incubated at a temperature of 100 ºC for 370 min, the ESP2/AuNP, EPS4/AuNP and FucoPol/AuNP biocomposites were incubated at 120 ºC, 90 ºC and 85 ºC respectively, with ESP2/AuNP incubated for 20 min and the remainder for 370 min. By visual inspection, it was possible to notice a color change, and the formation of AuNP was confirmed by UV-vis spectra, using a wavelength of 300-800 nm. Finally, the samples were dialyzed against distilled water with constant agitation, at room temperature, to obtain pure samples without excess ions. At the end of the analysis, some of the samples were stored at -4 ºC and others were lyophilized.

Finally, for the synthesis of EPSs/SeNP biocomposites, a Na_2SeO_3 stock solution was prepared which contained a 100 mM Se concentration, an ascorbic acid solution (200 mM), and EPS solutions (2 g/L). The EPSs were dissolved in distilled water and later the EPS1, EPS2, EPS3, EPS4, and FucoPol were adjusted to the pH values, being 8.38, 6.6, 6.48, 5.61, and 8.37 respectively. Then the Na_2SeO_3 solution was mixed with each EPS solution to obtain a 10 mM Se concentration for both. Afterwards, the ascorbic acid solution was added to the samples at a concentration of 5 mM, thus making a final volume of 5 mL. All samples were incubated at room temperature (~ 25 ºC) for 120 min, except the EPS4/SeNP biocomposite, which was incubated for a period of 240 min. The formation of SeNP was monitored by visual inspection and by reading the absorbance in the UV-vis spectrum, measured at 200-700 nm. As with previous experiments, the samples were dialyzed against distilled water with constant agitation, at room temperature, to obtain pure samples without excess ions and impurities.

2.3. Characterization of the bionanocomposites

The content of each element (Ag^+, Au^{3+}, and Se^{4+}) of the pure samples was determined by the atomic emission spectroscopy (ICP) method - Ultima, Horiba Jobin-Yvon, France, equipped with a 40.68 MHz RF generator, Czerny-Turnermonochromador with 1.00 m (sequential) and autosampler AS500.

The interaction between EPSs and nanoparticles was evaluated by Fourier Transform Infrared Spectroscopy (FTIR) (Nicolet 6700 FT-IR, ThermoElectron Corporation, Waltham,

MC, USA), with a full-reflectance, attenuated diamond crystal (ATR) accessory, using a wavelength range of 525 - 4500 cm^{-1}.

X-Ray Diffraction (XRD) analysis was used to determine the phase composition and crystalline structure of AgNPs, AuNPs, and SeNPs. In this method, X'Pert Pro X-ray diffractometer from PANalytical (Almelo, Netherlands) was used, equipped with an X'Celerator detector, in Bragg-Brentan geometry with Cu Kα line radiation (μ = 1.5406ºA). The 2 Θ scans were performed from 5 ° to 60 °, with a 0.03 ° step.

Both, the single EPSs and, the EPSs/NPs biocomposites were evaluated by Thermogravimetry (TGA), using a simultaneous thermal analyzer STA 449 F3 Jupiter, from NETZSCH Thermal Analysis, (Wittelsbacherstraße) in air, with heating rate of 20 K/min, from 0 to 550 ° C.

The Zeta potential of the nanosuspensions of Ag, Au, and Se was determined by analyzing the Zeta potential (Zetasiser Nano ZS, model ZEN from Malvern) using electrophoretic cells (disposable folded hair cells, reference DTS1070). The particle size of AgNP, AuNP, and SeNP was determined by Dynamic Light Spreading (DLS). A 10x dilution was made with mQ water in each sample. The analysis was performed at 25ºC, 633 nm (Photocor, model. Laser Helium-Neon), 20 mW, Brookhaven BI9000, 90 ºC. The zeta potential was realized at 25 ºC. The calculation of this potential was made based on the Smoluchowski equation (analyzes carried out by Professor Christian Grandfils, from CEIB, University of Liège, Belgium).

Cell based-assays were also conducted to evaluate the citotoxicity and wound healing activity of both EPSs and EPS/NPs biocomposites.

2.4. Cell based-assays

2.4.1. Cell lines and cell culture

Experiments were performed using confluent and differentiated HaCaT cells (human skin keratinocytes). HaCaT is a well-characterized cell line thad exhibits many of the morphological and functional properties of the normal epidermis (Boukamp et al., 1988). This cell line was obtained from Deutsches Krebsforschungszentrum (DFKZ, Germany), and cultured in Dulbecco's Modified Eagle's Medium (DMEM) supplemented with 10% (v/v) of heat-inactivated fetal bovine serum (FBS) and 1% (v/v) penicillin-streptomycin (PS). The cell culture medium and PS were purchased from Invitrogen (Gibco, Invitrogen Corporation, UK), while FBS was obtained from Biowest (Riverside, MO, USA). Cells were maintained at 37 ºC with 5% CO_2 in a humidified incubator and routinely grown as a monolayer in 75 cm^2 culture flasks.

2.4.2. Cytotoxicity evaluation

In order to evaluate the cytotoxicity of EPS and biocomposites, the protocol described by Concórdio-Reis et al., (2020b) was followed. The HaCaT cells were seeded into 96-well plates at a density of 4.5×10^4 cells/well and allowed to grow for 3 days. At the time of the assay, the cells were incubated with EPS (62.5, 125, 250, 500 and 1000 mg/L) or the EPS/NPs biocomposite, at the following concentrations: EPS1/AgNP (0.74, 1.48, 2.95 and 5.9 mg/L), EPS1/AuNP (1.65, 3.30, 6.60, and 13.19 mg/L), EPS1/SeNP (0.39, 0.78 , 1.55 and 3.1 mg/L), EPS2/AgNP (0.23, 0.46, 0.92, and 1.85 mg/L), EPS2/AuNP (0.26, 0.52, 1.03, and 2.05 mg/L), EPS2/SeNP (0.52, 1.04 , 2.08 and 4.16 mg/L), EPS3/AgNP (3.45, 6.90, 13.81, and 27.61 mg/L), EPS3/AuNP (2.62, 5.25, 10.50, and 20.99 mg/L), EPS3/SeNP (0.48, 0.95 , 1.90, and 3.81 mg/L), EPS4/AgNP (0.62, 1.23, 2.46, and 4.92 mg/L), EPS4/AuNP (1.97, 3.94, 7.88, and 15.77 mg/L), EPS4/SeNP (0.07. 0.13, 0.27, and 0.53 mg/L), and finally FucoPol/AgNP (0.20, 0.40, 0.81, and 1.61 mg/L), FucoPol/AuNP (2.49, 4.98, 9.96, and 19.93 mg/L) and FucoPol/ SeNP (0.17, 0.34, 0.68, and 1.36 mg/L), diluted in DMEM supplemented with 0.5% FBS and 1% PS. Cells incubated only with culture medium were considered as control. After 24 h, the cells were washed once with PBS (Sigma-Aldrich, USA), and cell viability was assessed using CellTiter 96® AQueous One Solution Cell Proliferation Assay (Promega, USA) containingMTS reagent, according to the manufacturer's instructions. The optical density was measured at 490 nm using a BioTek EPOCH2Microplate Reader (BioTek, USA) and cell viability was expressed in terms of percentage of living cells relative to the control. Experiments were expressed in terms of mean ± SD of at least two experiments, performed in triplicate.

2.4.3. Wound healing capacity

Based on the protocol described by Concórdio-Reis et al., (2020b), the scracht assay was performed to evaluate the wound healing capacity of both isolated EPSs and EPSs/NPs biocomposites. The HaCaT cells were seeded at a density of 1.0×10^5 cells/cm^2 in a 12-well plate and allowed to grow until reaching 100% confluence (48 h). The wound was created with a sterile pipette tip and each well washed twice with PBS in order to remove non-adherent cells. Subsequently, cells were incubated for 24 h with the EPSs and EPSs/NPs biocomposites, using the following concentrations: 100 and 500 mg/L (EPS1, EPS1/AgNP, EPS1/AuNP, EPS1/SeNP, EPS2, EPS2 /AgNP, EPS2/AuNP, EPS2/SeNP, EPS4, EPS4/AgNP, EPS4/AuNP, EPS4/SeNP); 25 and 100 mg/L (EPS3, EPS3/AgNP, EPS3/AuNP and EPS3/SeNP), and finally, 50, 100 and 500 mg/L (FucoPol, FucoPol/AgNP, FucoPol/AuNP and FucoPol/ SeNP), diluted in DMEM supplemented with 0.5% FBS and 1% PS. Cells incubated with only culture medium were also included as negative control. Photos of the same scratch region were taken using an

inverted phase-contrast microscope (Olympus CKX41, Japan) at two different time points: 0 and 24 hours. Image analysis was performed using ImageJ 1.47v software (USA) and the wound area measured between the limits. The area of the recovered wound was calculated as a percentage, following the equation (Eq. 4) and the wound recovery results were determined as a ratio relative to the control.

$$\text{Wound area recovered (\%)} = \frac{(\textbf{Initial area}) - (\textbf{Final area})}{\textbf{Initial area}} \textbf{x } \textbf{100} \qquad \textbf{(4)}$$

The results were expressed in terms of mean ± SD of at least one experiment carried out in duplicate.

3. Results and discussion

3.1. FucoPol production and extraction

FucoPol was produced during the cultivation of the bacterium *Enterobacter* A47, in a mineral medium with glycerol as the sole carbon source, and the cultivation took 96 hours (4 days). The characteristic profile of the cultivation, namely, the cell growth of *Enterobacter* A47 and EPS production, using glycerol as the only carbon source is shown (Figure 3).

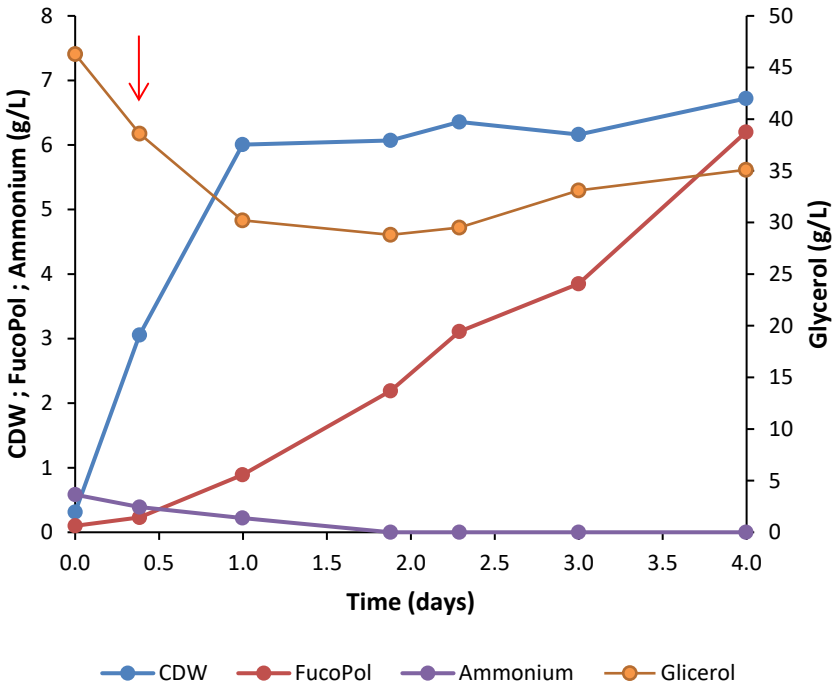

Figure 3. Typical culture profile for *Enterobacter* A47, using glycerol as the sole carbon source. The feed-bach phase was started on day 0.4 (red arrow), that is, after 8 hours of cultivation.

In the batch phase (~ 24 h) the culture grew exponentially, reaching a maximum dry cell weight of about 6 g/L. After this phase, a slight decrease in dry cell weight (CDW) was observed. This decrease in CDW may be related to several factors, such as loss of cell viability, due to the restricted conditions of oxygen and ammonia imposed on the bioreactor (Torres et al., 2011), and also, due to the dilution of the broth, as NaOH and the feeding solution were entering, and the concentration of cells decreased, due to the removal of samples from the broth. However, at around 48 h the CDW started to increase slightly until reaching a maximum of 7.05 g/L at 76 h, which subsequently decreased slightly, with a final CDW of 6.72 g/L at 96 h (Figure 3).

During the EPS cultivation run, a change in the broth viscosity was observed; acquired a viscous aspect referring to the beginning of the EPS synthesis process. The viscosity observed and which has been increasing is a typical characteristic observed in many microbial cultures aimed at the production of extracellular polysaccharides and is generally an indicator of the end of the race since the broth culture loses homogeneity (Freitas et al., 2011b).

It was possible to verify that an EPS production (6.20 g/L) was slightly lower than the values normally reported in the literature. Also, according to figure 3, it is possible to observe that, at the end of 96 hours, a CDW value corresponding to 6.72 g/L was reached, which is in line with the range of values reported in the literature. The net yield of EPS in glycerol was slightly lower than those reported in previous studies, with a value of 0.12 gEPS/gGlycerol. Finally, at the end of the cultivation trial, the productivity of 1.53 g/(L.d) was reached, a value slightly lower than those reported in the literature. Table 6 presents a summary of the kinetic parameters obtained by the cultivation trial in a bioreactor of *Enterobacter* A47 using glycerol as the sole carbon source, compared to previous studies.

Table 6. Summary of the kinetic parameters obtained by the cultivation trial in a bioreactor of Enterobacter A47 using glycerol as the sole carbon source, compared to previous studies.

	EPS (g/L)	**CDW_{max} (g/L)**	**$Y_{P/S}$ (gP/gS)**	**r_P (g/(L.d))**	**Resferences**
Cultivation assay	6.20	6.72	0.12	1.53	This study
Literature	7.23-7.97	5.80-7.68	0.28-0.47	1.89-3.72	(Alves et al., 2009; Freitas et al., 2014; Freitas, et al., 2011b; Torres et al., 2011)

Analyzing the table, it is possible to conclude that the values of the parameters of EPS cultivation, even not being within the range of values reported in the literature, present very similar results. This difference may be related to some difference in the EPS quantification methods.

3.2. Exopolysaccharides characterization

All EPSs involved in this study were properly characterized in terms of their composition in sugars (Table 7), as well as their acyl substituents, sulfate, and total protein (Table 8).

Table 7. Composition in sugars of each EPS.

mol% sugar					
%mol	EPS1	EPS2	EPS3	EPS4	FucoPol
Fucose	0.0	0.0	15.7	0.0	34.9
Glucose	27.9	67.0	39.1	2.4	33.9
Galactose	4.9	21.2	16.3	0.4	0.0
Rhamnose	0.3	1.1	7.1	0.0	0.0
Mannose	56.1	0.4	16.1	0.0	0.0
Glucosamine	0.0	0.0	0.0	20.6	0.0
Galactosamine	0.0	0.0	0.0	20.6	25.8
Glucuronic acid	8.8	10.0	3.5	55.9	5.0
Galacturonic acid	2.0	0.3	2.3	0.0	0.0
Reference	This study	This study	This study	(Martin-Pastor et al., 2019)	This study

Table 8. Composition in total acyl substituent's, total protein, and sulphate of each EPS.

	EPS1	**EPS2**	**EPS3**	**EPS4**	**FucoPol**
Acyl Substituints (wt.%)	6	1.6	0.3	3.7	8.15
Total protein (wt.%)	5.2	5.7	4.9	5.1	11.6
Sulphate (wt.%)	2.8	3.3	3.4	1.7	0.0

EPSs that have negatively charged components in their composition, such as residues of acyl substituents (e.g., pyruvate and succinate), acid sugars like glucuronic acid, and sulfate, give EPSs an anionic nature, thus sustaining an electrostatic attraction of ions, and the potential for the formation of ion complexes with positively charged compounds (Concórdio-Reis et al., 2020b; Freitas et al., 2011a).

As for the composition in sugars, the EPS understudy shares the characteristics of EPSs reported in the literature. For example, EPS2 and EPS3 have in common glucose, and glucuronic acid, which are sugars found in the composition of xanthan gum, the first biopolymer produced by an industrial process, in addition to having applications in the food, pharmaceutical, and cosmetics industries (Freitas et al., 2011b). Other examples of EPSs reported in the literature that have characteristics similar to the EPSs in this study, such as gellan that contains glucose, rhamnose, and glucuronic acid, and alginate, consisting of glucuronic acid, such as EPS4. Gelan, as well, xanthan gum, has potential application in the food and pharmaceutical industry (Fialho et al., 2008), while alginate has potential application in medicine, as surgical dressings, and wound treatment (Peña et al., 2008).

3.3. Definition of conditions for bionanocomposites synthesis

3.3.1. Silver nanocomposites

For the synthesis of AgNPs, preliminary tests were performed (Table 3 in materials and methods), in order to define the optimal conditions, taking into account the following factors (temperature, time, pH, and Ag^+ concentration), that would result into the formation of nanoparticles stabilized by the different EPS.

The selected values were based on the literature, albeit with some modifications. Some of the experiments were performed at the pH value of EPS solutions prepared in deionized water (pH ~ 5.4) without any change. Navarro Gallón et al., (2019), prepared AgNPs, with EPS synthesized by *Botryococcus braunii* (*B. braunii*, LB572), with a Ag^+ concentration of 3.5 mM, at pH 8. Incubation took place for 1 h at 90 ° C. They also describe that the reduction of Ag^+ to Ag^0, indicating the formation of AgNP, occurred a few seconds after the start of incubation. Vanaja et al., (2013) also prepared AgNPs with extracts of *Cissus quadrangularis*, a plant of the Vitaceae family, using different concentrations of Ag^+ (1 - 5 mM), varying the pH (4-8), the temperature (30 - 70 °C), and the time interval (minimum of 10 min and maximum of 24 h), resulting in AgNPs with different characteristics, such as the color of the solution and the shape of the spectrum. On the other hand, Concórdio-Reis et al., (2020b), also prepared AgNP with EPS FucoPol, at room temperature, with Ag^+ concentrations of 1 and 10 mM. The reaction lasted 24 hours and resulted in the synthesis of stable FucoPol-AgNPs. The references mentioned above were some of the references that served as a starting point to have a notion of values used for each factor to synthesize AgNPs, thus justifying some of the values selected to perform the preliminary tests. To confirm that AgNPs were formed due to the presence of the EPS, control samples were prepared under the same conditions using distilled water. Control samples remained colorless, and a color change occurred only in the presence of EPS under some conditions (Table 9), which was confirmed by UV-vis spectra (Figure 4).

Table 9. Results obtained from preliminary tests for each EPS. For each EPS, suspensions containing EPS and Ag^+ (image on the right) and control samples (images on the left) are shown.

Experiment	EPS1	EPS2	EPS3	EPS4	FucoPol
1					
2					
3	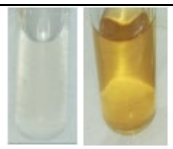				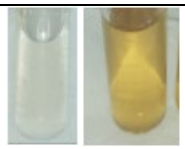
4					

Early results show that not all conditions resulted in AgNPs. Table 10 shows the result of all suspensions of each EPS and shows that in all EPSs, only in experiment 3, the formation of AgNP occurred, which can be visualized by changing the color of the solution (image on the right), while a control sample remained colorless (left image). In the other experiments, both the control and the samples (with solutions of Ag^+ and EPS) remained colorless, showing that AgNP synthesis did not occur. Figure 4 shows a characteristic spectrum of AgNPs (Figure 4A), corresponding to one of the EPSs from experiment 3, and another spectrum that does not correspond to the characteristic spectrum of AgNP (Figure 4B).

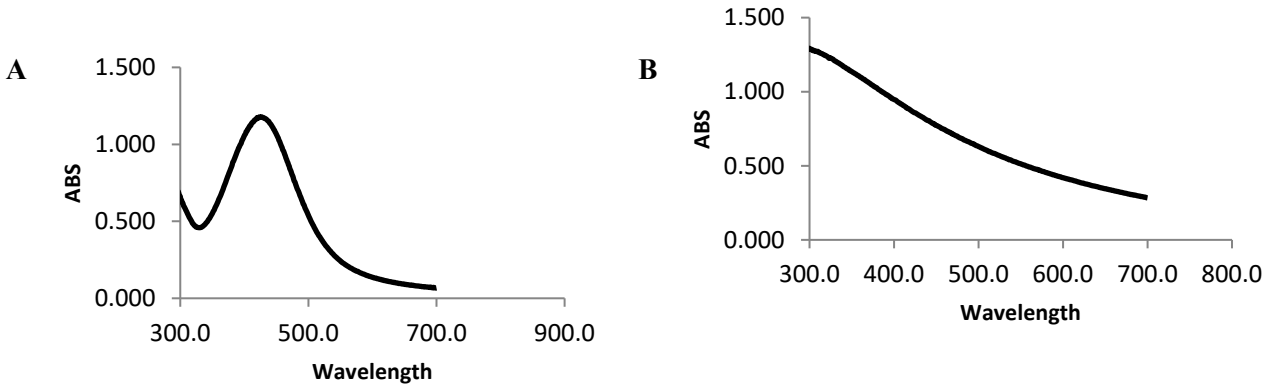

Figure 4. Examples of spectra with the SPR band characteristic of AgNPs (4A) and spectra that do not correspond to the synthesis of AgNPs (4B).

These tests were extremely important because they provided results to select conditions that result in stable AgNPs.

3.3.1.1. Selection of conditions for biocomposites synthesis

Among the various values tested for each factor, for the different EPSs, those that showed the best results were chosen. Table 10 shows the values chosen for each factor to synthesize AgNPs.

Table 10. Selected values of each factor to synthesize AgNPs.

NPs	T (ºC)	pH	Tempo (min)	$[Ag^+]$ (mM)
EPS1/AgNP	80	8.81	380	11
EPS2/AgNP	80	9.16	380	11
EPS3/AgNP	85	9.2	380	11
EPS4/AgNP	85	9.38	380	11
FucoPol/AgNP	85	8.96	380	11

3.3.2. Gold nanocomposite

3.3.2.1. Preliminary tests

For the synthesis of AuNPs, preliminary tests were performed (Table 11), in order to select the conditions, taking into account factors (temperature, time, pH, and Au^{3+} concentration), that would lead to the formation of stable AuNPs with each tested EPS.

Table 11. Preliminary values used in the tests for the synthesis of AuNP

	Factors			
Experiment	**Temperature (ºC)**	**pH**	**Time (min)**	**[Au^{3+}] mM**
1	60	9	60	1
2	80	~ 5.4	360	1
3	100	~5.4	180	0.5
4	100	~5.4	10	0.1

The values used for each factor for the preliminary tests in the synthesis of AuNPs were based on literature reports. Temperatures up to 100°C, pH between 4 and 9 reaction times of 5-300 min, and Au^{3+} concentration between 0.1 and 2 mM have been reported (Aswathy Aromal & Philip, 2012; Philip et al., 2011; Smitha et al., 2009). Experiment 1 was carried out at 60 ºC and pH 9, with a Au^{3+} concentration of 1 mM, for 1 h. Experiments 2, 3, and 4 were carried out without changing the pH value of the solutions (pH ~ 5.4), but different temperatures, reaction times, and Au^{3+} concentrations were used. To confirm whether the synthesis of AuNPs occurred only in the presence of the EPS, control samples were prepared under the same conditions, using deionized water without the addition of EPS. Therefore, the control samples remained colorless, whereas, in the EPS samples, a color change occurred under some conditions (Table 12), indicating the formation of AuNP which was confirmed by UV-vis spectra (Figure 5).

Table 12. Results obtained from preliminary tests for each EPS. For each EPS, suspensions containing EPS and Au^{3+} (image on the right) and control samples (images on the left) are shown.

Experiment	EPS1	EPS2	EPS3	EPS4	FucoPol
1					
2		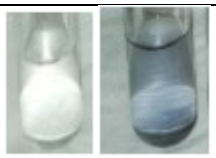			
3	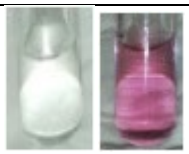	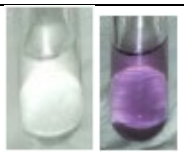			
4					

The results of the suspensions show that, some of the conditions tested, namely, experiments 2 and 3, resulted in the formation of AuNPs, and experiment 4, only worked for EPS4. In these experiments, the control remained colorless (images on the left), while suspensions with different shades of purple (images on the right) can be seen, depending on the EPS and the conditions tested. In figure 5, it is possible observe both spectra with SPR bands characteristic of the AuNP formation (5A), for the conditions that worked, and spectra corresponding to the suspensions that remained colorless (5B).

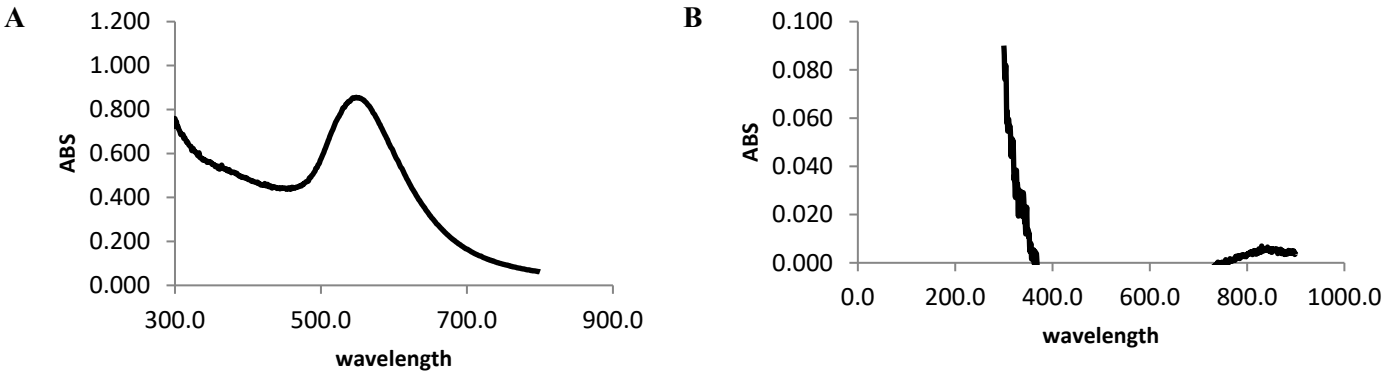

Figure 5. Examples of spectra with the SPR band characteristic of AuNPs (A) and spectra that do not correspond to the synthesis of AuNPs (B).

3.3.2.2. Synthesis optimization

Based on preliminary tests, it was possible to define ranges of values (Table 13) to be used for each factor (time, temperature, pH, and Au^{3+} concentration), in order to be able to synthesize stable AuNPs. Design Expert was used to build an experience matrix (Table 14), which generated a set of values to be tested, with a total of 24 experiments, 8 of which are central points, thus being able to assess the impact of the various factors in the synthesis AuNPs and, in the end, determine the ideal condition for their production. With the experiment matrix, it was possible to perform experiments, combining different values of pH, temperature, time, and Au^{3+} concentration. This combination of values was evaluated by visual inspection, changing the colors of the samples (from colorless to a purple solution), which were confirmed by the UV-vis absorption spectra, which presented a plasmon resonance (SPR) surface characteristic of metallic gold. With the spectra obtained for each condition, it was possible to calculate and analyze the generated response (Table 14), thus evaluating the impact of each factor in the synthesis of AuNPs.

Table 13. Values range defined for each factor in the preparation of AuNP.

Factors	Low level (-1)	Central point (0)	High level (+1)
Temperature (ºC)	80	100	120
pH	5	7	9
Time	5	182.5	360
[Au^{3+}]	0.1	0.55	1

For the test optimization process, the response was calculated using equation (3) described in the materials and methods section. With the results obtained for each set of factor interactions, the Design Expert was used to present the responses obtained (Table 14) and to be able to analyze which factors were significant and which ranges of values would be ideal for synthesizing the biocomposites. According to the responses, it was possible to see the impact of each factor and its interactions on the synthesis of AuNPs.

Table 14. Conditions were tested for the synthesis of AuNP with different EPSs and their responses.

	Factors				Responses ψ				
Run	Time (min)	T (ºC)	pH	[Au^{3+}]	**EPS1**	**EPS2**	**EPS3**	**EPS4**	**FucoPol**
1	5	80	5	0.1	0.0	0.0	0.0	0.0	0.0
2	5	120	5	1	0.0	0.0	9.9×10^{-6}	0.0	2.2×10^{-6}
3	5	80	9	1	0.0	0.0	0.0	0.0	0.0
4	5	120	9	0.1	0.0	0.0	0.0	0.0	0.0
5	360	80	5	1	3.4×10^{-6}	2.2×10^{-6}	6.0×10^{-6}	9.4×10^{-6}	9.9×10^{-6}
6	360	120	5	0.1	1.2×10^{-6}	1.6×10^{-6}	8.5×10^{-7}	8.9×10^{-7}	0.0
7	360	80	9	0.1	0.0	0.0	0.0	0.0	0.0
8	360	120	9	1	0,0	2.7×10^{-6}	2.5×10^{-6}	5.1×10^{-6}	0.0
9 (C)	182.5	100	7	0.55	4.0×10^{-6}	2.7×10^{-6}	4.1×10^{-6}	5.4×10^{-6}	2.2×10^{-6}
10 (C)	182.5	100	7	0.55	5.0×10^{-6}	3.0×10^{-6}	4.3×10^{-6}	5.2×10^{-6}	2.1×10^{-6}
11 (C)	182.5	100	7	0.55	4.1×10^{-6}	3.7×10^{-6}	3.7×10^{-6}	5.5×10^{-6}	2.2×10^{-6}
12 (C)	182.5	100	7	0.55	4.0×10^{-6}	3.4×10^{-6}	4.0×10^{-6}	6.0×10^{-6}	2.3×10^{-6}
13	5	80	5	0.1	0.0	0.0	0.0	0.0	0.0
14	5	120	5	1	0.0	0.0	10.0×10^{-6}	0.0	2.3×10^{-6}
15	5	80	9	1	0.0	0.0	0.0	0.0	0.0
16	5	120	9	0.1	0.0	0.0	0.0	0.0	0.0
17	360	80	5	1	3.4×10^{-6}	2.9×10^{-6}	5.3×10^{-6}	9.1×10^{-6}	9.7×10^{-6}
18	360	120	5	0.1	1.2×10^{-6}	1.8×10^{-6}	1.1×10^{-7}	9.1×10^{-7}	0.0
19	360	80	9	0.1	0.0	0.0	0.0	0.0	0.0
20	360	120	9	1	0.0	$1,9 \times 10^{-6}$	0.0	9.6×10^{-6}	0.0
21 (C)	182.5	100	7	0.55	4.1×10^{-6}	3.8×10^{-6}	3.8×10^{-6}	5.3×10^{-6}	2.1×10^{-6}
22 (C)	182.5	100	7	0.55	4.0×10^{-6}	3.5×10^{-6}	4.2×10^{-6}	5.0×10^{-6}	1.9×10^{-6}
23 (C)	182.5	100	7	0.55	4.0×10^{-6}	3.0×10^{-6}	4.1×10^{-6}	5.5×10^{-6}	1.9×10^{-6}
24 (C)	182.5	100	7	0.55	4.7×10^{-6}	3.2×10^{-6}	4.2×10^{-6}	5.3×10^{-6}	2.0×10^{-6}

According to the answers presented for each factor, it is possible to conclude in which conditions the synthesized AuNPs were more stable, and in which conditions their synthesis does not occur. For example, at pH 9, most of the responses were equal to zero, for all EPSs, a positive response to that pH was rarely obtained. And also, the higher the temperature, the Au^{3+}

concentration, and the incubation time, the better the responses, except EPS3, which showed better results with only 5 min of incubation.

With the statistical analysis (ANOVA) (Table S1 in appendix), the results showed that, for the EPS1/AuNP biocomposite, both factors were significant, as well as their interactions, causing an impact on the synthesis of AuNPs. The statistical analysis also showed that for this biocomposite the curvature was significant, with a non-significant lack of fit adjustment and a value of $R^2 > 0.94$. The graphs presented (Figure 6) show the results and the impact of the interaction of the significant factors and respective regions with the ideal values to be used.

RSM model

The RSM model is a powerful model used to optimize analytical methods by building mathematical models in factorial experiments to describe the role of various factors in a univariate or multivariate response (Ertürk, 2019). RSM was used to assess the combined effect and define the working region to synthesize the best biocomposites.

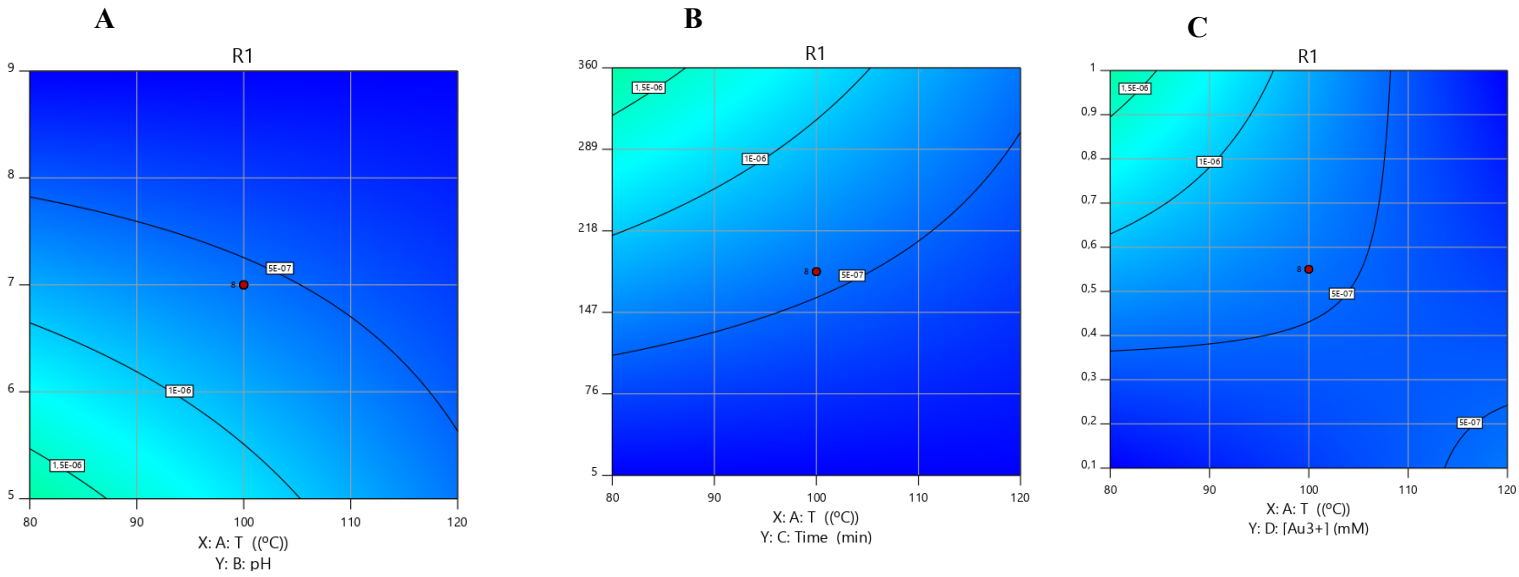

Figure 6. Contour plots of the AuNP desirability measure, mediated by EPS1, under various conditions: A (pH and temperature), B (time and temperature), and C (Au concentration and temperature). The colors ranging from blue to green indicate the minimum and maximum values, respectivelly. The values that are closest to the green zone are considered ideal for synthesizing AuNPs.

With the graphs that represent the interaction of the different factors, it was possible to determine the range of ideal values for each factor to synthesize AuNPs. Table 15 presents a summary of the value ranges for each factor that can be used in the synthesis of stable AuNPs for EPS1.

Table 15. The value ranges considered ideal for synthesizing EPS1/AuNP biocomposite

Temperature (ºC)	Time (min)	pH	[Au]
80 - 100	350 - 360	5.0 – 5.5	0.9 – 1.0

Thus, to produce stable AuNPs, a value must be chosen for each factor within the range shown in the table.

In the EPS2/AuNP synthesis, according to the statistical analysis, (Table S2 in the appendix), the results showed that not all factors were significant. One of the factors that were not significant was the temperature, as well as its interaction with the time factor. The model showed an $R^2 > 0.91$, a non-significant lack of fit, and a significant curvature, thus resulting in a significant model. Figure 7, show the interactions of the significant factors and the respective ranges of optimal values for each of the factors to synthesize this biocomposite.

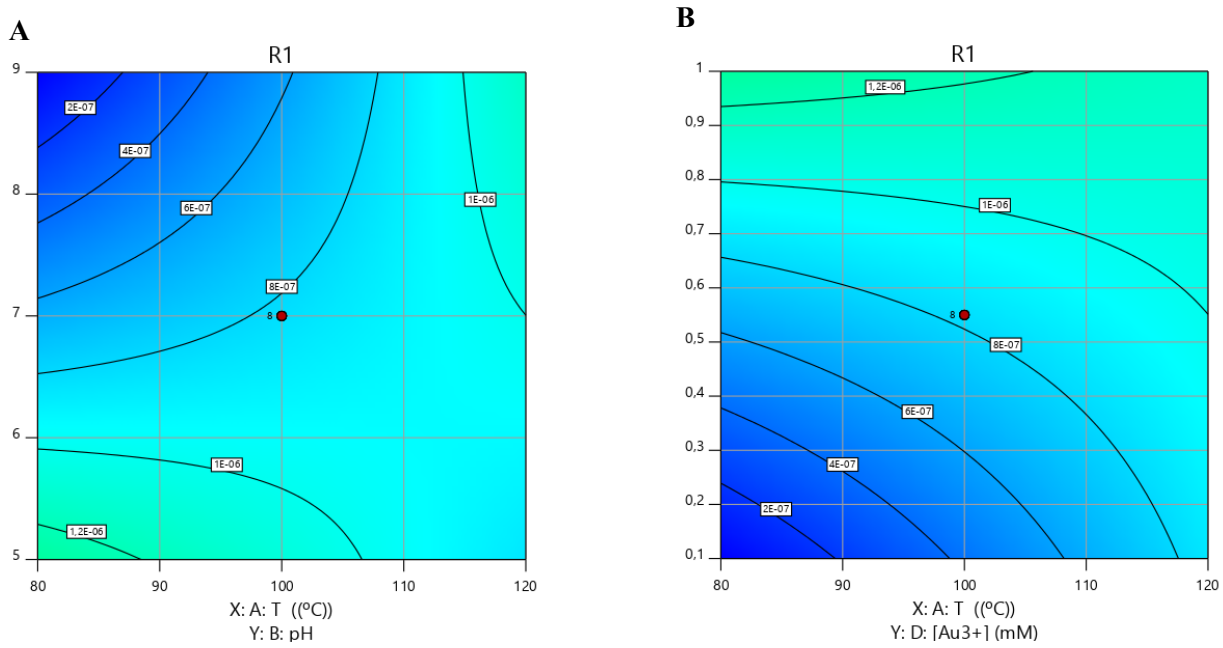

Figure 7. Contour plots of the AuNP desirability measure, mediated by EPS2, under various conditions: A (pH and temperature), and B (Au concentration and temperature). The colors ranging from blue to green indicate the minimum and maximum values, respectivelly. The values that are closest to the green zone are considered ideal for synthesizing AuNPs.

Table 16 shows the results of the ranges of values considered optimal for the synthesis of EPS2/AuNPs according to the results presented in the graphs.

Table 16. The value ranges considered ideal for synthesizing EPS2/AuNP biocomposite.

Temperature (ºC)	pH	[Au]
80 - 100	5.0 – 5.4	0.9 – 1.0

Contrary to the results presented for the EPS1/AuNP biocomposite, in the EPS2/AuNP biocomposite, the time factor is not noticed, as can be seen in the graphs. This is because the interaction of the other factors with the time factor is not significant.

An ANOVA statistical analysis for the EPS3/AuNP biocomposite (Table S3 in the appendix), showed that all factors were significant and the interactions (temperature and pH, temperature and concentration of Au^{3+} and temperature and time) were significant and impact the synthesis of AuNPs. The model showed a value of $R^2 > 0.99$, significant curvature, and lack of fit significant adjustment. These results allow us to conclude that the model used is significant. The graphs (Figure 8) show the interactions of the different factors.

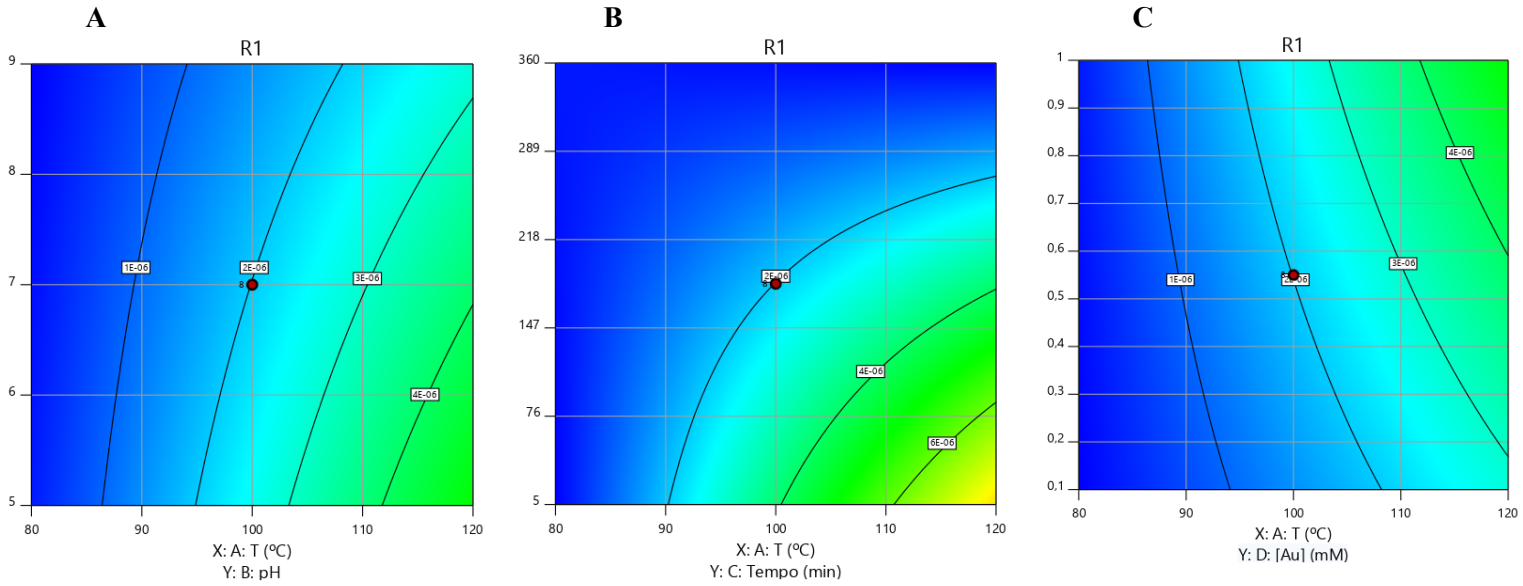

Figure 8. Contour plots of the AuNP desirability measure, mediated by EPS3, under various conditions: A (pH and temperature), B (time and temperature), and C (Au concentration and temperature). The colors ranging from blue to green/yellow indicate the minimum and maximum values, respectivelly. The values that are closest to the green/yellow zone are considered ideal for synthesizing AuNPs.

The range of values to be used for each factor in the synthesis of the EPS3/AuNP biocomposite, as illustrated by the graphs is summarized (Table 17).

Table 17. The value ranges considered ideal for synthesizing EPS3/AuNP biocomposite.

Temperature (ºC)	Time (min)	pH	[Au]
100 - 120	5.0 - 30	5.0 – 5.5	0.9 – 1.0

According to the results presented, the preparation of AuNPs should be done with low pH values, around 5, and at high temperatures, around 120ºC. Unlike the biocomposites described previously, where it took a few hours of incubation to obtain stable AuNPs, for the EPS3/AuNP biocomposite, only a few minutes of incubation are needed.

In the synthesis of the EPS4/AuNP biocomposite, according to the statistical analysis (ANOVA), only the time and the concentration of Au^{3+} presented themselves as significant factors (Table S4 in the appendix), and as for the interaction of the different factors, only the interaction of the temperature with pH proved to be significant. However, the curvature in this drawing is significant; the lack of fit is also significant, which is not good for the model, as the goal is for the model to fit. However, this model presented an $R^2 > 0.92$. Figure 9 shows the significant interaction, which in this case is between temperature and pH and respective areas with values considered optimal for their synthesis.

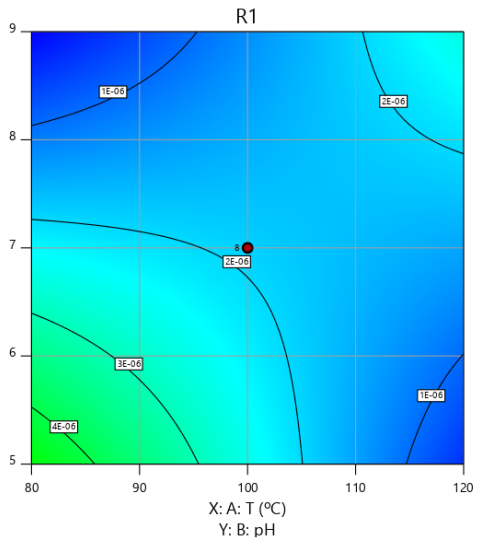

Figure 9. Contour plots of the AuNP desirability measure, mediated by EPS4, showing the interaction of two factors: pH and temperature. Colors ranging from blue to green indicate the minimum and maximum values, respectively. The values closest to the green zone are considered ideal for the synthesis of AuNPs.

The range of values to be used for each factor in the synthesis of the EPS4/AuNP biocomposite, as illustrated in the graphs, is summarized (Table 18). In this table, only the factors of significant interaction are presented.

Table 18. The value ranges considered ideal for synthesizing EPS4/AuNP biocomposite.

Temperature (ºC)	pH
80 - 98	4.5 – 5.5

Once the range of ideal values is determined, interaction is made, and in this case, the only significant interaction was between temperature and pH, so they are the only factors present in the table.

Finally, the statistical analysis (Table S5 in appendix) regarding the synthesis of the biocomposite FucoPol/AuNP, showed results showing that all factors and all interactions were significant, causing an impact on the synthesis of this biocomposite. The model showed an $R^2 >$ 0.99, a significant curvature, and a non-significant lack of fit. The graphs (Figure 10) show the interactions of the different factors.

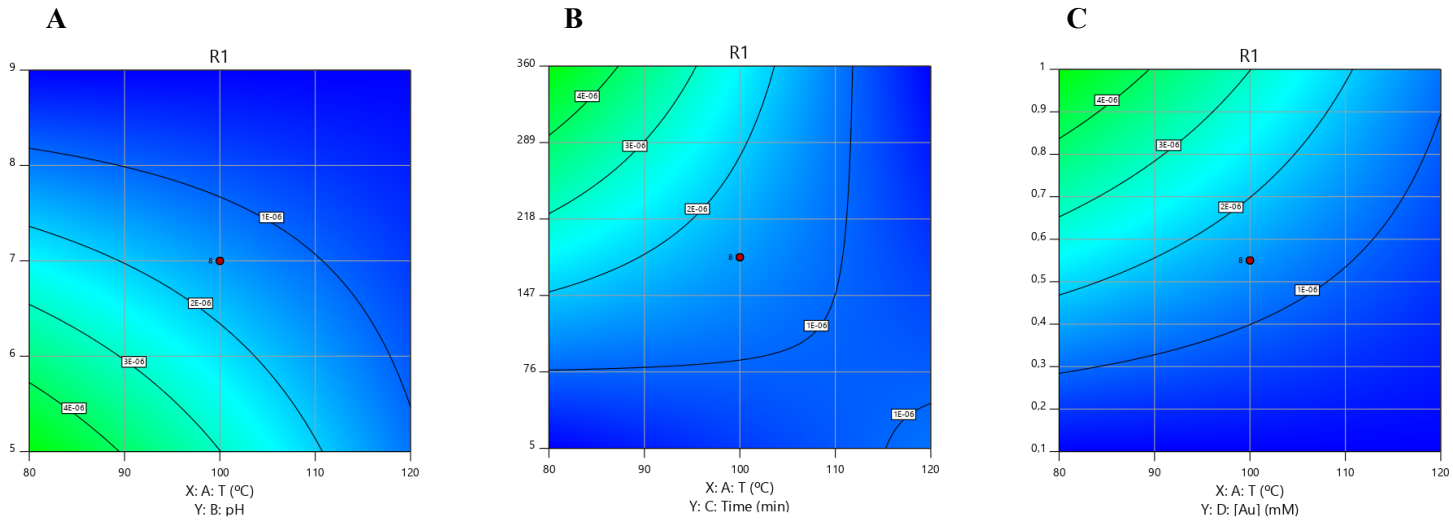

Figure 10. Contour plots of the AuNP desirability measure, mediated by FucoPol, under various conditions: A (pH and temperature), B (time and temperature), and C (Au concentration and temperature). The colors ranging from blue to green indicate the minimum and maximum values, respectively. The values that are closest to the green zone are considered ideal for synthesizing AuNPs.

In the graphs it is possible to observe a more greenish region, indicating how the ideal values of each factor are to be used in the synthesis of this biocomposite. Table 19 presents a summary of the values of each factor considered ideal in the synthesis of FucoPol/AuNP.

Table 19. The value ranges considered ideal for synthesizing FucoPol/AuNP biocomposite

Temperature (ºC)	Time (min)	pH	[Au]
80 - 100	330 - 360	5.0 – 5.5	0.9 – 1.0

Therefore, to prepare the FucoPol/AuNP biocomposite it will be necessary to choose values for each factor that are within the ranges presented.

3.3.2.3. Selection of conditions for biocomposites synthesis

Among the various values tested for each factor, for the different EPSs, those that showed the best results were chosen. Table 20 shows the values chosen for each factor to synthesize AuNPs.

Table 20. Selected values of each factor to synthesize AuNPs.

NPs	T (ºC)	pH	Time (min)	[Au^{3+}] (mM)
EPS1/AuNP	100	5.21	370	1.2
EPS2/AuNP	100	5.19	370	1.2
EPS3/AuNP	120	4.68	20	1.2
EPS4/AuNP	90	4.92	370	1.2
FucoPol/AuNP	85	5.08	370	1.2

3.3.3. Selenium nanocomposites

3.3.3.1. Preliminary tests

In order to define the conditions, taking into account several factors such as temperature, time, pH, and Se^{4+} concentration, that lead to SeNPs formation, some preliminary tests (Table 21) were carried out, based on examples from the literature.

Table 21. Preliminary values used in the tests for the synthesis of SeNP.

	Factors			
Experiment	Temperature (ºC)	pH	Time (min)	[Se^{4+}] mM
1	Room temperature	~5.4	120	10
2	50	~ 5.4	360	2
3	80	9	5	5
4	35	~5.4	60	10

Zhang et al., (2004) described the process of synthesis of SeNPs in the presence of polysaccharides, using a concentration of Se^{+4} of 10 mM, at two different temperatures: at room temperature and 80°C. The reaction took place for 120 min and resulted in the synthesis of stable polysaccharide-SeNPs. The execution of tests for experiments 1 to 4 was based on this article, in order to know what values are normally used to synthesize SeNPs. In experiment 1, the conditions tested were similar to those described in the reference, except for the pH value, which corresponds to the pH of the original EPS solutions (~ 5.4). As for experiments 2, 3 and 4, one or another factor was similar to the reference, but in general different conditions were tested to see how the synthesis of SeNPs took place. To confirm under what conditions SeNPs were formed, control samples were prepared under the same conditions, using deionized water, without EPS. Control samples remained colorless, and a color change (pale yellow) occurred under some conditions. Table 22, it is possible to see the results of the synthesis of SeNPs, which was confirmed by UV-vis spectra (Figure 11), where it is possible to observe spectra with SPR bands characteristic of SeNP formation (Figure 11A), and a spectrum where SeNPs do not form (Figure 11B).

Table 22. Results obtained from preliminary tests for each EPS. For each EPS, suspensions containing EPS and Se^{4+} (image on the right) and control samples (images on the left) are shown.

Experiment	EPS1	EPS2	EPS3	EPS4	FucoPol
1	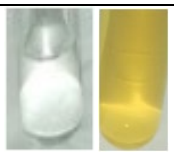	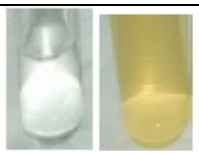	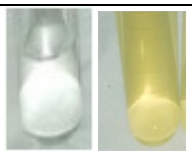		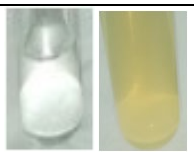
2					
3					
4					

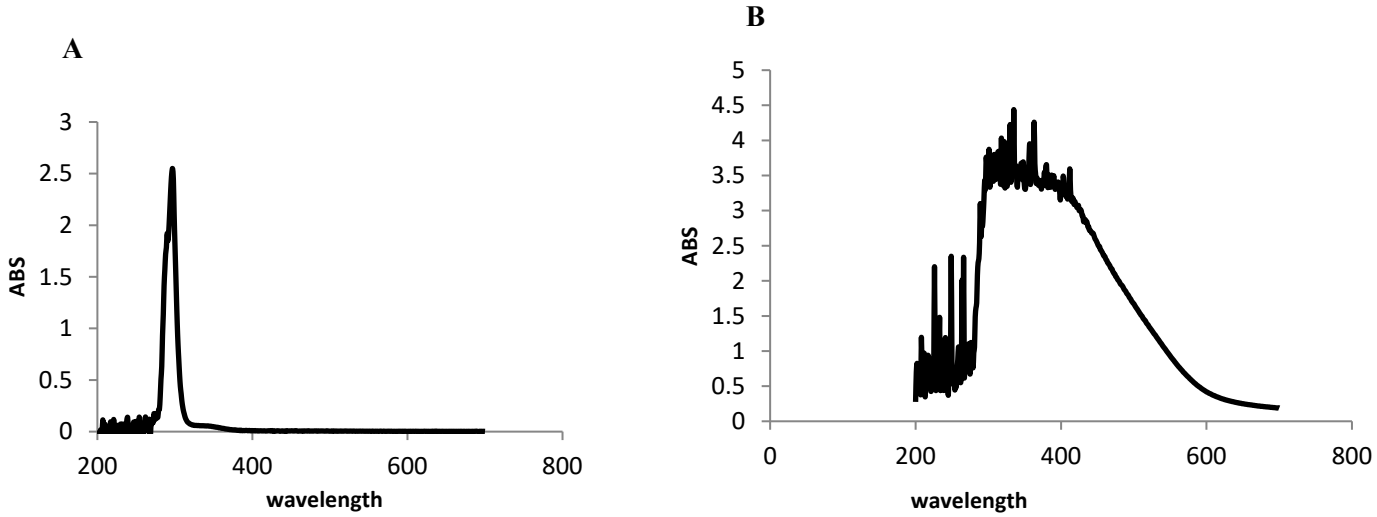

Figure 11. Examples of spectra with the SPR band characteristic of SeNPs (A) and spectra that do not correspond to the synthesis of SeNPs (B).

According to the results presented, it is possible to verify by the color of the suspensions that, under some conditions tested, result in the synthesis of SeNPs (room temperature and 35 °C, pH ~5.4, time 120 min and 60 min, Se^{+4} concentration 10 mM). In these experiments, the control remained colorless (images on the left), while suspensions with different shades of orange / pale yellow (images on the right) indicate synthesis of SeNP.

3.3.3.2. Synthesis optimization

Preliminary tests were essential to define the ranges of values to be used for each factor (temperature, pH, time, and Se concentration) (Table 23), to synthesize stable SeNPs. Design Expert was used to generate an experience matrix, which generated a set of values to be tested, with a total of 24 experiments, 8 of which are central points, thus being able to evaluate the impact of different factors in the synthesis of SeNPs and, in the end, determine the ideal conditions. With the experiments matrix, it was possible to perform experiments, combining values of the different factors. This combination of values was evaluated by visual inspection, changing the colors of the samples (from colorless to pale yellow), which were confirmed by the UV-vis absorption spectra, which presented a characteristic SPR of Se. For each spectrum, the response generated (Table 24) was calculated by combining the factors for each synthesized biocomposite.

Table 23. Values range defined for each factor in the preparation of SeNP.

Factors	Low level (-1)	Central point (0)	Higth level (+1)
Temperature (ºC)	20	35	50
pH	6	8	10
Time	5	122.5	240
[Se^{4+}]	2	6	10

For the test optimization process, for the SeNPs, the response was calculated using equation (3) described in the materials and methods. The Design Expert was used to generate the experience matrix, which after performing the tests it was possible to obtain the answer for each set of factors (Table 24). According to the responses, it was possible to perceive the impact of each factor on the synthesis of SeNP.

Table 24. Conditions were tested for the synthesis of SeNP with different EPSs and their responses.

	Factors				Responses ψ				
Run	Time (min)	T (ºC)	pH	[Se]	**EPS1**	**EPS2**	**EPS3**	**EPS4**	**FucoPol**
1	5	20	6	2	0.0	0.0	0.0	0.0	2.7×10^{-4}
2	5	20	10	10	5.0×10^{-4}	0.0	0.0	0.0	4.7×10^{-4}
3	5	50	6	10	4.6×10^{-4}	4.9×10^{-4}	5.2×10^{-4}	0.0	1.6×10^{-4}
4	5	50	10	2	0.0	0.0	0.0	0.0	2.0×10^{-4}
5	240	20	6	10	4.7×10^{-4}	4.9×10^{-4}	5.4×10^{-4}	4.8×10^{-4}	3.0×10^{-4}
6	240	20	10	2	0.0	0.0	0.0	0.0	1.7×10^{-4}
7	240	50	6	2	0.0	0.0	0.0	0.0	0.0
8	240	50	10	10	0.0	0.0	0.0	0.0	1.7×10^{-4}
9 (C)	122.5	35	8	6	4.8×10^{-4}	5.2×10^{-4}	5.4×10^{-4}	0.0	6.3×10^{-4}
10(C)	122.5	35	8	6	5.2×10^{-4}	5.3×10^{-5}	5.2×10^{-4}	0.0	2.3×10^{-4}
11(C)	122.5	35	8	6	4.8×10^{-4}	5.2×10^{-4}	4.9×10^{-4}	0.0	8.7×10^{-4}
12(C)	122.5	35	8	6	4.8×10^{-4}	5.0×10^{-4}	4.8×10^{-4}	0.0	2.9×10^{-4}
13	5	20	6	2	0.0	0.0	0.0	0.0	2.5×10^{-4}
14	5	20	10	10	4.9×10^{-4}	0.0	0.0	0.0	4.6×10^{-4}
15	5	50	6	10	0.0	5.0×10^{-4}	5.7×10^{-4}	0.0	3.4×10^{-4}
16	5	50	10	2	0.0	0.0	0.0	0.0	1.9×10^{-4}
17	240	20	6	10	4.7×10^{-4}	5.0×10^{-4}	5.0×10^{-4}	5.0×10^{-4}	2.9×10^{-4}
18	240	20	10	2	0.0	0.0	0.0	0.0	2.6×10^{-4}
19	240	50	6	2	0.0	0.0	0.0	0.0	0.0
20	240	50	10	10	0.0	0.0	0.0	0.0	1.6×10^{-4}
21(C)	122.5	35	8	6	5.2×10^{-4}	5.1×10^{-4}	5.0×10^{-4}	0.0	3.1×10^{-4}
22(C)	122.5	35	8	6	4.4×10^{-4}	5.1×10^{-4}	4.7×10^{-4}	0.0	3.1×10^{-4}
23(C)	122.5	35	8	6	4.9×10^{-4}	5.3×10^{-4}	4.7×10^{-4}	0.0	3.2×10^{-4}
24(C)	122.5	35	8	6	4.9×10^{-4}	4.9×10^{-4}	4.7×10^{-4}	0.0	4.1×10^{-4}

The results show that for a pH equal to 10 and a concentration of Se^{4+} of 2 mM the responses were practically all zero, for both biocomposites. For the EPS4/SeNP biocomposite, most of the responses were equal to zero, except in the conditions where the solution was used with a pH equal to 6, at 20 ºC, and with a concentration of Se^{4+} of 10 mM. The responses also show that, in general, that using 2 mM Se^{+4} concentrations and pH 10 solutions, SeNPs do not normally

form. The statistical analysis (ANOVA), allowed identifying which factors were significant and which had an impact on the synthesis of stable SeNPs.

For the synthesis of the EPS1/SeNP biocomposite, the statistical analysis (Table S6 in the appendix), demonstrated that only the pH and Se^{4+} concentration factors were significant in the synthesis of this biocomposite. The combination of the time factor and the temperature has shown to have an impact on the synthesis of SeNPs, allowing determining the regions with the ideal values for their synthesis (Figure 12). The statistical analysis also showed that for this biocomposite the curvature was significant, lack of fit non-significant adjustment and $R^2 > 0.99$ (Table S6 in the appendix).

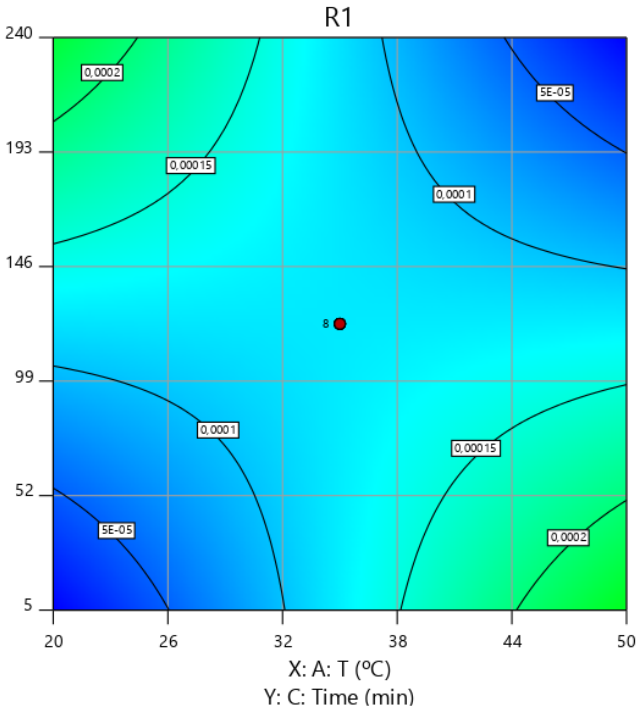

Figure 12. Contour plots of the SeNP desirability measure, mediated by EPS1, showing the interaction of two factors: temperature and time. Colors ranging from blue to green indicate the minimum and maximum values, respectively. The values closest to the green zone are considered ideal for the synthesis of SeNPs.

The range of values to be used for each factor in the synthesis of the EPS1/SeNP biocomposite, as illustrated in the graph, is summarized (Table 25). In this table, only the factors whose interactions were significant are shown.

Table 25. The value ranges considered ideal for synthesizing EPS1/SeNP biocomposite.

Temperature (ºC)	Time (min)
20-25	5-50

The results presented indicate the range of temperature and time values that can be used to synthesize SeNPs.

In the synthesis of the EPS2/ SeNP biocomposite, according to the statistical analysis (Table S7 in appendix), only factors such as the temperature and the Se concentration and the respective interaction between them were considered significant. The remaining factors (pH and time) showed a p-value > 0.05, so there was no significance in the synthesis of this biocomposite. This design showed significant curvature, non-significant lack of fit, and a value of $R^2 > 0.81$. Figure 13 shows the interaction between temperature and the Se concentration, at which it is possible to determine the range of values considered ideal to synthesize this biocomposite.

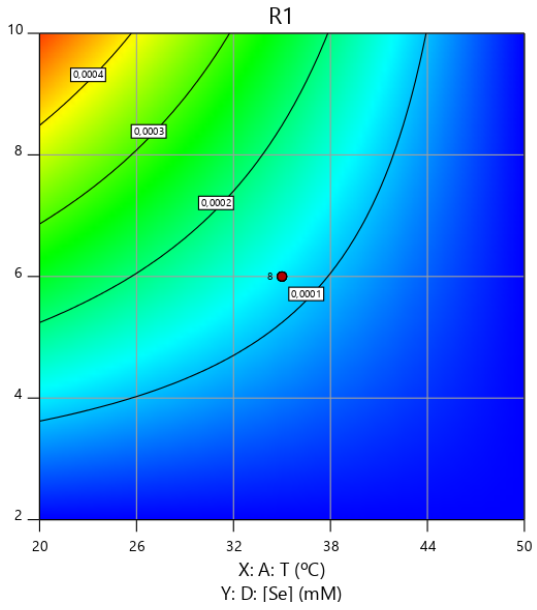

Figure 13. Contour plots of the SeNP desirability measure, mediated by EPS2, showing the interaction of two factors: temperature and Se concentration. Colors ranging from blue to red indicate the minimum and maximum values, respectively. The values closest to the red zone are considered ideal for the synthesis of SeNPs.

The range of values to be used for each factor or interaction of factors considered significant in the synthesis of the EPS2/SeNP biocomposite, as shown in the graph, is summarized (Table

26). In this table, only the factors whose interactions were significant, as shown displayed on the graph.

Table 26. The value ranges considered ideal for synthesizing EPS2/SeNP biocomposite.

Temperature (ºC)	[Se] (mM)
20-26	9.0-10

The results presented indicate the range of temperature and Se concentration values that can be used to synthesize SeNPs.

An ANOVA statistical analysis for the EPS3/SeNP biocomposite (Table S8 in appendix), showed that not all factors were significant. As in the synthesis of the EPS2/SeNP biocomposite, in the synthesis of this biocomposite, only factors such as temperature and Se concentration, as well as the interaction of these factors were considered significant in the synthesis of the biocomposite. In this design, the curvature was significant, the lack of fit appeared to be non-significant and showed an $R^2 > 0.99$. Figure 14 presents a graph of the interaction of temperature with the concentration of Se, to which it is possible to identify the region with the ideal values to synthesize the EPS3/SeNPs biocomposite.

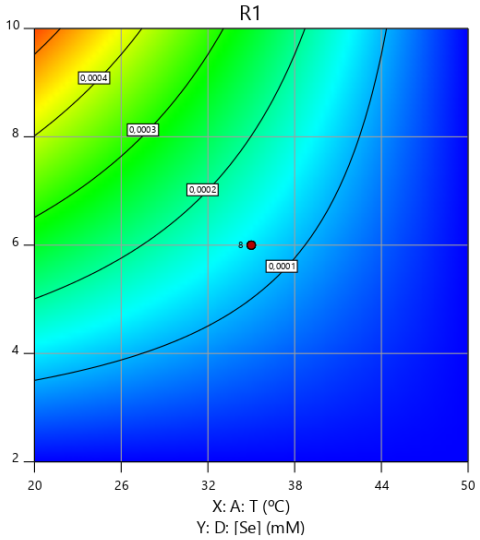

Figure 14. Contour plots of the SeNP desirability measure, mediated by EPS3, showing the interaction of two factors: temperature and Se concentration. Colors ranging from blue to red indicate the minimum and maximum values, respectively. The values closest to the red zone are considered ideal for the synthesis of SeNPs.

The range of values to be used for each factor or interaction of factors considered significant in the synthesis of the EPS3/SeNP biocomposite, as shown in the graph, is summarized (Table

27). In this table, only the factors whose interactions were significant, as shown displayed on the graph.

Table 27. The value ranges considered ideal for synthesizing EPS3/SeNP biocomposite.

Temperature (°C)	[Se]
20-23	9.6 - 10

The results presented indicate the range of temperature and Se concentration values that can be used to synthesize the EPS3/SeNPs biocomposite.

In the synthesis of the EPS4/SeNP biocomposite, according to the statistical analysis (Table S9 in appendix), all factors (time, pH, temperature, and Se concentration) appeared to be significant in the synthesis of the biocomposite, in addition to all interactions between the factors be significant as well. This design showed significant curvature, non-significant lack of fit, and a value of $R^2 > 0.99$. Figure 15 shows the interaction between the different factors, in which it is possible to determine the range of values for each factor considered ideal for synthesizing the EPS4/SeNP biocomposite.

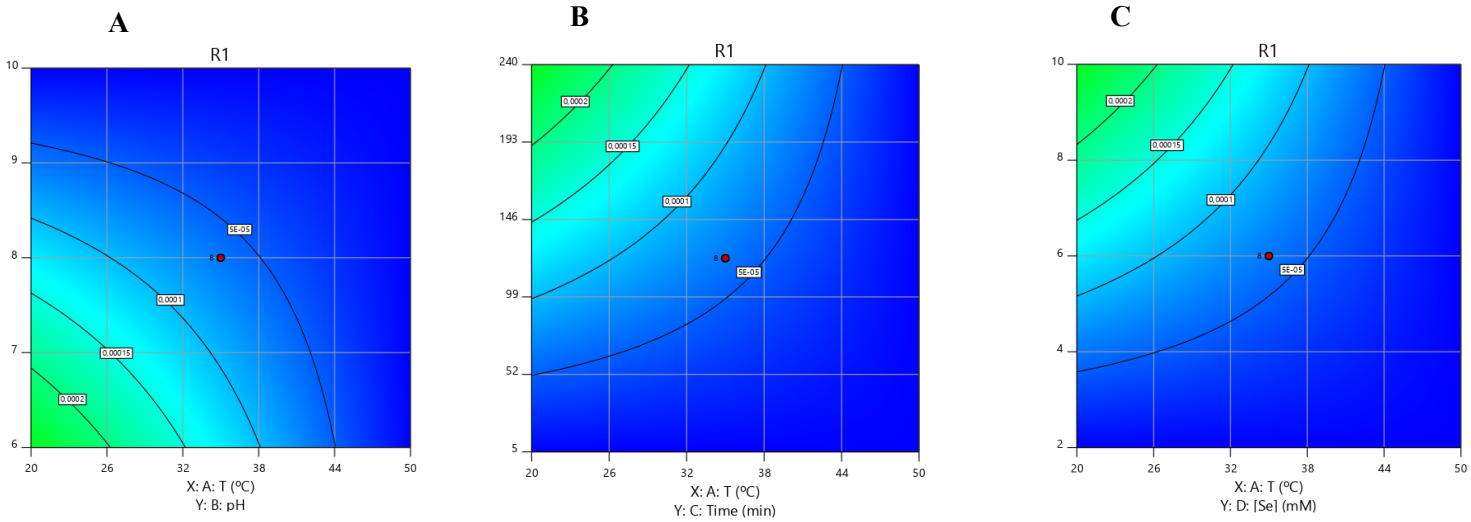

Figure 15. Contour plots of the SeNP desirability measure, mediated by EPS4, under various conditions: A (pH and temperature), B (time and temperature), and C (Se concentration and temperature). The colors ranging from blue to green indicate the minimum and maximum values. The values that are closest to the green zone are considered ideal for synthesizing SeNPs.

The range of values to be used for each factor or interaction of factors considered significant in the synthesis of the EPS4/SeNP biocomposite, as shown in the graph, is summarized (Table 28).

Table 28. The value ranges considered ideal for synthesizing EPS4/SeNP biocomposite.

Temperature (ºC)	Time (min)	pH	[Se] (mM)
20-26	190 - 240	6.0 – 6.8	8.3 - 10

The results presented indicate the range of values for each factor to be used in order to synthesize a stable biocomposite.

Finally, in the synthesis of the FucoPol/SeNP biocomposite, the statistical analysis (Table S10 in the appendix) showed that only the Se concentration was significant. The other factors (time, pH, and temperature) had a p-value > 0.05, which means that they were not significant in the synthesis of this biocomposite. Although only the Se concentration is significant, the design showed significant curvature, lack of fit significant adjustment, and a value of $R^2 > 0.59$, thus making the model invalid. Therefore, to assess the impact of factors on the synthesis of this biocomposite, it would be necessary to resort to a new model.

3.3.3.3. Selection of conditions for biocomposites synthesis

Among the various values tested for each factor, for the different EPSs, those that showed the best results were chosen. Table 29 shows the values chosen for each factor to synthesize SeNPs.

Table 29. Selected values of each factor to synthesize SeNPs.

NPs	T (ºC)	pH	Time (min)	$[Se^{4+}]$ (mM)
EPS1/SeNP	T.amb.	8.38	120	10
EPS2/SeNP	T.amb.	6.6	120	10
EPS3/SeNP	T.amb.	6.48	120	10
EPS4/SeNP	T.amb.	5.61	240	10
FucoPol/SeNP	T.amb.	8.37	120	10

3.4. Preparation of EPS-NPs nanocomposites.

The preparation of the biocomposites was carried out under the conditions determined in the previous sections. In the case of AgNP, the preparation conditions were selected based on the results of the preliminary experiments, while for AuNPs and SeNPs, synthesis was carried out based on the optimization experiments, and for each factor, a value was chosen within the range considered optimal.

3.4.1. Preparation of EPS-AgNPs nanocomposites

The synthesis of AgNP was performed by reducing Ag^{+} to Ag^{0}, using distilled water as a solvent. The Ag^{+} concentration used was 11 mM for all tested EPSs. All biocomposites were incubated for 380 min. What differentiated in the preparation of the different biocomposites was the incubation temperature and pH. For the biocomposites EPS1/AgNP and EPS2/AgNP, the incubation temperature was 80 ºC for both, while the pH was 8.81 and 9.16 respectively, while for the biocomposites EPS3/AgNP, EPS4/AgNP, and FucoPol/AgNP, the incubation temperature was 85 ºC for both and the pH value was 9.2, 9.38 and 8.96, respectively. It is important to note that the pH was adjusted before adding the Ag^{+} solution to the EPS solution. At the end of the incubation, in addition to the visual inspection that allowed to detect the color change from colorless to yellowish, the formation of AgNP was also confirmed by the UV-vis absorption spectrum (Figure 16), at a wavelength range of 200-700 nm, where it was possible to observe a characteristic SPR band of each biocomposite. According to Figure 16, it is possible to see a strong peak at around 450 nm, due to the reduction of ionic silver (Ag^{+}) to elemental silver (Ag^{0}). There are also differences in the bandwidth of each biocomposite, and this is due to the variation in size, morphology, and stability of the AgNPs (Rasulov et al., 2016).

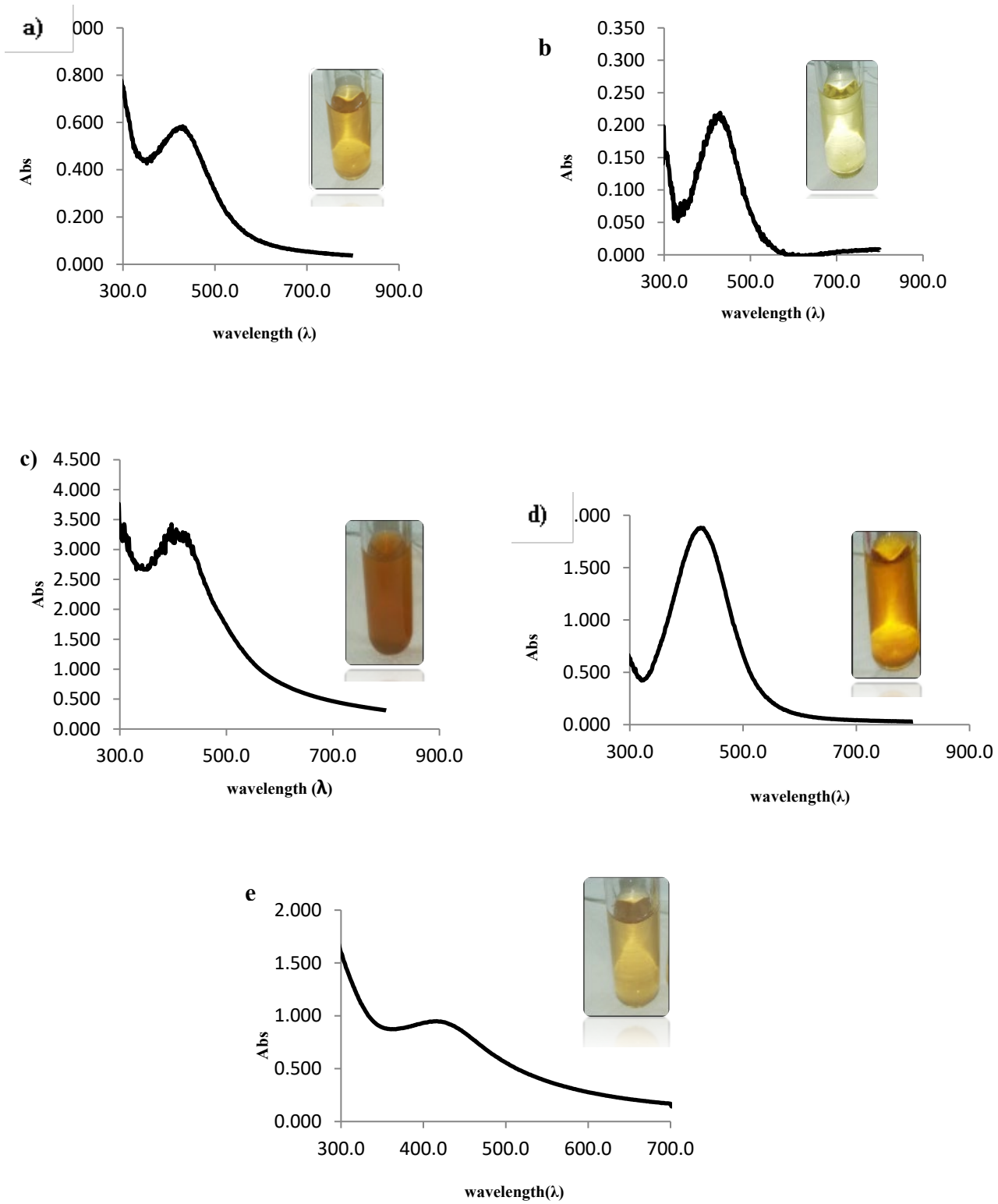

Figure 16. UV-vis absorption spectra and respective EPSs/Ag^{+} biocomposite suspensions. EPS1/AgNP (a), EPS2/AgNP (b), EPS3/AgNP (c), EPS4/AgNP (d) and FucoPol/AgNP (e).

3.4.2. Preparation of EPS-AuNPs biocomposites

For the preparation of EPS/AuNP biocomposites, the results of the RSM analysis of the interaction of the different factors that determined the ranges of optimal values for the preparation of biocomposites were used. AuNP was synthesized by reducing Au^{3+} to Au, using distilled water as a solvent. The samples were obtained at an Au^{3+} concentration of 1.2 mM for all EPSs. The pH values of the EPS solutions were adjusted to around 5 (i.e., 5.21, 5.19, 4.68, 4.92, and 5.08 corresponding to EPS1, EPS2, EPS3, EPS4, and FucoPol, respectively). The samples containing the EPS solution with Au^{3+} were incubated at different temperatures, namely, 120 ºC for the EPS3/AuNP biocomposite, 100 ºC for the biocomposites EPS1/AuNP and EPS2/AuNP, 90 ºC for the EPS4/AuNP and 85 ºC for the FucoPol/ AuNP. A reaction time of 370 min, was used for preparing all biocomposites, except for the EPS3/AuNP for which na incubation time of 20 min was used. At the end of the incubation, a color change of the solution was observed, which changed from colorless to purple (Figure 17), indicating the formation of AuNP. Such observations were confirmed by the UV-vis absorption spectrum (Figure 17), where the spectra show the SPR band characteristic of each biocomposite. In these spectra, it is possible to observe a strong peak at 530 nm, characteristic of the metallic Au. According to Philip, (2010), an SPS band with a peak around 540 nm is indicative of almost spherical NPs. However, there is a certain variation in the position of the SPR band in the UV-vis spectrum, and this is because the SPR band is sensitive to the size of the particles, the shape, the refractive index, and also the interaction of the particles with the medium (Aswathy Aromal & Philip, 2012).

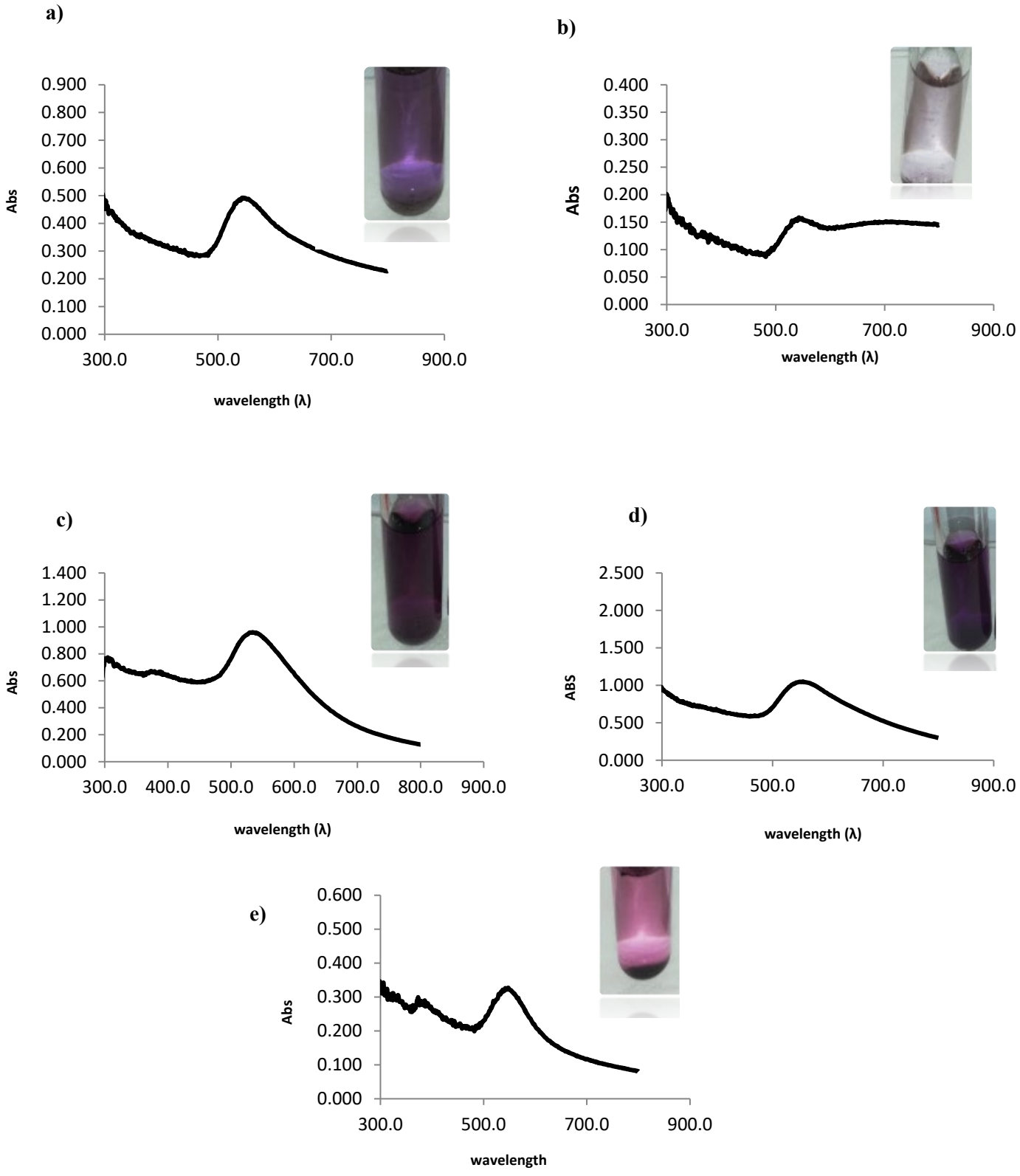

Figure 17. UV-vis absorption spectra and respective EPSs/Au biocomposites suspensions. EPS1/Au (a), EPS2 /Au(b), EPS3/Au (c), EPS4/Au (d) and FucoPol/Au (e).

3.4.3. Prepartion of EPS-SeNPs biocomposites

The preparation of EPS/SeNP biocomposites was carried out by reducing the precursor SeO_3^{2-} to elemental selenium (Se^0) (Yan et al., 2018), using distilled water as a solvent, in the presence of $C_6H_8O_6$ and EPSs. EPS solutions were adjusted to pH values indicated for each, being 8.38, 6.6, 6.48, 5.61, and 8.37, for EPS1, EPS2, EPS3, EPS4, and FucoPol, respectively. The samples were obtained at a concentration of 10 mM Se and 5 mM $C_6H_8O_6$ and incubated at room temperature (~ 25ºC) protected from light. They were incubated for a period of 120 minutes, except the EPS4/SeNP biocomposite, which remained for 240 min. The SeNP formation process was monitored by visual inspection, detecting a color change from colorless to pale yellow-orange (Figure 18). Cai et al., (2018), indicating an amorphous or monoclinic appearance of the Se particles since the trigonal is known for presenting a black colored solution (Yan et al., 2018). The formation of SeNPs was confirmed by the UV-vis absorption spectra (Figure 18), where a characteristic band of each biocomposite appears, with a strong peak around 290 nm, although previous studies have reported the presence of a peak intense around 260 nm (Cai et al., 2018) and 265 nm (Yan et al., 2018). However, this change in resonance can be explained by the stability of the synthesized SeNPs, as well as by the size and morphology of the SeNP.

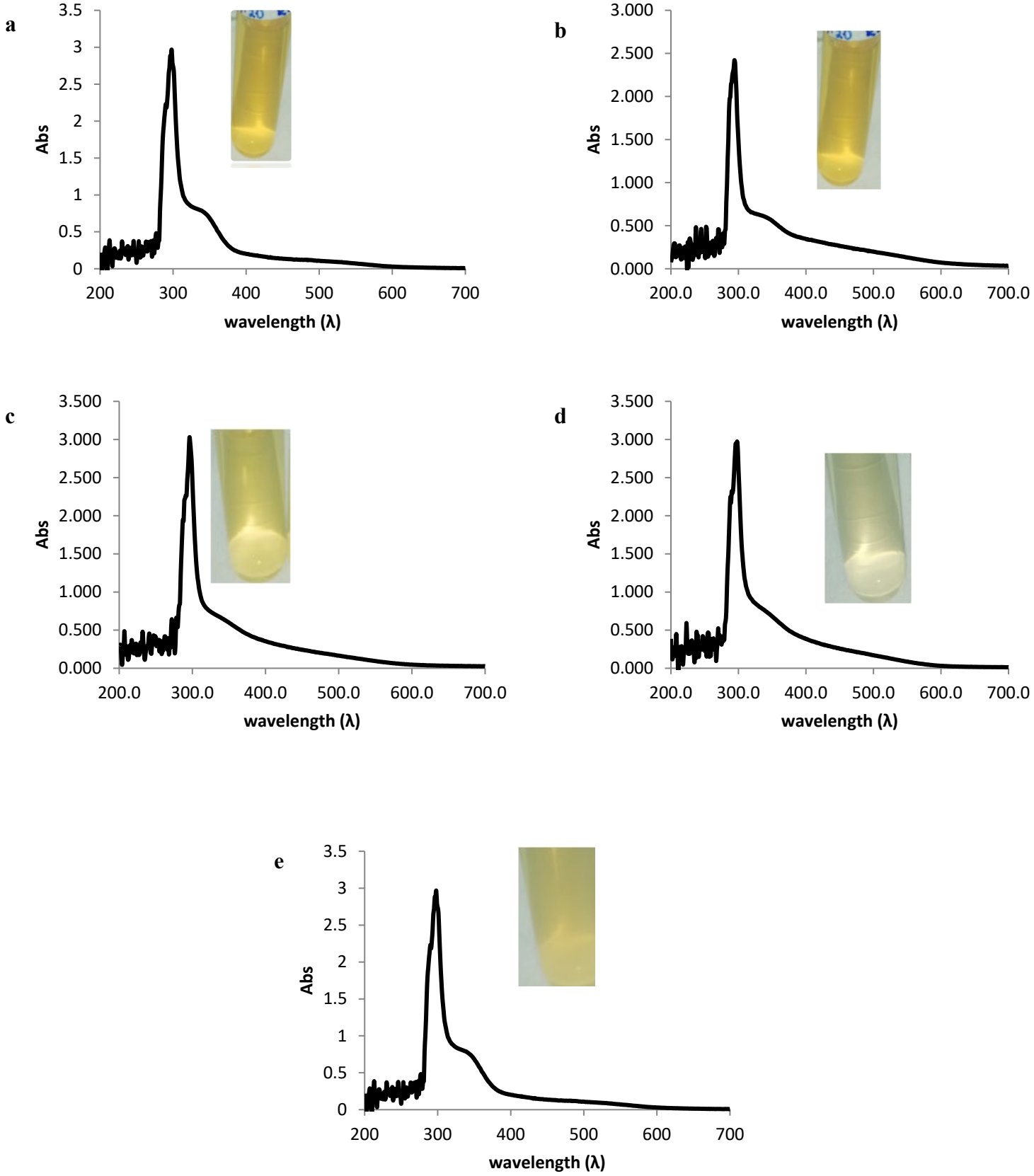

Figure 18. UV-vis absorption spectra and respective EPSs/Se biocomposites suspensions. EPS1/Se (a), EPS2/SeNP(b), EPS3/Au (c), EPS4/SeNP (d) and FucoPol/SeNP (e).

3.5. Bionanocomposites physical-chemical characterization

To evaluate the chemical properties of biocomposites, atomic emission spectroscopy (ICP), and infrared spectroscopy (FTIR) were used. The ICP analysis aimed to determine the amount of inorganic ion in the nanoparticle biocomposites (Table 30).

Table 30. Quantity of metal in EPSs/NPs biocomposites.

	Biocomposite name	Metal Concentration (mg/L)
AgNP	EPS1/AgNP	11.80
	EPS2/AgNP	3.69
	EPS3/AgNP	55.21
	EPS4/AgNP	9.84
	FucoPol/AgNP	3.22
AuNP	EPS1/AuNP	26.38
	EPS2/AuNP	4.10
	EPS3/AuNP	41.98
	EPS4/AuNP	31.53
	FucoPol/AuNP	39.85
SeNP	EPS1/SeNP	6.20
	EPS2/SeNP	8.31
	EPS3/SeNP	7.61
	EPS4/SeNP	1.06
	FucoPol/AgNP	2.72

Analyzing the table it is concluded that, for each set of biocomposites of each metal, even using the same conditions, the amount of metal present in the nanoparticles is different. For example, for the EPSs/AgNP biocomposites, in both syntheses, 11 mM Ag^{+} was used, however, the concentration of this metal is different in all biocomposites.

FTIR analysis was used to characterize the chemical surface of nanoparticles, that is, to detect possible ion reduction reactions and the establishment of Ag^{+}, Au^{3+}, and Se^{4+} and stabilization atoms in EPSs.

Figures 19-23 show the FTIR spectra of EPSs and EPSs/NPs biocomposites. The spectra are quite similar to each other, presenting bands characteristic of EPSs and respective biocomposites. Figures 19-23 (A) show the spectra corresponding to the EPSs alone. According to the results (Figure 19-23), it is possible to observe a slight change in most of the absorption peaks after the interaction of EPSs (Figure 19A-23A-dashed lines) with AgNP (Figure 19B-23B), AuNP (Figure 19C-23C) and SeNP (Figure 19D–23D). Both EPS spectra alone as well as biocomposites have a wide and intense band around 3300 cm^{-1}, which represents the O-H stretching of hydroxyl groups (Chen et al., 2016). At this peak, more significant changes were observed when comparing EPSs with biocomposites. This peak may be involved in links between EPSs with AgNP, AuNP, and SeNP. The peaks that appear to be around 2900 cm^{-1} may correspond to the C-H elongation of the CH_2 or CH_3 groups (Cai et al., 2018; Farinha et al., 2015). The peaks observed around 1700 cm^{-1} and 1030 cm^{-1}, may indicate the C = O stretch of the carbonyl fractions found in the acyl substituents and the C-O and C-C vibrations of the glycosidic bonds (D. Araújo et al., 2020). There is also a band around 1700/1600 cm^{-1} (marked in red), that can indicate the interaction -COO- of the EPS groups with AgNP, AuNP, and SeNP (Philip, 2010). Groups corresponding to hydroxyl, carboxyl, seem to have relevant importance in the interaction with metals, being found in uronic acids, acyls, among others.

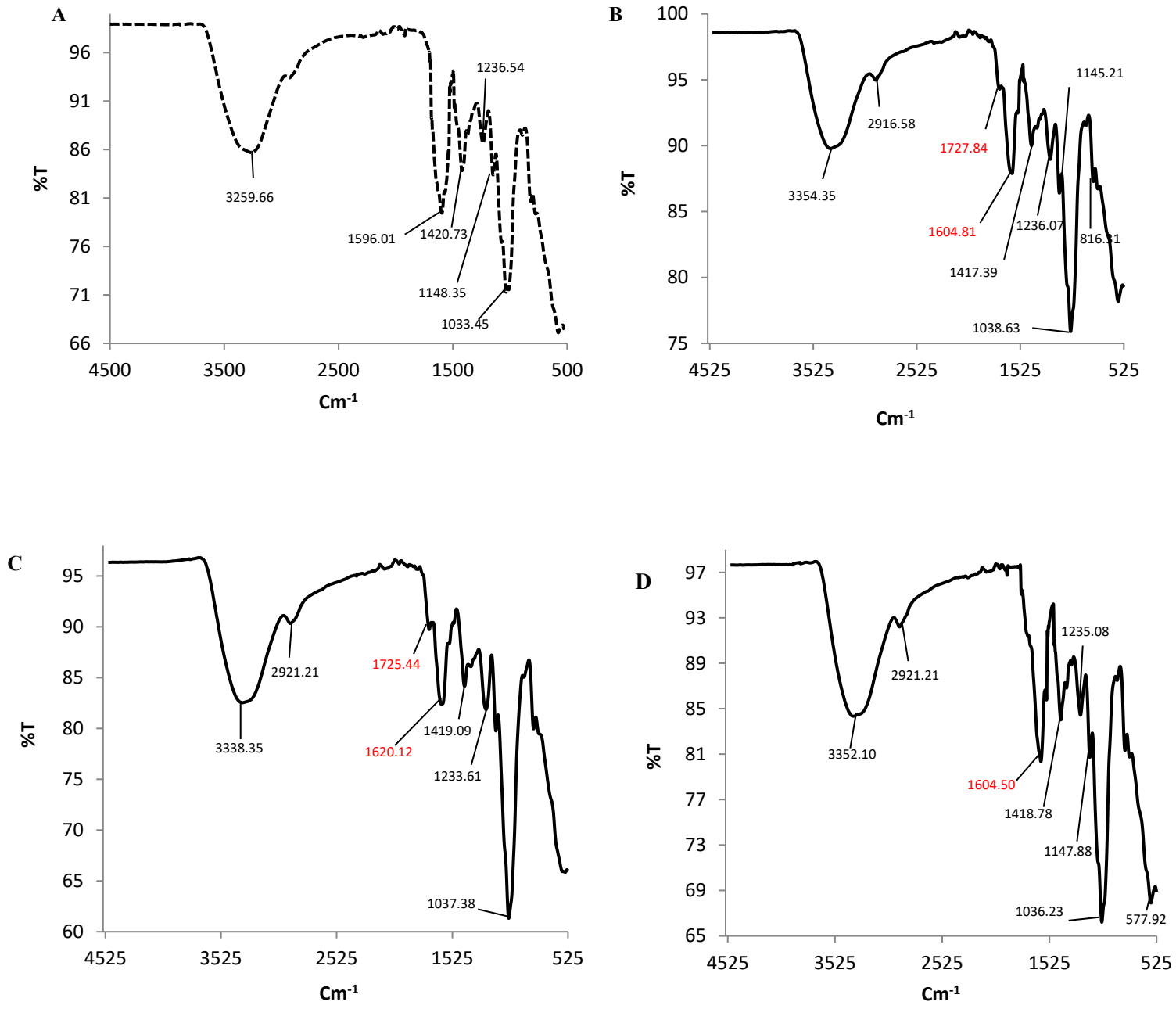

Figure 19. FTIR spectrum of EPS1 (A) and EPS1/AgNP(B), EPS1/AuNP (C) EPS1/SeNP (D) biocomposites.

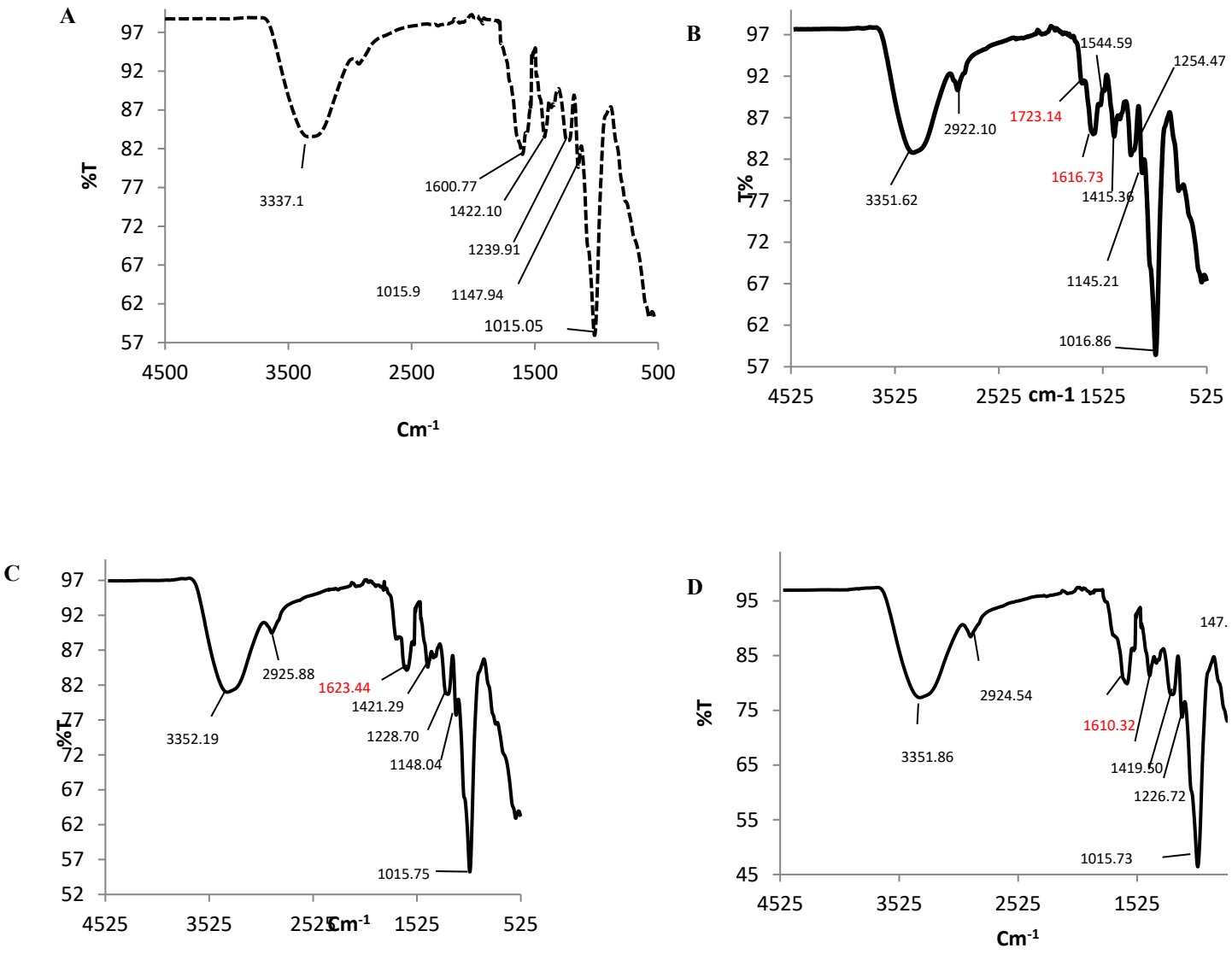

Figure 20. FTIR spectrum of EPS2 (A) and EPS2/AgNP(B), EPS2/AuNP (C) EPS2/SeNP (D), biocomposites.

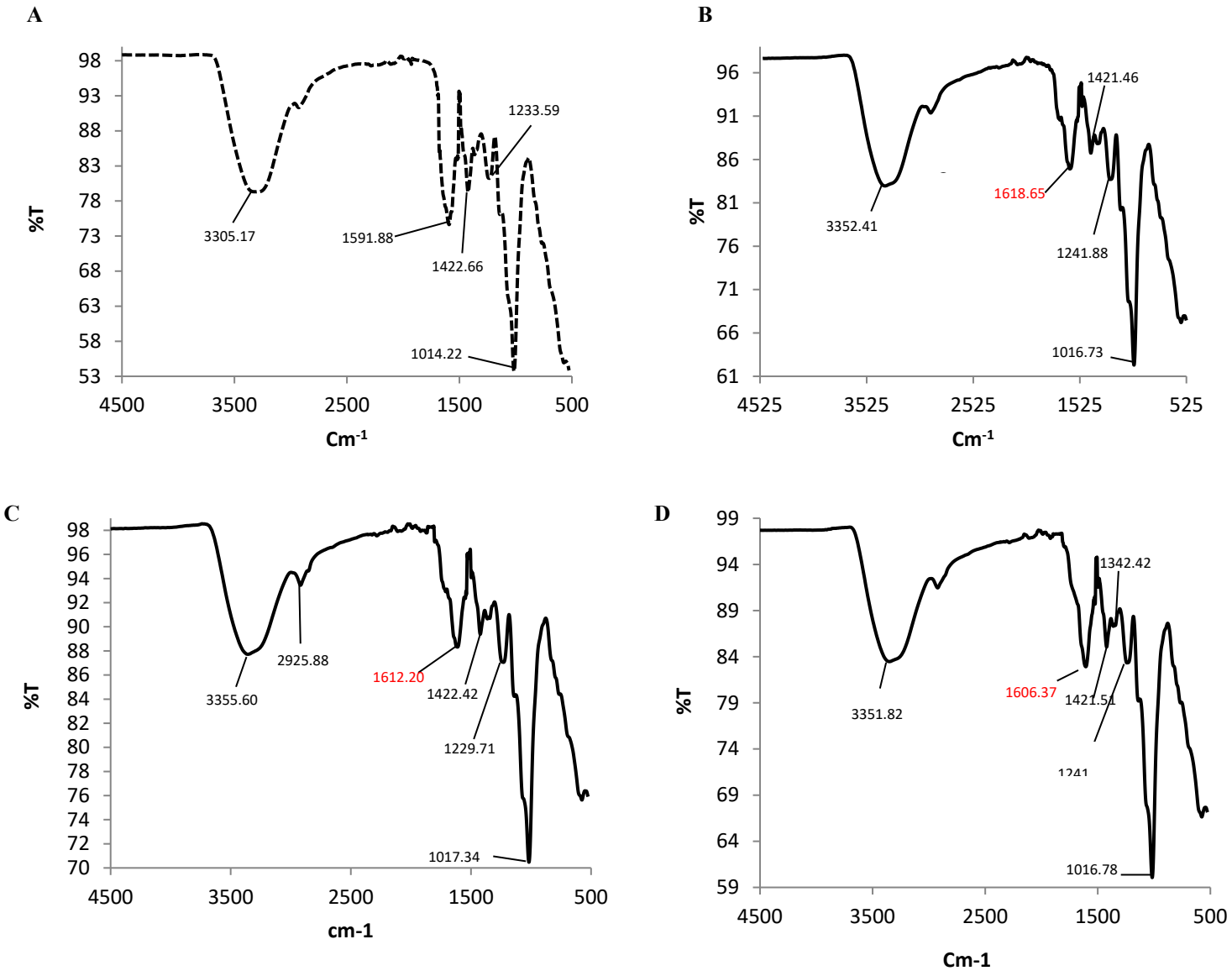

Figure 21. FTIR spectrum of EPS3 (A) and EPS3/AgNP(B), EPS3/AuNP (C) EPS3/SeNP (D), biocomposites.

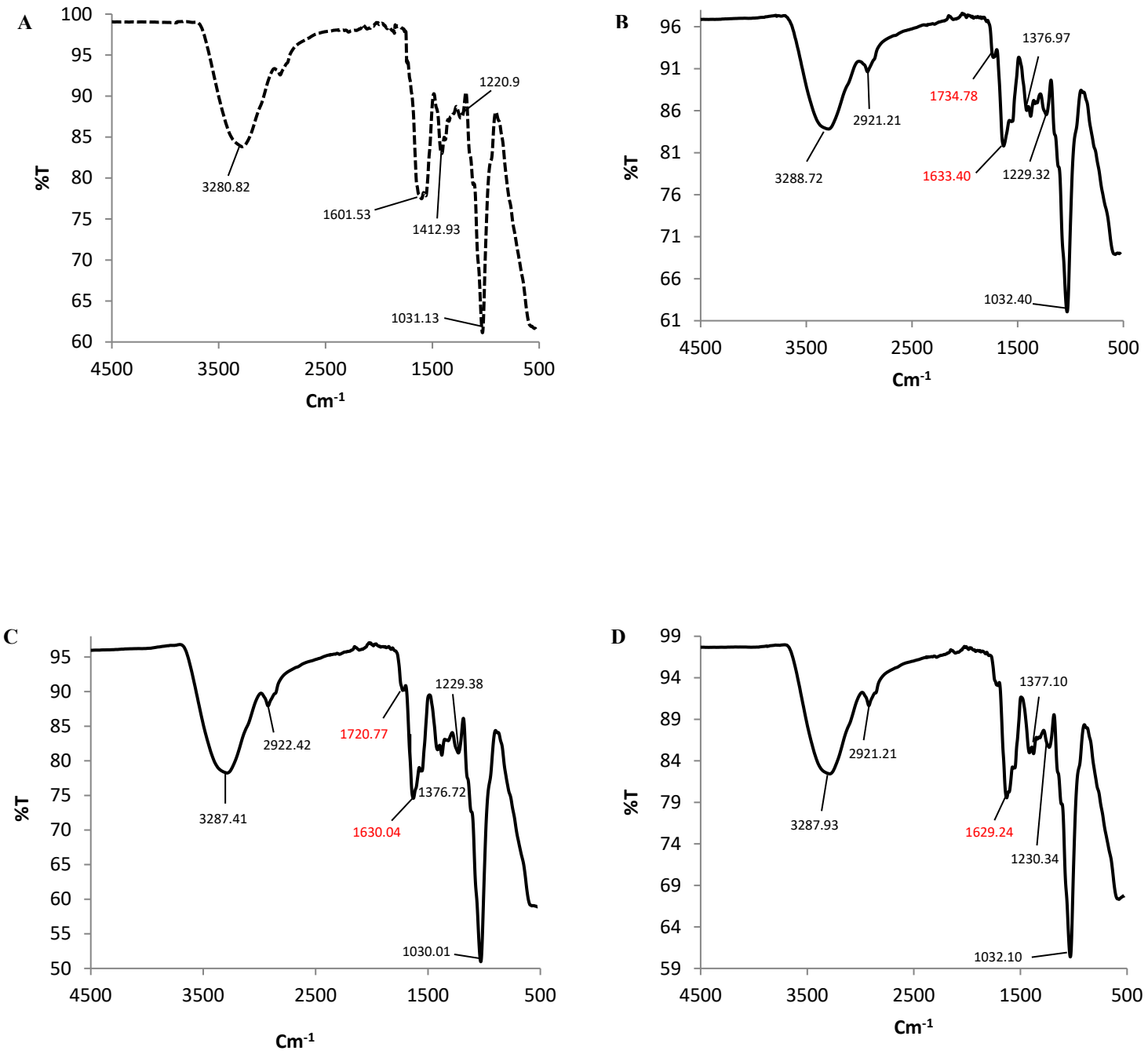

Figure 22. FTIR spectrum of EPS4 (A) and EPS4/AgNP(B), EPS4/AuNP (C) EPS4/SeNP (D), biocomposites.

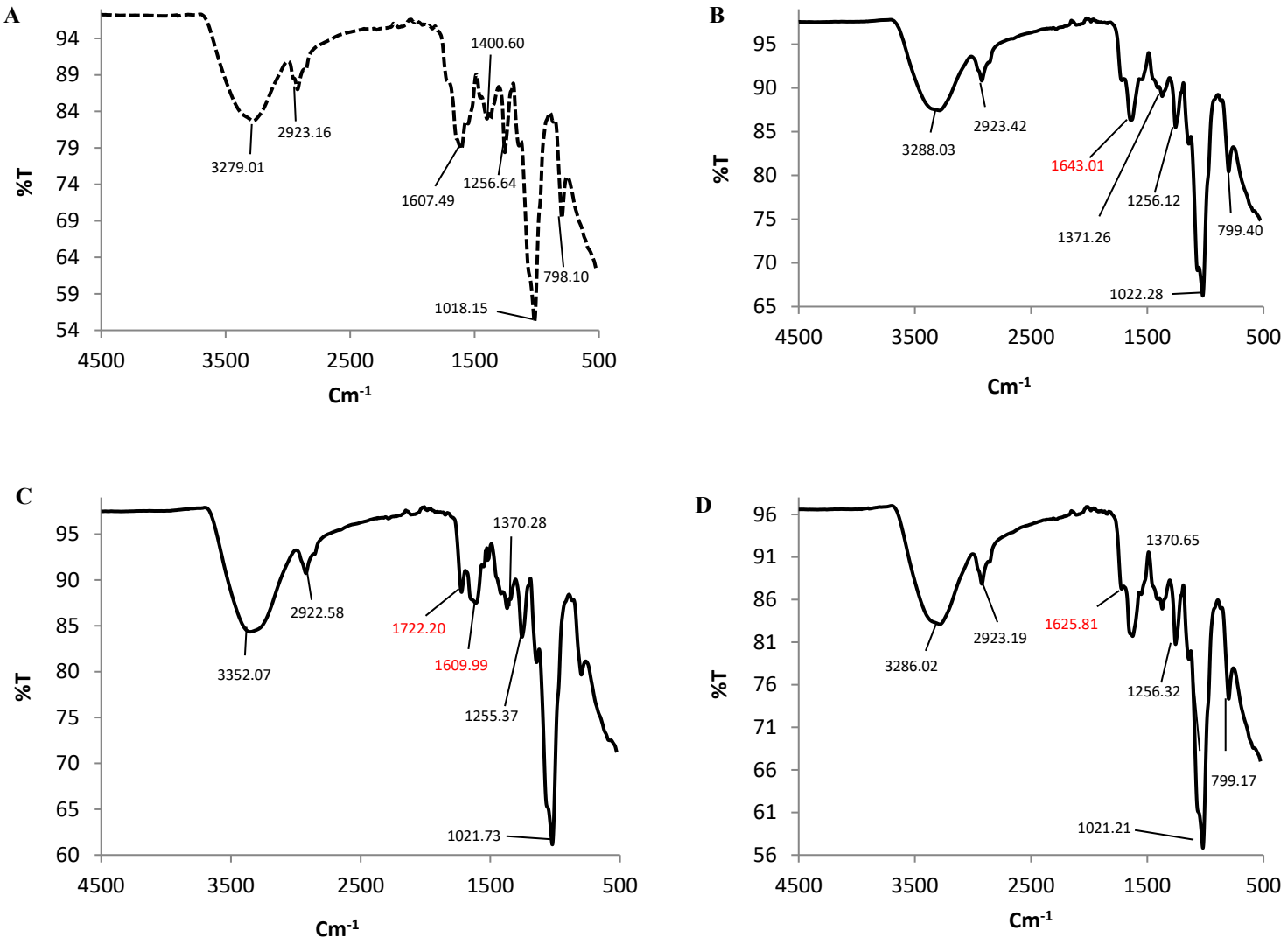

Figure 23. FTIR spectrum of FucoPol (A) and FucoPol /AgNP (B), FucoPol /AuNP (C), FucoPol /SeNP (D), biocomposites.

Despite the FTIR spectra presented, they belong to different elements, the bands show some similarity. That is, the absorption peaks of the different EPSs and biocomposites are not very far apart.

3.5.1. Themal characterization

Figures A1-A5 (a-d present in the appendix), shows the thermal degradation curves of EPSs and EPSs/NPs biocomposites. In general, in the TGA, decomposition in the range of 0 - 100 ºC, the peak is generally attributed to water evaporation; at peak around 300 ºC, degradation of the molecule's saccharide structure is attributed (Álvarez et al., 2014), and finally, the degradation around 400 -500 ºC, usually corresponds to the complete degradation of the

polymer (Álvarez et al., 2014). Table 31 shows the degradation curves corresponding to each EPS and each synthesized biocomposite.

Table 31. Degradation curves corresponding to each EPS and each synthesized biocomposite.

	First degradation curve (ºC)	Mass loss (%)	Second degradation curve (ºC)	Mass loss (%)	Third degradation curve (ºC)	Mass loss (%)
EPS1	33-193	19	194-489	40	_	_
EPS1/AgNP	34-164	13	163-493	50	_	_
EPS1/AuNP	34-164	12	164-493	49	_	_
EPS1/SeNP	34-172	15	172-491	48	_	_
EPS2	33-189	17	188-497	45	_	_
EPS2/AgNP	34-162	12	162-490	52	_	_
EPS2/AuNP	34-163	12	162-488	50	_	_
EPS2/SeNP	34-160	11	160-486	50	_	_
EPS3	34-183	18	184-490	44	_	_
EPS3/AgNP	34-162	9	161-488	51	_	_
EPS3/AuNP	34-141	8	140-485	51	_	_
EPS3/SeNP	36-169	10	169-489	50	_	_
EPS4	35-184	17	185-485	49	_	_
EPS4/AgNP	34-154	12	154-492	53	_	_
EPS4/AuNP	35-153	8	153-482	51	_	_
EPS4/SeNP	37-166	10	166-491	55	_	_
FucoPol	37-167	11	167-383	48	383-497	10
FucoPol/AgNP	34-162	9	162-483	62	_	_
FucoPol/AuNP	36-157	9	158-48	64	_	_
FucoPol/SeNP	33-161	13	163-496	62	_	_

Most EPSs and biocomposites showed two degradation curves, except FucoPol which presented three degradation curves. According to the results presented, the biocomposites formed by FucoPol (FucoPol/AgNP, FucoPol/AuNP and FucoPol/SeNP), showed the greatest loss of mass in the second degradation curve, around 60%, while, for the remaining biocomposites and EPSs, the percentage of mass in the second degradation curve was around 40% and 50%.

3.5.2. Crystallinity

As previously reported, XRD was used to determine the phase composition and crystalline structure of the polymers and nanoparticles under study. EPS1 (Figure 24A), its XRD pattern exhibited broadband at approximately 23º, which explains the amorphous nature of this polymer. Likewise, the EPS1/SeNP biocomposite (Figure 24D), also exhibited a large band around 21º, indicating that even with SeNP it continues with an amorphous structure, that is, no Bragg peak was exhibited. Meanwhile, the EPS1/AgNP biocomposite diffractogram (Figure 24B), exhibited a Bragg peak characteristic of metallic silver at 38.3 in the 2θ region, combining crystallographic planes of (111). The EPS1/AuNP biocomposite (Figure 24C) exhibited two Bragg peaks, characteristic of metallic gold at 38.3 and 44.5 in the 2θ region, combining crystallographic planes of (111) and (200). For both AgNP and AgNP, the observed diffraction peaks are reflections of a face-centered cubic structure (Aswathy Aromal & Philip, 2012; Sivakumar et al., 2017).

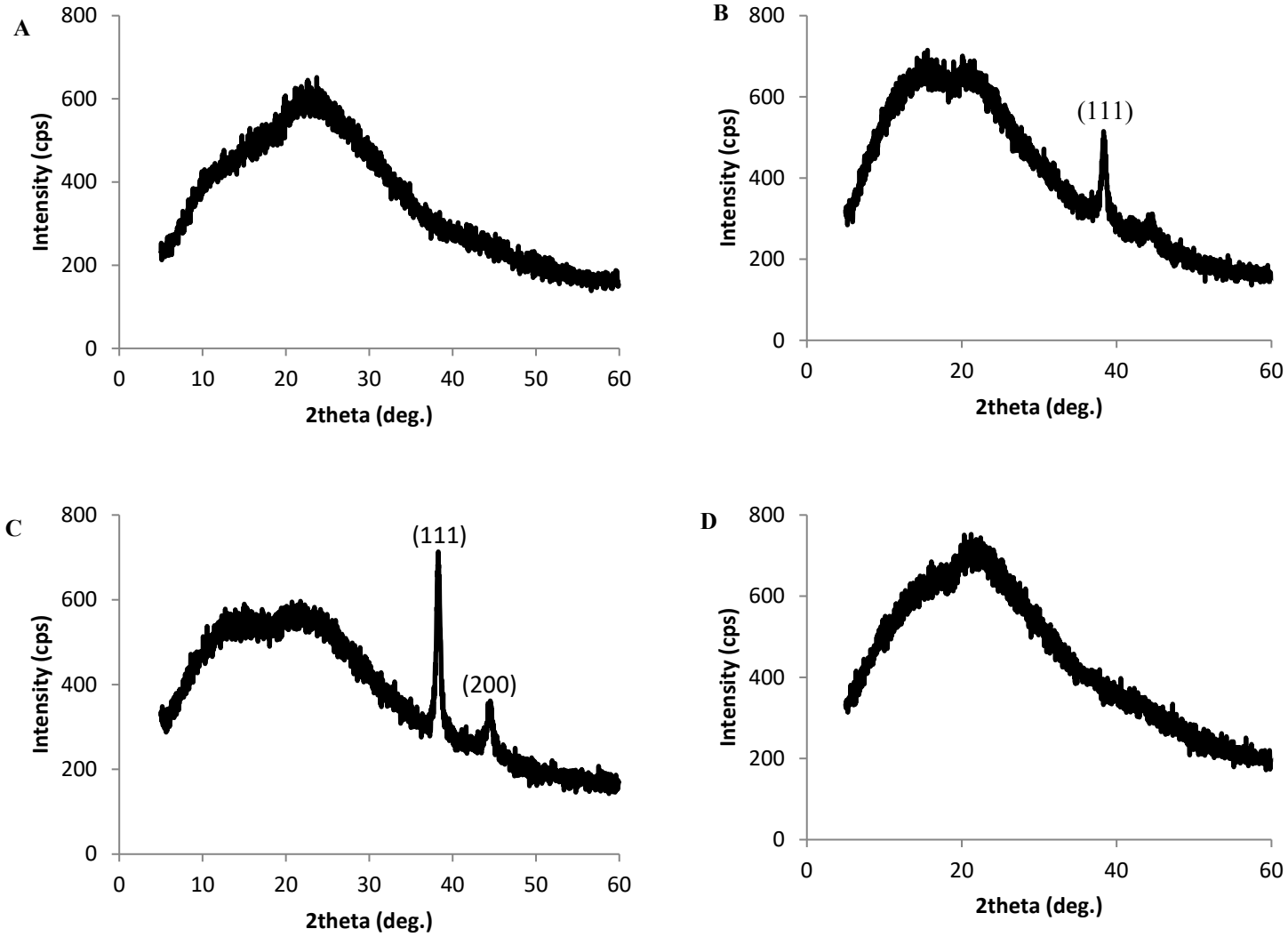

Figure 24. Diffractograms of EPS1 (A), EPS1/AgNP biocomposite (B), EPS1/AuNP biocomposite (C), and EPS1/SeNP biocomposite (D).

The EPS2 diffractogram (Figure 25A), as well as the EPS2/AgNP (Figure 25B) and EPS2/SeNP (Figure 25D) biocomposites, did not show any Bragg peak, indicating an amorphous morphology for these compounds or else it can be explained by the low adhesion of the nanoparticles, in the case of AgNP, since in the case above, it presents clear Bragg peaks, characteristic of a crystalline structure. In the case of the EPS2/SeNP biocomposite, it was reported by Cai et al., (2018), Se, normally presents two Bragg peaks in the 2θ region, on a 24º and 30º throne, indicating the presence of crystalline Se, but in the presence of EPSs, these characteristic peaks disappear completely, causing the SeNP to remain in an amorphous phase. In contrast, the EPS2/AuNP biocomposite (Figure 25C), exhibited a Bragg peak, around 38.2º, in the 2θ region, combining the crystallographic plane of (111).

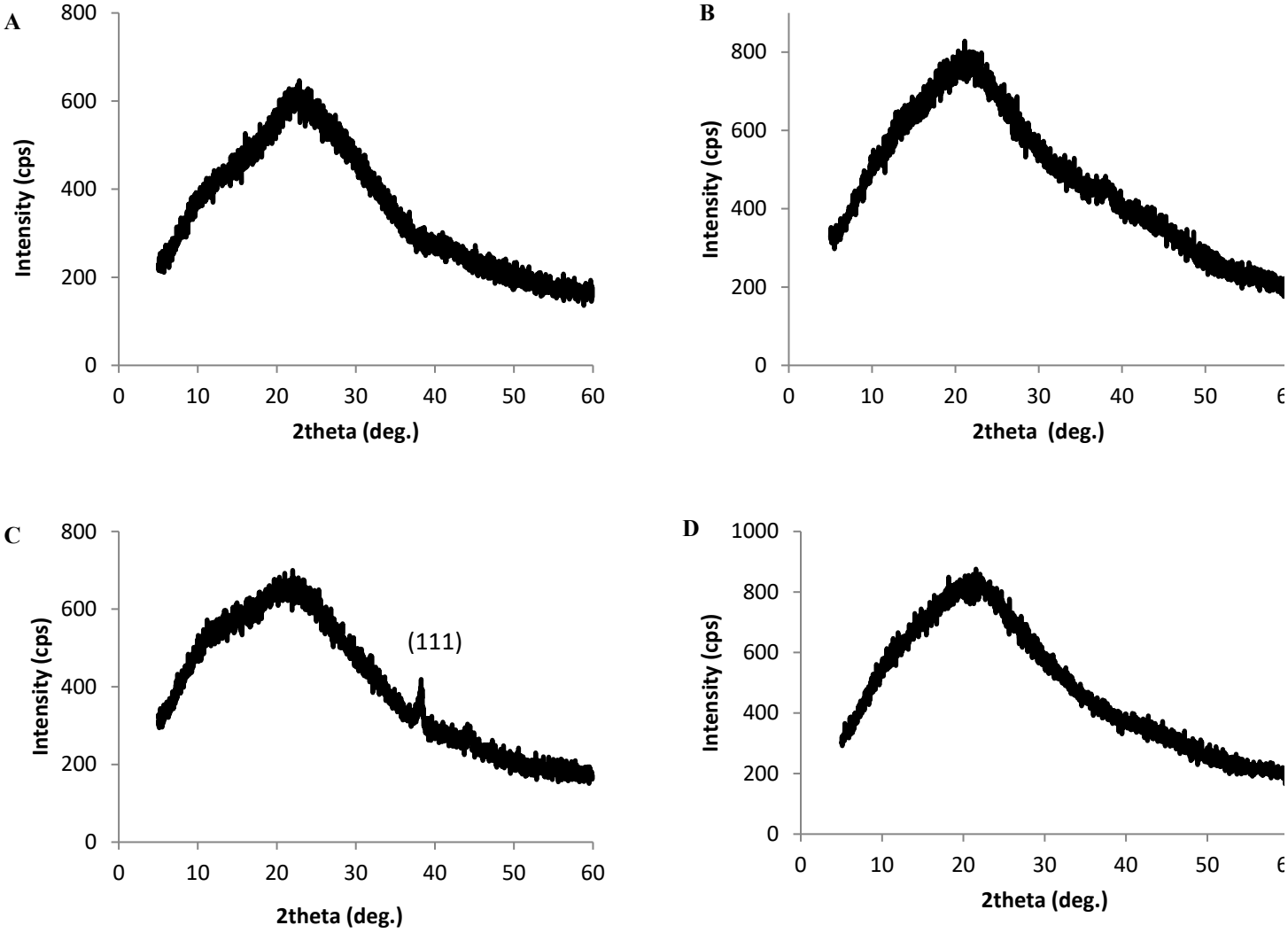

Figure 25. Diffractograms of EPS2 (A), EPS2/AgNP biocomposite (B), EPS2/AuNP biocomposite (C), and EPS2/SeNP biocomposite (D).

The XRD pattern of both, EPS3 (Figure 26A) and EPS3/SeNP biocomposite (Figure 26D), exhibited broadband around 24º and 21º, thus not having Bragg peaks. The EPS3/AgNP biocomposite (Figure 26B) exhibited Bragg peaks characteristic of metallic silver in 28, 32.5, 38.4, 46.4, 54.9, 55, 55.2, 55.5 and 57.7, in the region of 2θ. In addition to this, the EPS3/AuNP biocomposite (Figure 26C), also exhibited Bragg peaks at 38.2 and 44.4 in the 2θ region, corresponding to metallic gold.

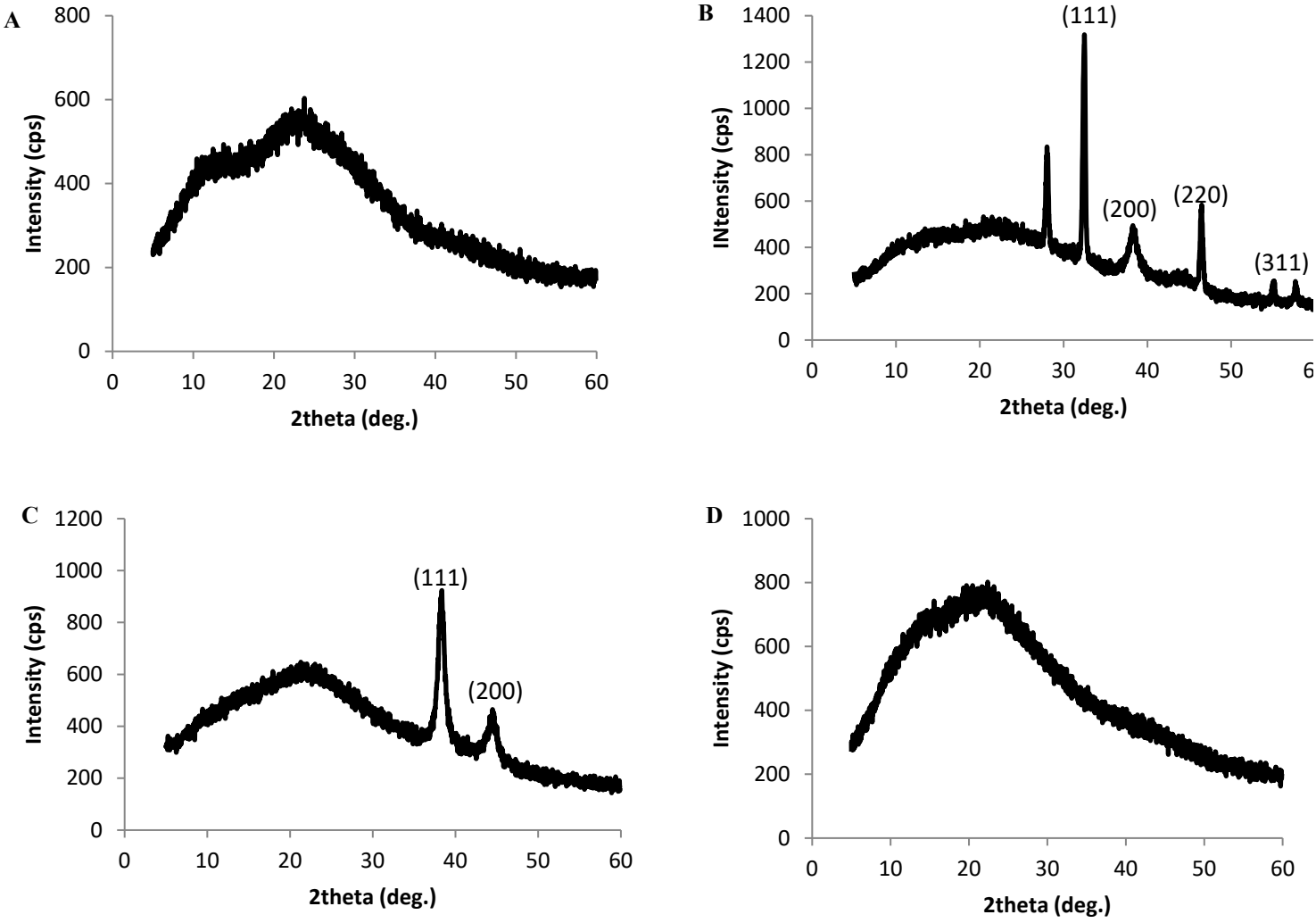

Figure 26. Diffractograms of EPS3 (A), EPS3/AgNP biocomposite (B), EPS3/AuNP biocomposite (C), and EPS3/SeNP biocomposite (D).

The EPS4 diffractogram (Figure 27A), as well as the EPS4/AgNP (Figure 27B) and EPS4/SeNP (Figure 27D) biocomposites, did not exhibit any Bragg peak, which indicates that the polymer has an amorphous structure and that the characteristic peaks of AuNP, disappear, leaving the biocomposite in an amorphous phase, which indicates low adherence of the nanoparticles, therefore. On the other hand, the XRD pattern of the EPS4/AuNP biocomposite (Figure 27C), exhibited two Bragg peaks at 38.2 and 44.3 in the theta region, combining the crystallographic planes of (111) and (200).

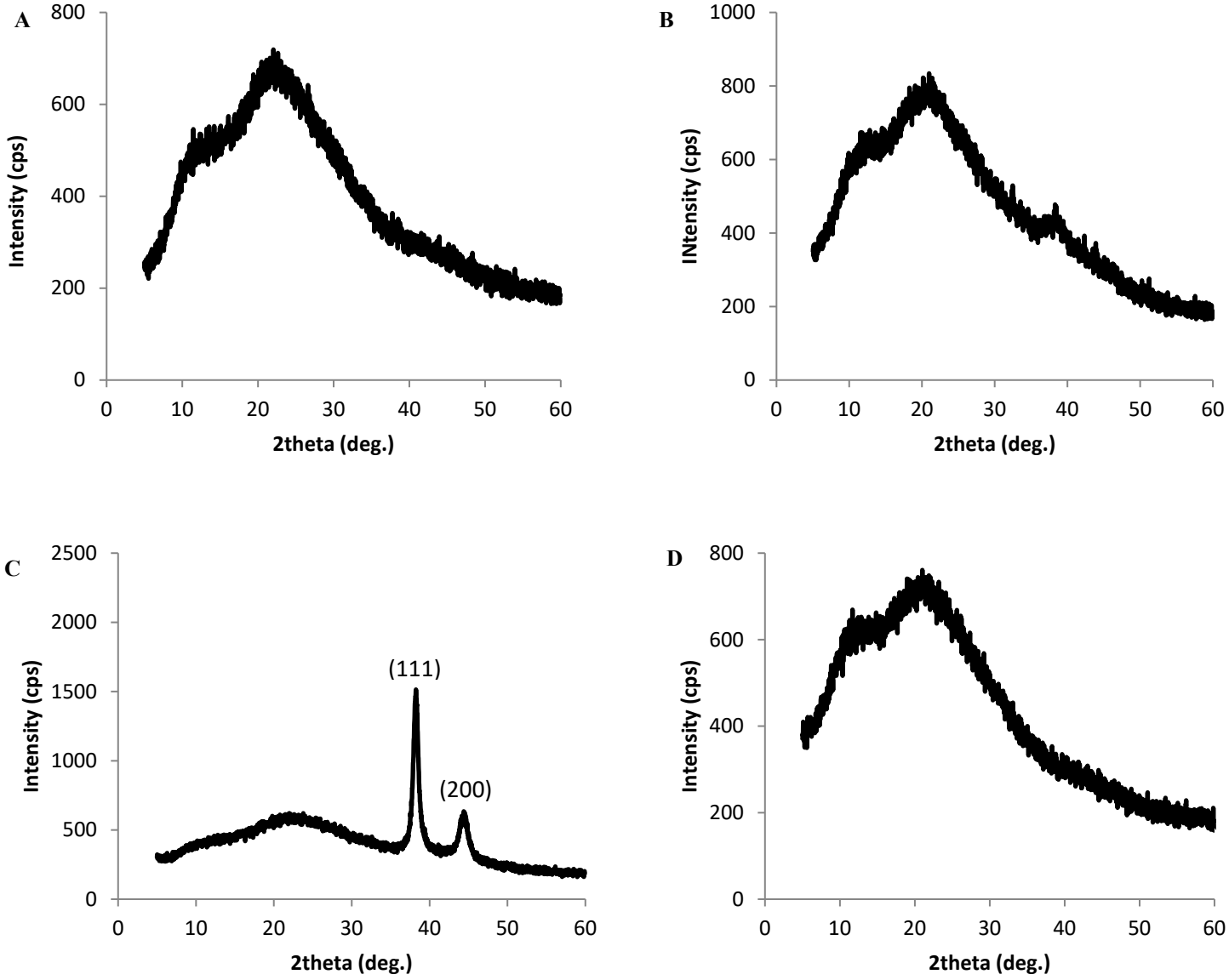

Figure 27. Diffractograms of EPS4 (A), EPS4/AgNP biocomposite (B), EPS4/AuNP biocomposite (C), and EPS4/SeNP biocomposite (D).

FucoPol (Figure 28A) exhibited a pattern of XRD which was not possible to observe any Bragg peak, exhibiting only broadband around 20º, explaining the amorphous nature of this polymer. The same pattern was observed in the biocomposites FucoPol/AgNP (Figure 28B) and FucoPol/SeNP (Figure 28D). The FucoPol/AuNP biocomposite (Figure 26C), was the only diffractogram that exhibited a Bragg peak at 38.3 in the 2θ region, combining the crystallographic plane of (111). According to (Aswathy Aromal & Philip, 2012), the peak corresponding to the plane (111) is more intense than the other planes, suggesting that (111) is the predominant orientation.

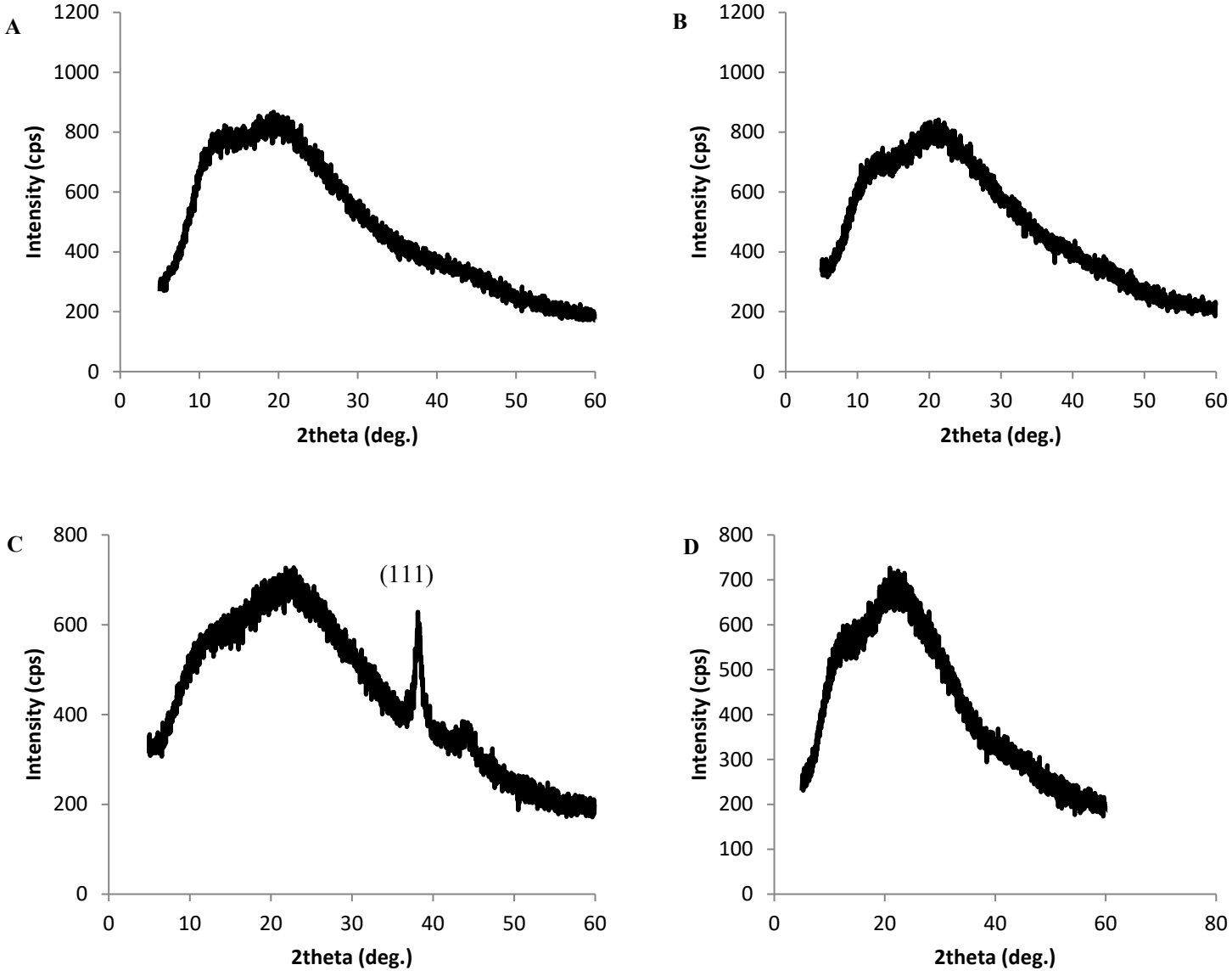

Figure 28. Diffractograms of FucoPol (A), Fucopol/AgNP biocomposite (B), FucoPol/AuNP biocomposite (C), and FucoPol /SeNP biocomposite (D).

3.5.3. Particle size and zeta potencial

The size of AgNP, AuNP and SeNP was determined by measuring the diameter of the particles. Table 32 shows the sizes corresponding to the biocomposites synthesized by the different EPSs.

Table 32. Presentation of the size of the different biocomposites.

	DLS (nm)	
Biocomposite	**Mean**	**SD**
EPS1/AgNP	191	15
EPS2/AgNP	120	5
EPS3/AgNP	168	17
EPS4/AgNP	260	19
FucoPol/AgNP	661	73
EPS1/AuNP	468	27
EPS2/AuNP	128	8
EPS3/AuNP	120	8
EPS4/AuNP	109	6
FucoPol/AuNP	995	78
EPS1/SeNP	230	21
EPS2/SeNP	435	29
EPS3/SeNP	357	59
EPS4/SeNP	234	6
FucoPol/SeNP	600	53

According to the results, it is possible to observe that the AgNPs and AuNPs, synthesized with FucoPol presented a significantly larger size when compared to the NPs synthesized with the other EPSs. For SeNPs, the one synthesized with EPS3 showed a larger size, although it does not have much difference concerning the one synthesized with FucoPol. About AuNPs, synthesis of 10 nm, 25 nm, and 50 nm NPs was previously reported (Jia et al., 2017). Regarding SeNPs, Liu et al., (2018) reported experiences carried out where they obtained SeNPs with diameters of 14 nm, 17 nm, 29 nm, 49 nm, 50 nm, and 65 nm. Thus, it is possible to conclude that the size of the biocomposites synthesized in this study has some similarity to those reported in the literature.

The zeta potential (Table 33) was measured to estimate the electrostatic stabilization of AgNP, AuNP, and SeNP.

Table 33. Presentation of the zeta potential of the different biocomposites.

	Zeta Potencial (mV)	
Biocomposite	**Mean**	**SD**
EPS1/AgNP	- 42.00	1.18
EPS2/AgNP	-37.83	3.33
EPS3/AgNP	-40.47	0.38
EPS4/AgNP	-39.20	0.98
FucoPol/AgNP	-40.37	0.94
EPS1/AuNP	-42.37	1.27
EPS2/AuNP	-28.13	0.25
EPS3/AuNP	-34.37	0.84
EPS4/AuNP	-32.20	0.95
FucoPol/AuNP	-30.17	0.67
EPS1/SeNP	-46.43	1.36
EPS2/SeNP	-36.73	2.29
EPS3/SeNP	-39.53	0.46
EPS4/SeNP	-40.57	1.43
FucoPol/SeNP	-38.87	0.21

The negative charge of biocomposites prevents aggregation and increases stability in addition to helping with their antimicrobial properties (Barapatre et al., 2016). Both biocomposites showed a zeta potential around -30/-40 mV, except the EPS2/AuNP biocomposite containing a zeta potential of -28.13 mV. In previous studies, AgNPS zeta potential of -51.81 ± 3.01 mV using *Botryococcus braunii* and -12.16 ± 2.41 mV using *Chlorella pyrenoidosa* as reducing and stabilizing agents (Navarro Gallón et al., 2019) has been reported. For AuNPs, Stiolica et al., (2017) reported zeta potential in the range of -27 mV to -95 mV, and Yan et al., (2018) reported zeta potential values of -17, -28, and -29 mV for SeNPs.

3.6. Exopolysaccharides and bionanocomposites biological characterization

3.6.1. Cytotoxicity

Keratinocytes attract, stimulate and coordinate the actions of different types of cells that are involved in wound healing processes, in addition to recapitulating the skin's epidermal barrier layer (Wojtowicz et al., 2014). In this work, the ability of EPSs and biocomposites to promote cell migration was evaluated using the HaCaT human keratinocyte cell line. First, the cytotoxicity of the samples (62.5 mg/L to 1000 mg/L) was evaluated after 24 h and the results are shown (Figure 29).

The results showed that none of the EPSs and biocomposites induced cytotoxicity in HaCaT cells, except the EPS3/AgNP biocomposite (Figure 29C) which significantly decreased cell viability by approximately 91-93%, relative to control, at concentrations above 125 mg/L , in terms of polymer content, equivalent to concentrations above 6.9 mg/L in terms of Ag^{+} content.

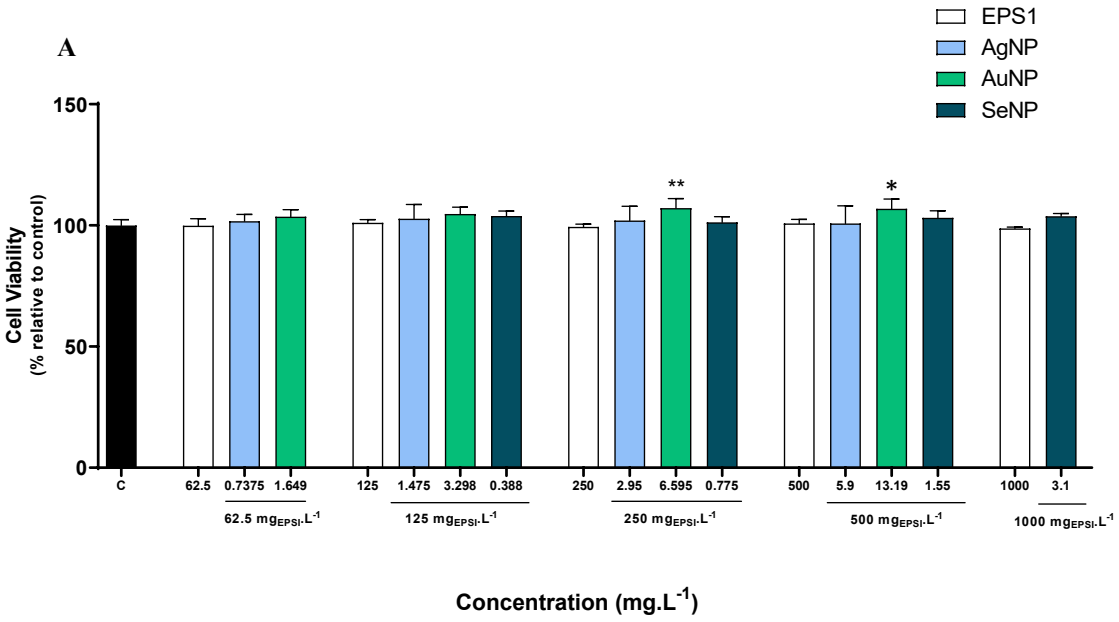

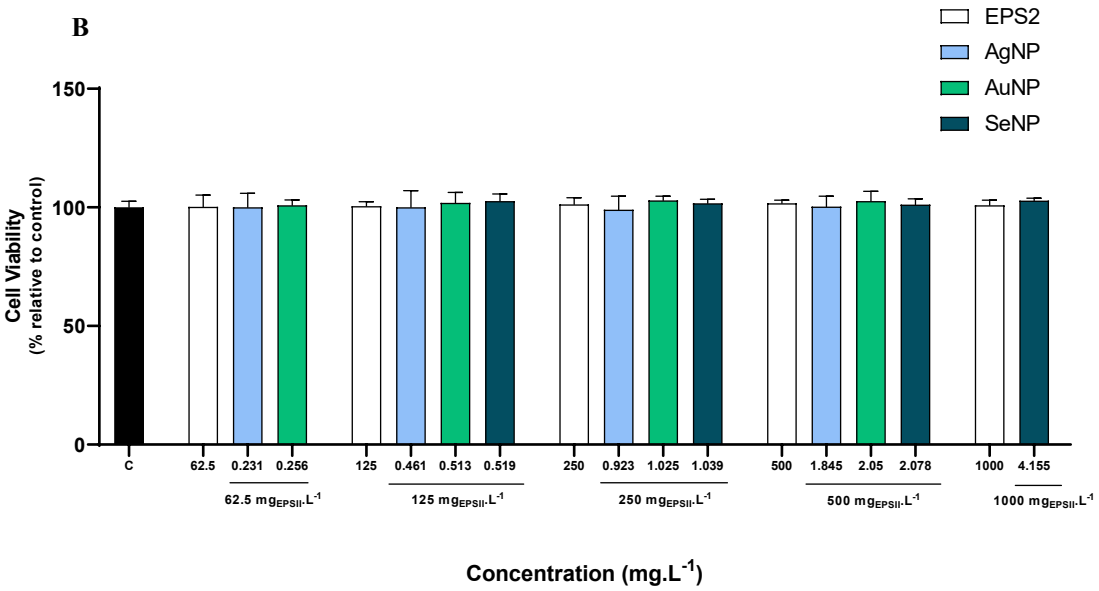
B
EPS2
AgNP
AuNP
SeNP
Cell Viability
(% relative to control)
150
100
50
0
C
62.5
0.231
0.256
125
0.461
0.513
0.519
250
0.923
1.025
1.039
500
1.845
2.05
2.078
1000
4.155
62.5 mg$_{EPSII}$.L^{-1}
125 mg$_{EPSII}$.L^{-1}
250 mg$_{EPSII}$.L^{-1}
500 mg$_{EPSII}$.L^{-1}
1000 mg$_{EPSII}$.L^{-1}
Concentration (mg.L^{-1})

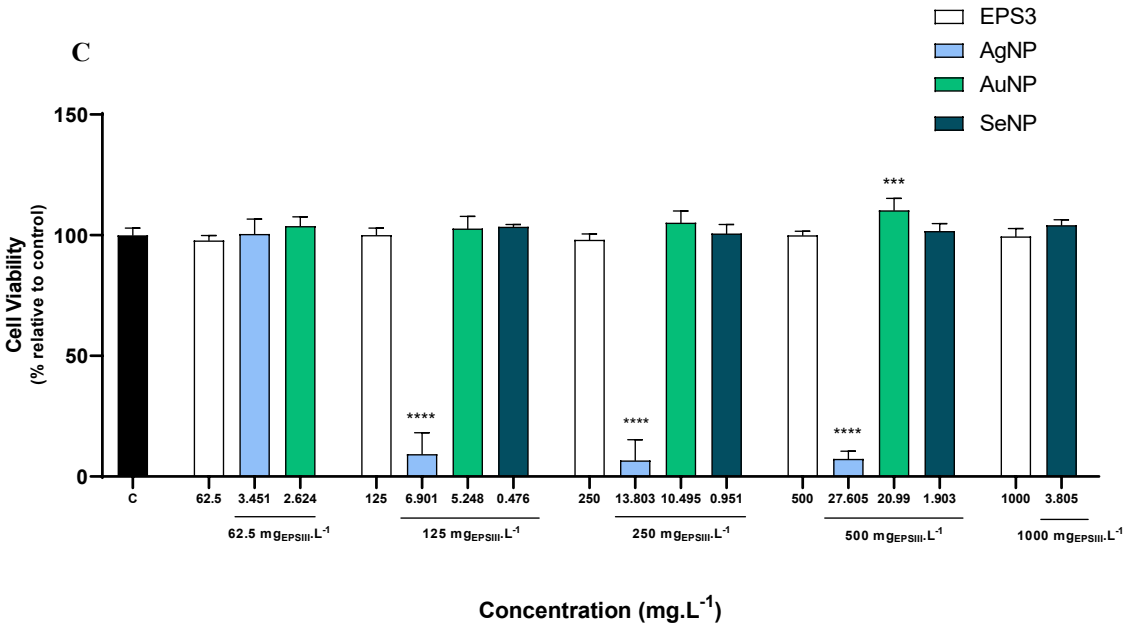
C
EPS3
AgNP
AuNP
SeNP
Cell Viability
(% relative to control)
150
100
50
0
****
****
****
***
C
62.5
3.451
2.624
125
6.901
5.248
0.476
250
13.803
10.495
0.951
500
27.605
20.99
1.903
1000
3.805
62.5 mg$_{EPSIII}$.L^{-1}
125 mg$_{EPSIII}$.L^{-1}
250 mg$_{EPSIII}$.L^{-1}
500 mg$_{EPSIII}$.L^{-1}
1000 mg$_{EPSIII}$.L^{-1}
Concentration (mg.L^{-1})

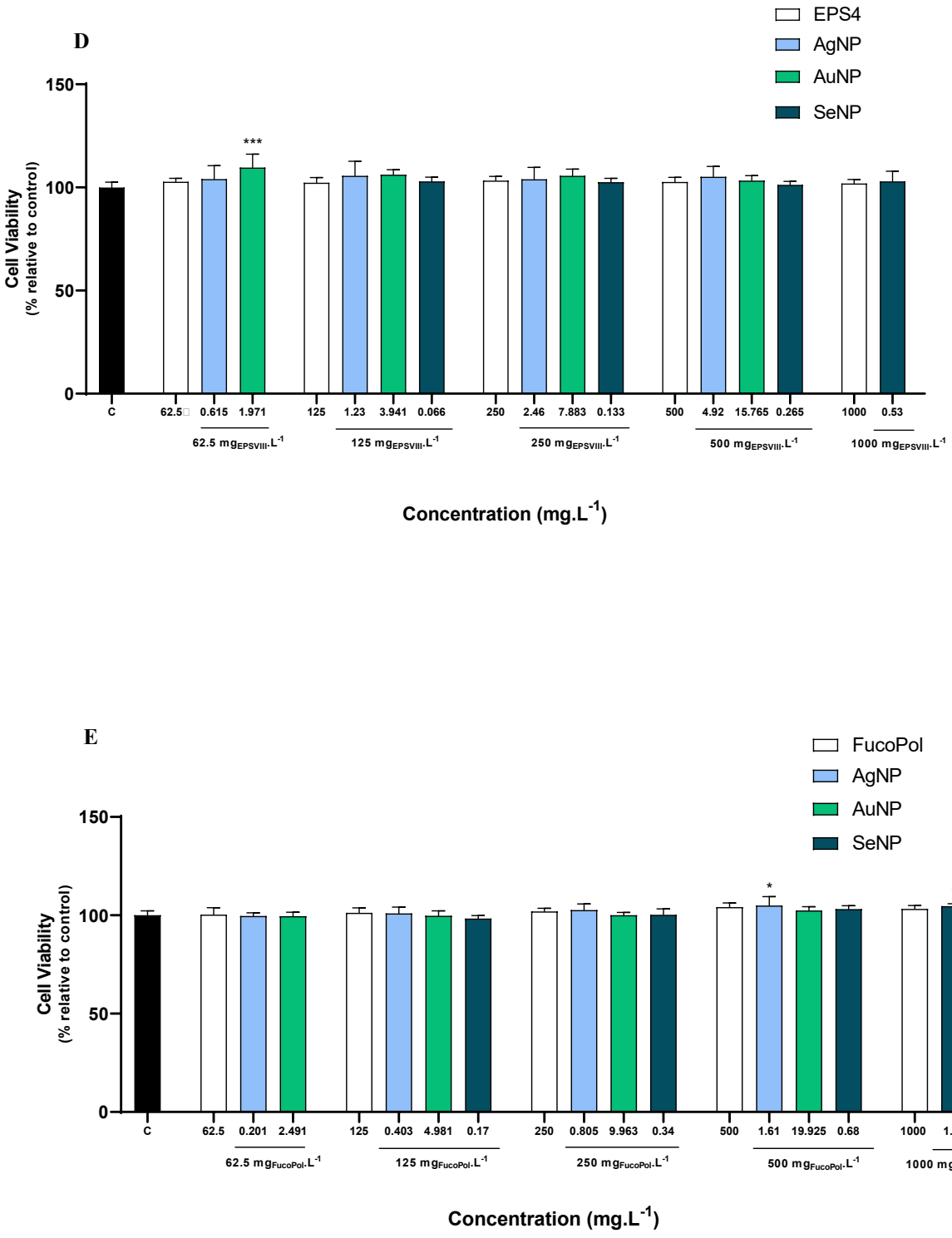

Figure 29. Cytotoxicity effect of EPS1 and EPS1/NPs biocomposite (A), EPS2 and EPS2/NPs biocomposite (B), EPS3 and EPS3/NPs biocomposite (C), EPS4 and EPS4/NPs biocomposite (D), and FuccoPol and FucoPol/NPs biocomposite (E), on HaCaT cells line after 24 h of incubation. Significant differences (* $p \leq 0.05$, ** $p \leq 0.01$, ** * $p \leq 0.001$, **** $p \leq 0.0001$).), when compared to the control (C), were tested by one-way ANOVA followed by post-hoc Bonferroni multiple comparison test.

The cytotoxic effect of the EPS3/AgNP biocomposite can be explained by the high concentration of Ag^+ (6.9 mg/L, 13.8 mg/L and 27.6 mg/L). This result has already been reported by other authors who demonstrated that NPs containing silver elements have a cytotoxic effect on HaCaT cells from a certain concentration (Zanette et al., 2011). For AuNP and SeNP no cytotoxic effect was observed, suggesting that these samples can be safe for skin applications at the concentrations tested. Punuri et al., (2012) reported the use of AuNPs in two different cell lines (human cervical cancer and human breast cancer), demonstrating that treatment with AuNPs did not induce any cytotoxic effects, causing no significant damage or death to the treated cells. Concordantly, Pivodová et al., (2015) also demonstrated that AuNPs did not cause significant cytotoxic effect on fibroblasts and keratinocytes cells. In addition, Yang et al., (2017), performed studies where they demonstrated that SeNPs exhibited low cytotoxic activity against SPCA-1 and HeLa cells. It is important to mention that in generall the samples promoted an increase in cell viability, some of them slightly (EPS1/AgNP, EPS1/AuNP, EPS2/AuNP, EPS2/SeNP, EPS3/SeNP, EPS4/AgNP, EPS4/SeNP, FucoPol/AgNP, and FucoPol/SeNP) with an increase in cell viability by approximately 1-2 % compared to the control and others more significantly (EPS1/AuNP, EPS3/AuNP, and EPS4/AuNP), with an increase in cell viability in up to 10 % relative to control, sugesting that a proliferative effect might be occurring at certain concentrations. However, future cytotoxicity evaluation studies should be performed using other human skin cell lines, including fibroblasts and melanocytes, to confirm the safety of the samples.

3.6.2. Wound healing capacity

The wound healing capacity of EPS and biocomposites was analysed after 24 h incubation by the scratch assay. In this assay, the migration of HaCaT cells was evaluated through the measurement of the area between wound edges at 0 and 24h and the wound recovery was calculated as a ratio relative to control (relative wound recovery). For FucoPol, three different concentrations (50, 100, and 500 mg/L) were tested (Figure 30).

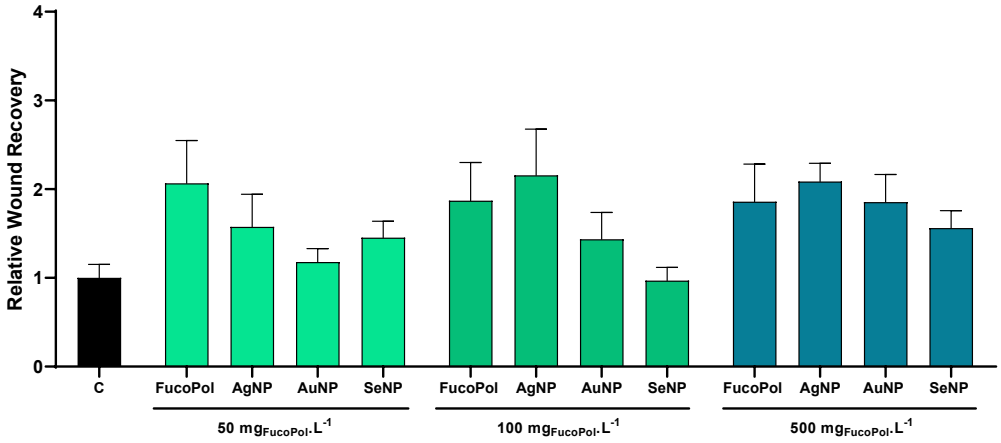

Figure 30. Scratch assay. Migration assessment of HaCaT cell line after treatment with FucoPol and FucoPol/NPs biocomposites for 24 h.

The results presented show that FucoPol alone, at a concentration of 50 mg/L, provided greater cell migration when compared to FucoPol impregnated with nanoparticles containing elements such as Ag, Au, and Se. The relative wound recovery with FucoPol was twice that of the control, demonstrating the potential of this EPS in the treatment of wounds. By increasing the FucoPol concentration to 100 mg/L, the FucoPol/AgNP biocomposite provided greater cell migration (2.15 increase in relative wound recovery) compared to the control, and FucoPol alone (1.86). At a concentration of 500 mg/L EPS, the FucoPol/AgNP biocomposite continues to exhibit greater cell migration (an increase of 2.08), although FucoPol alone has been shown to have a good influence on wound healing (1.85). The biocomposites FucoPol/AuNP (1.85) and FucoPol/SeNP (1.56) at the concentration of 500 mg/L EPS also had a good effect on wound healing compared to the control. Figure 31 shows the phase-contrast images of wound recovery when treated with FucoPol (100 and 500 mg/L) and the biocomposites FucoPol/AgNP (100 and 500 mg/L) and FucoPol/AuNP (500 mg/L), compared to the control.

T= 0h **T= 24h**

A

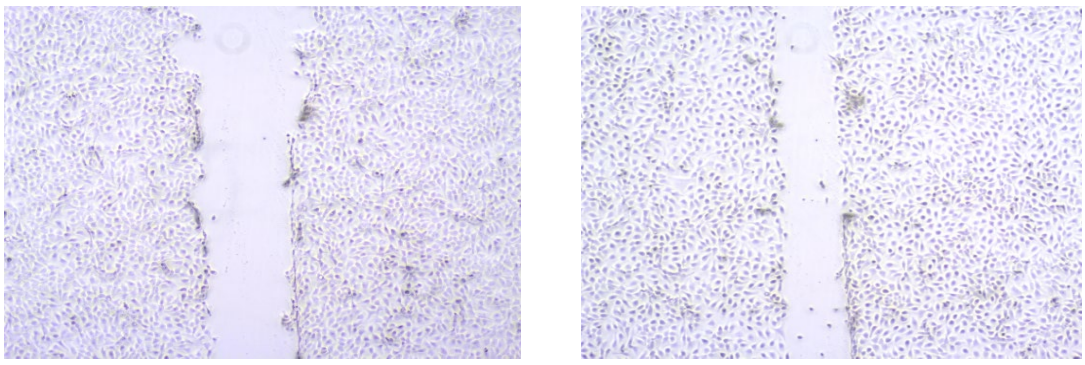

B

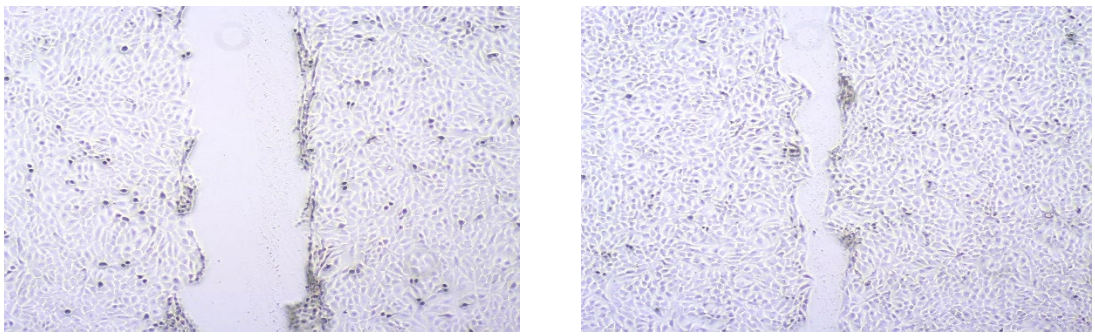

C

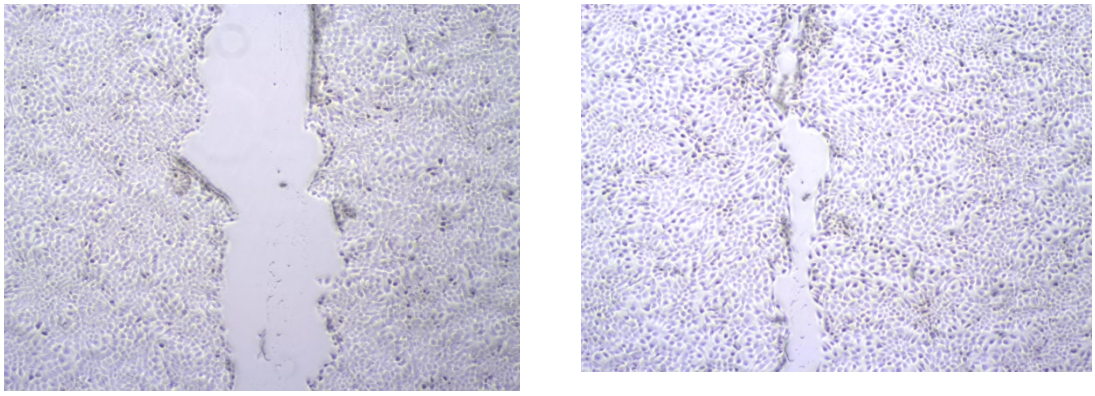

D

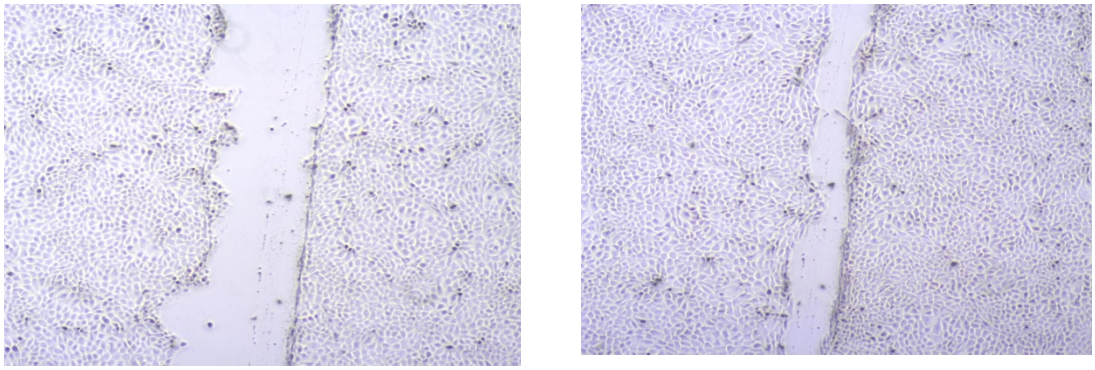

E

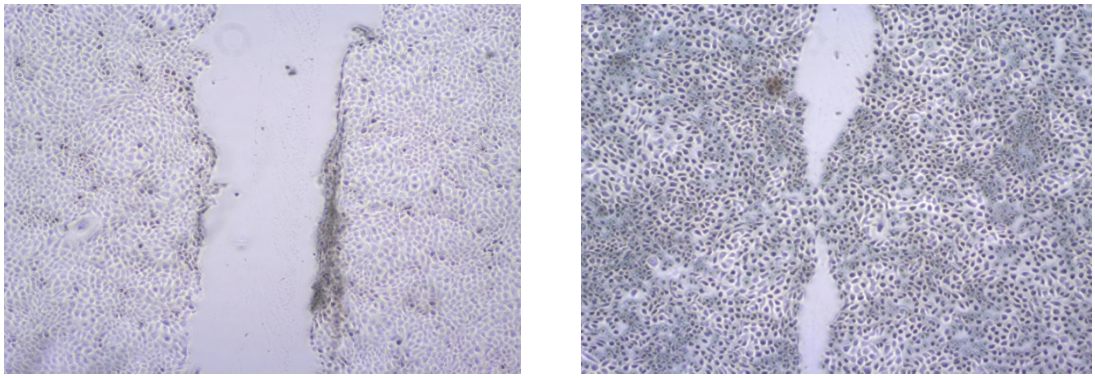

F

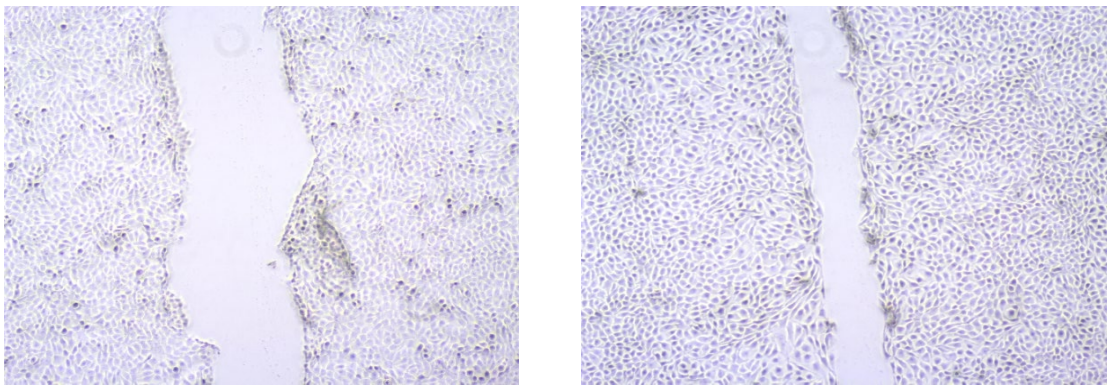

Figure 31. Evolution of wound healing in HaCaT cells line after treatment with FucoPol and biocomposites in different concentrations at time 0 and after 24 hours: control (A), FucoPol 100 mg/L (B), FucoPol/AgNP 100 mg/L (C), FucoPol 500 mg/L (D), FucoPol/AgNP 500 mg/L (E) and FucoPol/AuNP 500 mg/L (F).

These results allow us to conclude that FucoPol and respective biocomposites contributed to wound healing. Regarding FucoPol alone, there was no difference on cell migration for both concentrations tested (100 mg/L (B) and 500 mg/L (D)). It is notorious an evolution in wound healing with FucoPol alone at both concentrations (100 and 500 mg/L) when compared to the control. The FucoPol/AgNP and FucoPol/AuNP biocomposites have also been shown to be effective in wound healing, especially the FucoPol/AgNP 100 mg/L and 500 mg/L biocomposites. The FucoPol/AuNP biocomposite demonstrated a small reduction in the wound area but was not as significant. It is also noted that, although FucoPol provides cell migration and consequent wound healing, it is possible to observe greater effectiveness in wound healing with the FucoPol/AgNP biocomposite. Previous studies have reported the efficacy of FucoPol and the FucoPol/AgNP biocomposite in wound healing processes (Concórdio-Reis et al., 2020b), and the potential of AuNP as an adjunct to a compound in the treatment of cutaneous wounds (Leu et al., 2012). Still, it is possible to see both from the graphics and from the images that the wound recovery capacity, in general, seems to be dependent on the concentration of Ag, Au, and Se (shown only in the graphics), that is, the effectiveness is greater (decrease in the wound area) when there is an increase in the concentration of these elements. Regarding EPS1 (Figure 32), the polymer alone did not promote much considerable effects on the cell migration of HaCaT cells, however, the EPS1/AgNP (100 mg/L) and EPS1/AuNP (500 mg/L) biocomposite were shown to enhance the migration of HaCaT cells by two-fold when compared to control.

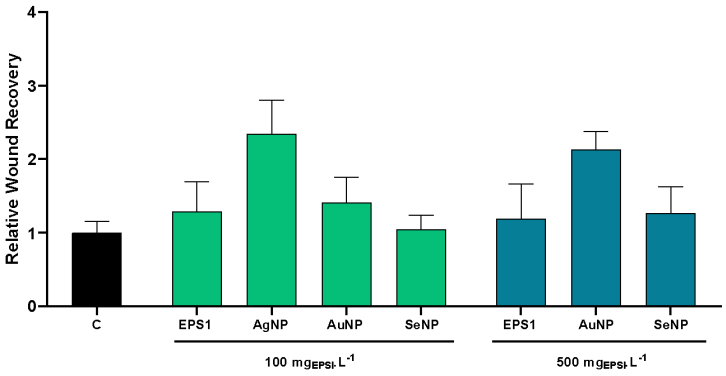

Figure 32. Scratch assay. Migration assessment of HaCaT cell line after treatment with EPS1 and EPS1/NPs biocomposites for 24 h.

These results show that, although EPS1/AgNP (100 mg/L) and EPS1/AuNP (500 mg/L) biocomposites demonstrate more significant results in cell migration (2.34 and 2.13 increase in relative wound healing, respectively) compared to the control. These results are confirmed by the photographs presented in Figure 33, comparing the wound areas at 0 h and after 24 h of incubation with EPS1 (100 and 500 mg/L) and respetive EPS1/AgNP (100 mg/L) and EPS1/AuNP (500 mg/L) biocomposites.

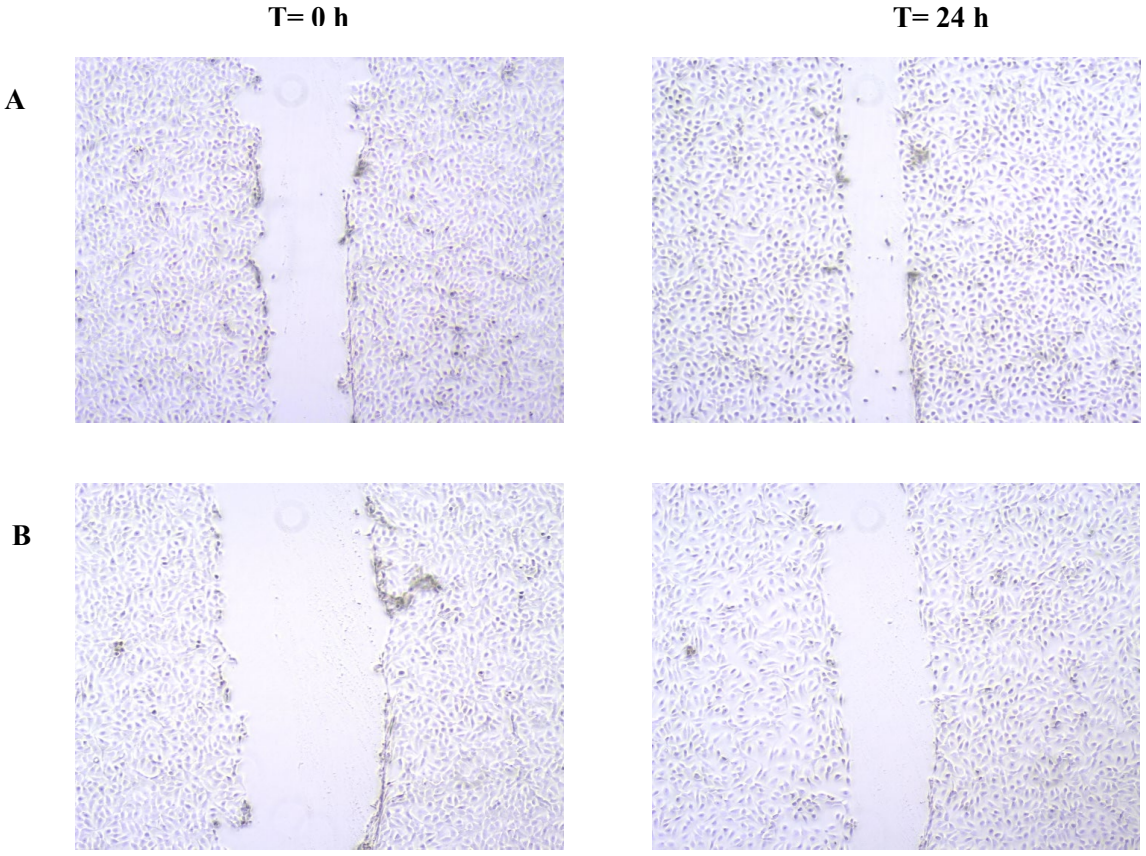

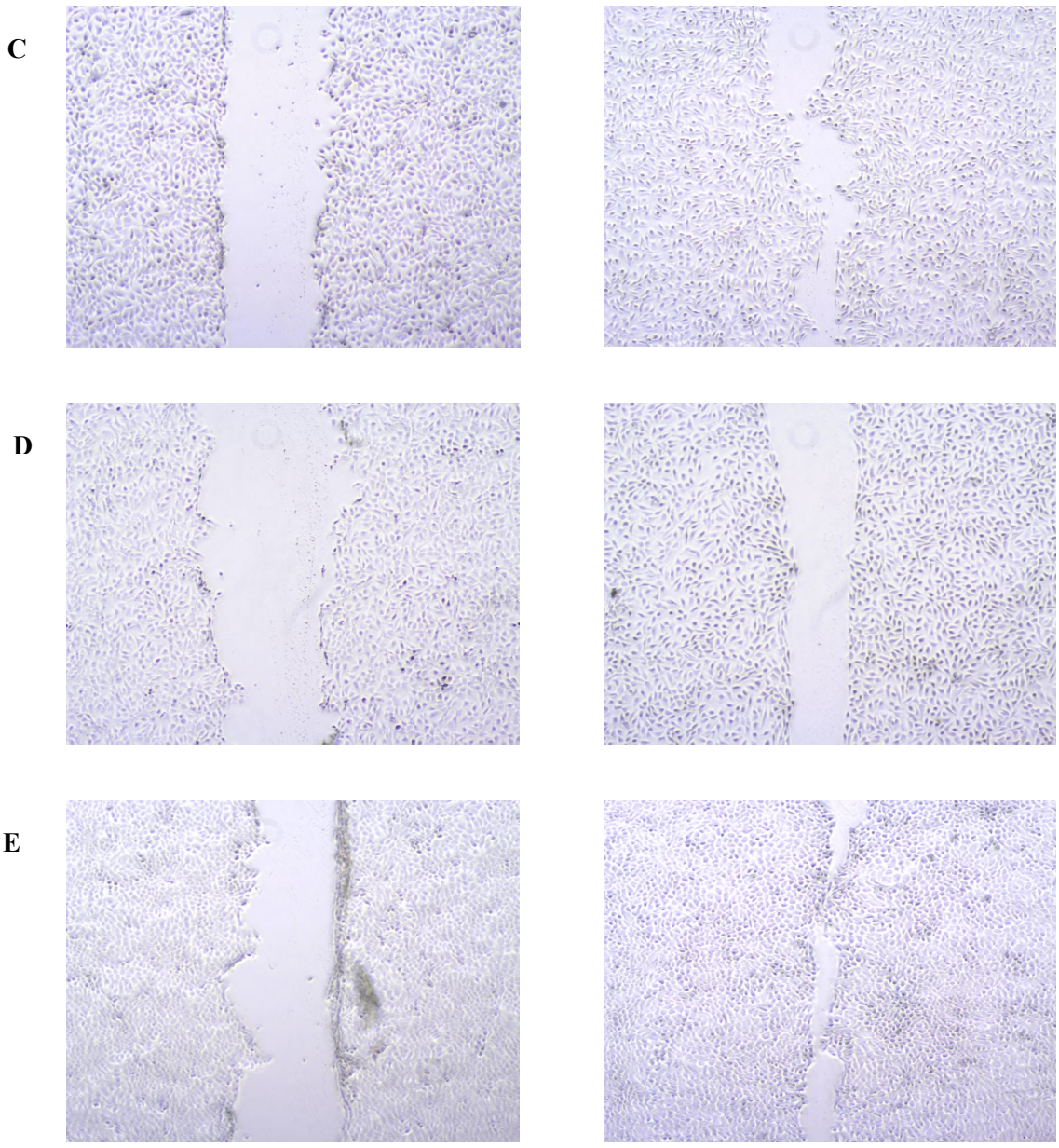

Figure 33. Evolution of wound healing in HaCaT cells line after treatment with EPS1 and biocomposites in different concentrations at time 0 and after 24 hours: control (A), EPS1 100 mg/L (B), EPS1/AgNP 100 mg/L (C), EPS1 500 mg/L (D) and EPS1/AuNP 500 mg/L (E).

These results reinforce the idea that EPS1 alone has not been shown to have significant effects on wound healing, however, the biocomposites EPS1/AgNP at a concentration of 100 mg/L (C) and EPS1/AuNP at a concentration of 500 mg/L, demonstrated have some effectiveness in wound healing. It is possible to notice a significant decrease in the wound area after treatment with these biocomposites, especially EPS1/AuNP. For the other EPS, namely EPS2 (Figure 34A), EPS3 (Figure 34B), EPS4 (Figure 34C), and respective biocomposites,

there was no relevant effect on HaCaT cell migration indicating that for the concentrations tested, these samples have moderate to no wound-healing effect.

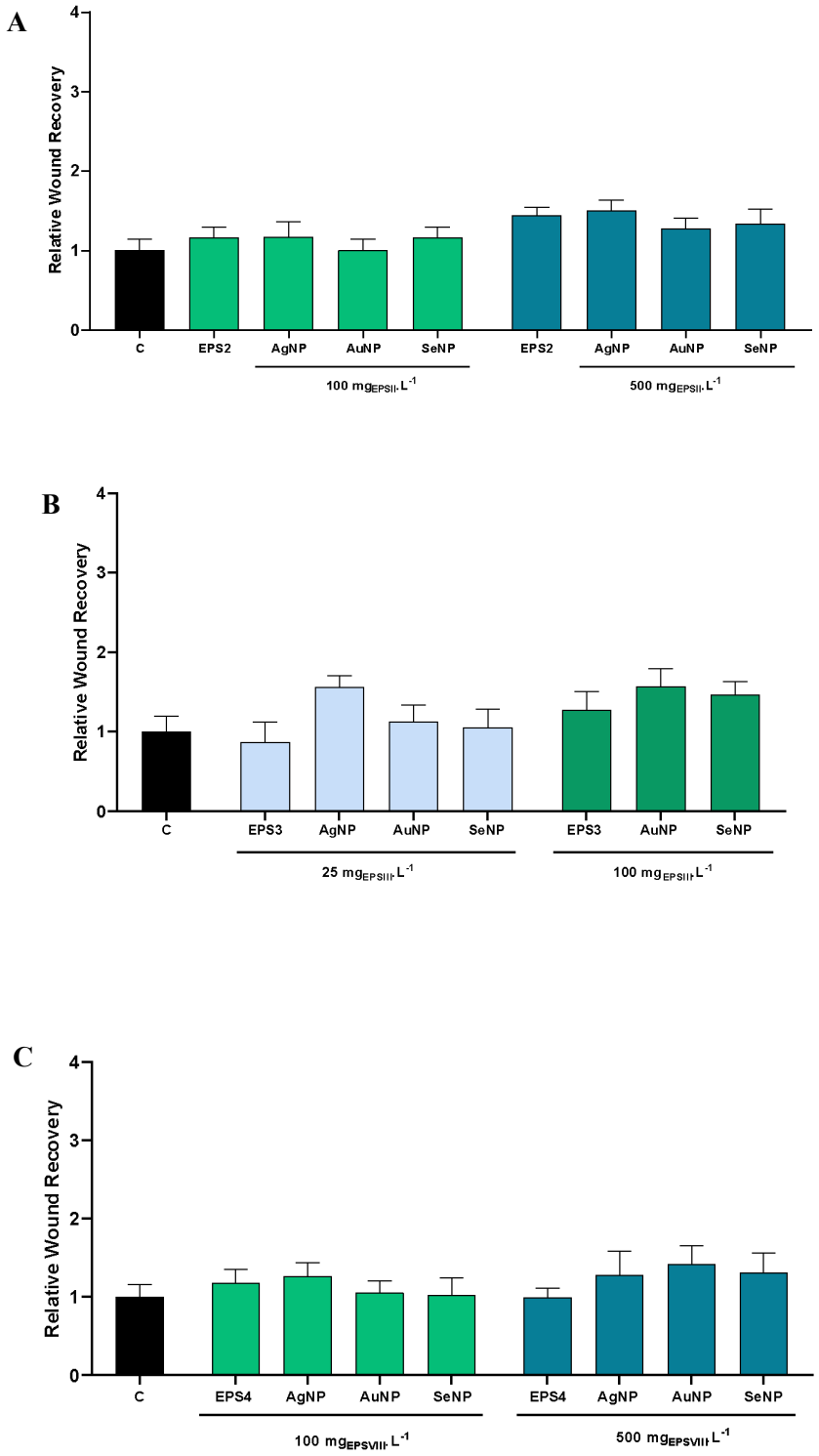

Figure 34. Scratch assay. Migration assessment of HaCaT cell line after treatment with EPS2 and EPS2/NPs biocomposites (A), EPS3 and EPS3/NPs biocomposites (B), EPS4 and EPS4/NPs biocomposites (C), for 24 h.

In general, the power of NPs in the wound healing process is notorious, especially AgNPS and AuNPS. In conclusion, our results suggest that FucoPol and its AgNPs and AuNPs biocomposites as well as EPS1/AgNP and EPS1/AuNP were the samples that showed greater efficacy in promoting skin wound healing, as they notably increased the migration of human skin keratinocytes, without inducing cytotoxic effects.

4. Conclusions

Silver, gold, and selenium nanoparticles were synthesized using a simple and green method, where a set of different EPS acted as reducing and stabilizing agents, respectively. FucoPol, a fucose-rich EPS, and four EPS secreted by marine isolates were used to prepare the metallic biocomposites. To synthesize the NPs, an experimental design and subsequent optimization of factors were previously carried out, which proved to play an important role, as they allowed the construction of response surface graphs, thus allowing the evaluation of the interaction effect between independent variables (time, temperature, pH and concentration of Ag^{+}, Au^{+3}, and Se^{+4}).

Biological characterization assays of EPSs and respective biocomposites, carried out in cells of the HaCaT lineage, showed that EPS, as well as EPSs/NPs biocomposites, did not show cytotoxic effects on human keratinocytes, except for the EPS3/AgNP biocomposite, demonstrated in a way overall, the presence of EPS in biocomposites helps to maintain greater cell viability. Furthermore, silver and gold nanoparticles have been shown to have a significant effect on the migration of keratinocytes, thus presenting potential effects on skin repair mechanisms, especially on wound healing processes.

5. Future work

In future works, in the case of nanoparticle synthesis, it is possible to adopt a different experimental design, to further optimize the different conditions used, especially the synthesis time, thus being able to obtain ideal nanoparticles in a shorter time. In the case of EPS, as well as biocomposites, they can be submitted to antibacterial tests to assess their antibacterial capacity with different types of bacteria and also assess the potential of NPs to increase or not the antibacterial effect of EPS if this effect exists. Still, it would be interesting to see if they have any antifungal effect and also to assess the anti-inflammatory activity of EPSs and their biocomposites, as it is an important factor in wound healing. Likewise, it would be relevant to test other skin cell lines, such as fibroblasts and melanocytes, to assess cell migration. In the case of SeNPs, evaluate their antioxidant effect and how each EPS behaves on this effect. Finally, develop wound care products based on these EPSs and their biocomposites.

6. References

Abbasi, E., Milani, M., Fekri Aval, S., Kouhi, M., Akbarzadeh, A., Tayefi Nasrabadi, H., Nikasa, P., Joo, S. W., Hanifehpour, Y., Nejati-Koshki, K., & Samiei, M. (2014). Silver nanoparticles: Synthesis methods, bio-applications and properties. *Critical Reviews in Microbiology*, *42*(2), 1–8. https://doi.org/10.3109/1040841X.2014.912200

Adrian, G., Mihai, M., & Vodnar, D. C. (2019). The Use of Chitosan, Alginate, and Pectin in the Biomedical and Food Sector—Biocompatibility, Bioadhesiveness, and Biodegradability. *Polymers*, *11(11)*, 1837. https://doi.org/10.3390/polym11111837

Álvarez, S., Cadavid, D., Sierra, D., Orozco, C., Vahos, D., Vahos, R., Ocampo, P., & Atehortúa, L. (2014). Comparison of Extraction Methods of Chitin from *Ganoderma lucidum* Mushroom Obtained in Submerged Culture. *BioMed Research International,* 2014, 1-7. http://dx.doi.org/10.1155/2014/169071

Alves, V. D., Freitas, F., Costa, N., Carvalheira, M., Oliveira, R., Gonçalves, M. P., & Reis, M. A. M. (2010). Effect of temperature on the dynamic and steady-shear rheology of a new microbial extracellular polysaccharide produced from glycerol byproduct. *Carbohydrate Polymers*, *79*(4), 981–988. https://doi.org/10.1016/j.carbpol.2009.10.026

Alves, V. D., Freitas, F., Torres, C. A. V., Cruz, M., Marques, R., Grandfils, C., Gonçalves, M. P., Oliveira, R., & Reis, M. A. M. (2009). Rheological and morphological characterization of the culture broth during exopolysaccharide production by *Enterobacter* sp. *Carbohydrate Polymers*, *January*. https://doi.org/10.1016/j.carbpol.2009.09.006

Anitha, A., Sowmya, S., Kumar, P. T. S., Deepthi, S., Chennazhi, K. P., Ehrlich, H., Tsurkan, M., & Jayakumar, R. (2014). Chitin and chitosan in selected biomedical applications. *Progress in Polymer Science*, *39*(9), 1644–1667. https://doi.org/10.1016/j.progpolymsci.2014.02.008

Antunes, S., Freitas, F., Sevrin, C., Grandfils, C., & Reis, M. A. M. (2017). Production of FucoPol by *Enterobacter* A47 using waste tomato paste by-product as sole carbon source. *Bioresource Technology*, *227*, 66–73. https://doi.org/10.1016/j.biortech.2016.12.018

Araújo, D., Concórdio-Reis, P., Marques, A. C., Sevrin, C., Grandfils, C., Alves, V. D., Fortunato, E., Reis, M. A. M., & Freitas, F. (2020). Demonstration of the ability of the bacterial polysaccharide FucoPol to flocculate kaolin suspensions. *Environmental Technology (United Kingdom)*, *41*(3), 287–295. https://doi.org/10.1080/09593330.2018.1497710

Ashokkumar, S., Ravi, S., Kathiravan, V., & Velmurugan, S. (2015). Synthesis of silver nanoparticles using *A. indicum* leaf extract and their antibacterial activity. *Spectrochimica Acta. Part A, Molecular and Biomolecular Spectroscopy*, *134*, 34–39. https://doi.org/10.1016/j.saa.2014.05.076

Aswathy Aromal, S., & Philip, D. (2012). Green synthesis of gold nanoparticles using *Trigonella foenum-graecum* and its size-dependent catalytic activity. *Spectrochimica Acta Part A: Molecular and Biomolecular Spectroscopy*, *97*, 1–5. https://doi.org/10.1016/j.saa.2012.05.083

Baharum, S. N., Beng, E. K., & Mokhtar, M. A. A. (2010). Marine Microorganisms: Potential application and challenges*Journal of Biological Sciences*, *10*(6), 555–564.

Barapatre, A., Aadil, K. R., & Jha, H. (2016). Synergistic antibacterial and antibiofilm activity of silver nanoparticles biosynthesized by lignin-degrading fungus. *Bioresources and Bioprocessing*, *3*(1). https://doi.org/10.1186/s40643-016-0083-y

Beam, J. W. (2009). Topical Silver for Infected Wounds. *Journal of Athletic Training*, *44*(5), 531–533. https://doi.org/10.4085/1062-6050-44.5.531

Belachew, T. F., Asrade, S., Geta, M., & Fentahun, E. (2020). *In Vivo* Evaluation of Wound Healing and Anti-Inflammatory Activity of 80% Methanol Crude Flower Extract of *Hagenia abyssinica* (Bruce) J.F. Gmel in Mice. *Evidence-Based Complementary and Alternative Medicine*, *2020*, 1–12. https://doi.org/10.1155/2020/9645792

Boateng, J., Matthews, K., Stevens, H., & Eccleston, G. M. (2008). Wound Healing Dressings and Drug Delivery Systems : A Review. *Journal of Pharmaceutical Sciences*, *97*(8), 2892–2923. https://doi.org/10.1002/jps

Boukamp, P., Petrussevska, R. T., Breitkreutz, D., Hornung, J., Markham, A., & Fusenig, N. E. (1988). Normal keratinization in a spontaneously immortalized aneuploid human keratinocyte cell line. *Journal of Cell Biology*, *106*(3), 761–771. https://doi.org/10.1083/jcb.106.3.761

Cai, W., Hu, T., Bakry, A. M., Zheng, Z., Xiao, Y., & Huang, Q. (2018). Effect of ultrasound on size, morphology, stability and antioxidant activity of selenium nanoparticles dispersed by a hyperbranched polysaccharide from *Lignosus rhinocerotis*. *Ultrasonics Sonochemistry*, *42*(October 2017), 823–831. https://doi.org/10.1016/j.ultsonch.2017.12.022

Casillo, A., Lanzetta, R., Parrilli, M., & Corsaro, M. M. (2018). Exopolysaccharides from Marine and Marine Extremophilic Bacteria: Structures, Properties, Ecological Roles and Applications. *Marine Drugs*, *16*(2), 69. https://doi.org/10.3390/md16020069

Chakraborty, J., Mangwani, N., Dash, H. R., Kumari, S., Kumar, H., & Das, S. (2016). Marine bacterial exopolysaccharides: Functional diversity and prospects in environmental restoration. *Marine Glycobiology: Principles and Applications*, *May*, 235–254.

Chaudhary, S., Umar, A., & Mehta, S. K. (2016). Selenium nanomaterials: An overview of recent developments in synthesis, properties and potential applications. *Progress in Materials Science*, *83*, 270–329. https://doi.org/10.1016/j.pmatsci.2016.07.001

Chen, X., Yan, J. K., & Wu, J. Y. (2016). Characterization and antibacterial activity of silver nanoparticles prepared with a fungal exopolysaccharide in water. *Food Hydrocolloids*, *53*, 69–74. https://doi.org/10.1016/j.foodhyd.2014.12.032

Cheng, Y., Xiao, X., Li, X., Song, D., Lu, Z., Wang, F., & Wang, Y. (2017). Characterization, antioxidant property and cytoprotection of exopolysaccharide-capped elemental selenium particles synthesized by *Bacillus paralicheniformis* SR14. *Carbohydrate Polymers*, *178*, 18–26. https://doi.org/10.1016/j.carbpol.2017.08.124

Concórdio-Reis, P., Pereira, J. R., Torres, C. A. V., Sevrin, C., Grandfils, C., & Freitas, F. (2018). Effect of mono- and dipotassium phosphate concentration on extracellular polysaccharide production by the bacterium *Enterobacter* A47. *Process Biochemistry*, *75*, 16–21. https://doi.org/10.1016/j.procbio.2018.09.001

Concórdio-Reis, P., Pereira, C. V., Batista, M. P., Sevrin, C., Grandfils, C., Marques, A. C., Fortunato, E., Gaspar, F. B., Matias, A. A., Freitas, F., & Reis, M. A. M. (2020b). Silver nanocomposites based on the bacterial fucose-rich polysaccharide secreted by *Enterobacter* A47 for wound dressing applications: Synthesis, characterization and in vitro bioactivity. *International Journal of Biological Macromolecules*, *163*, 959–969. https://doi.org/10.1016/j.ijbiomac.2020.07.072

Concórdio-Reis, P., Reis, M. A. M., & Freitas, F. (2020a). Biosorption of heavy metals by the bacterial exopolysaccharide fucopol. *Applied Sciences (Switzerland)*, *10*(19). https://doi.org/10.3390/APP10196708

Cruz, M., Freitas, F., Torres, C. A. V., Reis, M. A. M., & Alves, V. D. (2011). Influence of temperature on the rheological behavior of a new fucose-containing bacterial

exopolysaccharide. *International Journal of Biological Macromolecules*, *48*(4), 695–699. https://doi.org/10.1016/j.ijbiomac.2011.02.012

Czaja, W., Krystynowicz, A., Bielecki, S., & Brown, R. M. (2006). Microbial cellulose - The natural power to heal wounds. *Biomaterials*, *27*(2), 145–151. https://doi.org/10.1016/j.biomaterials.2005.07.035

De Araújo, I. W. F., Vanderlei, E. D. S. O., Rodrigues, J. A. G., Coura, C. O., Quinderé, A. L. G., Fontes, B. P., De Queiroz, I. N. L., Jorge, R. J. B., Bezerra, M. M., Rodrigues E Silva, A. A., Chaves, H. V., Monteiro, H. S. A., De Paula, R. C. M., & Benevides, N. M. B. (2011). Effects of a sulfated polysaccharide isolated from the red seaweed Solieria filiformis on models of nociception and inflammation. *Carbohydrate Polymers*, *86*(3), 1207–1215. https://doi.org/10.1016/j.carbpol.2011.06.016

de Carvalho, C. C. C. R., & Fernandes, P. (2010). Production of metabolites as bacterial responses to the marine environment. *Marine Drugs*, *8*(3), 705–727. https://doi.org/10.3390/md8030705

Değim, Z. (2008). Use of microparticulate systems to accelerate skin wound healing. *Journal of Drug Targeting*, *16*(6), 437–448. https://doi.org/10.1080/10611860802088572

Demidova-Rice, T. N., Hamblin, M. R., & Herman, I. M. (2012). Acute and Impaired Wound Healing. *Advances in Skin & Wound Care*, *25*(8), 349–370. https://doi.org/10.1097/01.ASW.0000418541.31366.a3

Dhivya, S., Vijaya, V., & Santhini, E. (2015). Wound dressings – a review. *BioMedicine*, *5*(4), 24–28. https://doi.org/10.7603/s40681-015-0022-9

Dutra, J. A. P., Carvalho, S. G., Zampirolli, A. C. D., Daltoé, R. D., Teixeira, R. M., Careta, F. P., Cotrim, M. A. P., Oréfice, R. L., & Villanova, J. C. O. (2017). Papain wound dressings obtained from poly(vinyl alcohol)/calcium alginate blends as new pharmaceutical dosage form: Preparation and preliminary eval- uation. *European Journal of Pharmaceutics and Biopharmaceutics*, *113*, 11–23. https://doi.org/10.1016/j.ejpb.2016.12.001

Ertürk, A. S. (2019). Controlled Production of Monodisperse Plant-Mediated AgNP Catalysts Using Microwave Chemistry: A Desirability-Function-Based Multiple-Response Optimization Approach. *ChemistrySelect*, *4*(32), 9300–9308. https://doi.org/10.1002/slct.201902197

Escárcega-González, C. E., Garza-Cervantes, J. A., Vázquez-Rodríguez, A., & Morones-Ramírez, J. R. (2018). Bacterial Exopolysaccharides as Reducing and/or Stabilizing Agents during Synthesis of Metal Nanoparticles with Biomedical Applications. *International Journal of Polymer Science*, *2018*, 1–15. https://doi.org/10.1155/2018/7045852

Farinha, I., Duarte, P., Pimentel, A., Plotnikova, E., Chagas, B., Mafra, L., Grandfils, C., Freitas, F., Fortunato, E., & Reis, M. A. M. (2015). Chitin – glucan complex production by *Komagataella pastoris*: Downstream optimization and product characterization. *Carbohydrate Polymers*, *130*, 455–464. https://doi.org/10.1016/j.carbpol.2015.05.034

Fialho, A. M., Moreira, L. M., Granja, A. T., Popescu, A. O., Hoffmann, K., & Sá-Correia, I. (2008). Occurrence, production, and applications of gellan: Current state and perspectives. *Applied Microbiology and Biotechnology*, *79*(6), 889–900. https://doi.org/10.1007/s00253-008-1496-0

Fialho, L., Araújo, D., Alves, V. D., Roma-Rodrigues, C., Baptista, P. V., Fernandes, A. R., Freitas, F., & Reis, M. A. M. (2021). Cation-mediated gelation of the fucose-rich polysaccharide FucoPol: preparation and characterization of hydrogel beads and their cytotoxicity assessment. *International Journal of Polymeric Materials and Polymeric Biomaterials*, *70*(2), 90–99. https://doi.org/10.1080/00914037.2019.1695205

Firdhouse, M. J., & Lalitha, P. (2015). Biosynthesis of Silver Nanoparticles and Its Applications. *Journal of Nanotechnology*, *2015*(September 2014), 1–18. https://doi.org/10.1155/2015/829526

Freitas, F., Alves, V. D., Gouveia, A. R., Pinheiro, C., Torres, C. A. V., Grandfils, C., & Reis, M. A. M. (2014). Controlled Production of Exopolysaccharides from *Enterobacter* A47 as a Function of Carbon Source with Demonstration of Their Film and Emulsifying Abilities. *Applied Biochemistry and Biotechnology*, *172*(2), 641–657. https://doi.org/10.1007/s12010-013-0560-0

Freitas, F., Alves, V. D., & Reis, M. A. M. (2011a). Advances in bacterial exopolysaccharides: from production to biotechnological applications. *Trends in Biotechnology*, *29*(8), 388–398. https://doi.org/10.1016/j.tibtech.2011.03.008

Freitas, F., Alves, V. D., Torres, C. A. V., Cruz, M., Sousa, I., Melo, M. J., Ramos, A. M., & Reis, M. A. M. (2011b). Fucose-containing exopolysaccharide produced by the newly isolated *Enterobacter* strain A47 DSM 23139. *Carbohydrate Polymers*, *83*(1), 159–165. https://doi.org/10.1016/j.carbpol.2010.07.034

Ghadi, R., Jain, A., Khan, W., & Domb, A. J. (2016). Microparticulate polymers and hydrogels for wound healing. In *Wound Healing Biomaterials* (Vol. 2). Elsevier Ltd. https://doi.org/10.1016/B978-1-78242-456-7.00010-6

Gopinath, K., Venkatesh, K. S., Ilangovan, R., Sankaranarayanan, K., & Arumugam, A. (2013). Green synthesis of gold nanoparticles from leaf extract of *Terminalia arjuna,* for the enhanced mitotic cell division and pollen germination activity. *Industrial Crops and Products*, *50*, 737–742. https://doi.org/10.1016/j.indcrop.2013.08.060

Gour, A., & Jain, N. K. (2019). Advances in green synthesis of nanoparticles. *Artificial Cells, Nanomedicine, and Biotechnology*, *47*(1), 844–851. https://doi.org/10.1080/21691401.2019.1577878

Guézennec, J., Moppert, X., Raguénès, G., Richert, L., Costa, B., & Simon-Colin, C. (2011). Microbial mats in French Polynesia and their biotechnological applications. *Process Biochemistry*, *46*(1), 16–22. https://doi.org/10.1016/j.procbio.2010.09.001

Gunasekaran, T., Nigusse, T., & Dhanaraju, M. D. (2011). Silver Nanoparticles as Real Topical Bullets for Wound Healing. *Journal of the American College of Clinical Wound Specialists*, *3*(4), 82–96. https://doi.org/10.1016/j.jcws.2012.05.001

Guo, Y., Pan, D., Li, H., Sun, Y., Zeng, X., & Yan, B. (2013). Antioxidant and immunomodulatory activity of selenium exopolysaccharide produced by *Lactococcus lactis* subsp. lactis. *Food Chemistry*, *138*(1), 84–89. https://doi.org/10.1016/j.foodchem.2012.10.029

Gupta, A., Landis, R. F., & Rotello, V. M. (2016). Nanoparticle-Based Antimicrobials: Surface Functionality is Critical. *F1000Research*, *5*(0), 364. https://doi.org/10.12688/f1000research.7595.1

Gutierrez, T., Berry, D., Yang, T., Mishamandani, S., McKay, L., Teske, A., & Aitken, M. D. (2013). Role of Bacterial Exopolysaccharides (EPS) in the Fate of the Oil Released during the Deepwater Horizon Oil Spill. *PLoS ONE*, *8*(6), e67717. https://doi.org/10.1371/journal.pone.0067717

Hamidi, M., Kozani, P. S., Kozani, P. S., Pierre, G., Michaud, P., & Delattre, C. (2019). Marine Bacteria versus Microalgae: Who Is the Best for Biotechnological Production of Bioactive Compounds with Antioxidant Properties and Other Biological Applications? *Marine Drugs*, *18*(1), 28. https://doi.org/10.3390/md18010028

Ho, J., Walsh, C., Yue, D., Dardik, A., & Cheema, U. (2017). Current Advancements and Strategies in Tissue Engineering for Wound Healing: A Comprehensive Review. *Advances*

in Wound Care, *6*(6), 191–209. https://doi.org/10.1089/wound.2016.0723

Huang, H., & Yang, X. (2004). Synthesis of polysaccharide-stabilized gold and silver nanoparticles: A green method. *Carbohydrate Research*, *339*(15), 2627–2631. https://doi.org/10.1016/j.carres.2004.08.005

Iravani, S. (2011). Green synthesis of metal nanoparticles using plants. *Green Chemistry*, *13*(10), 2638. https://doi.org/10.1039/c1gc15386b

Jayakumar, R., Prabaharan, M., Sudheesh Kumar, P. T., Nair, S. V., & Tamura, H. (2011). Biomaterials based on chitin and chitosan in wound dressing applications. *Biotechnology Advances*, *29*(3), 322–337. https://doi.org/10.1016/j.biotechadv.2011.01.005

Jayaseelan, C., Ramkumar, R., Rahuman, A. A., & Perumal, P. (2013). Green synthesis of gold nanoparticles using seed aqueous extract of *Abelmoschus esculentus* and its antifungal activity. *Industrial Crops and Products*, *45*, 423–429. https://doi.org/10.1016/j.indcrop.2012.12.019

Jensen, P. R., & Fenical, W. (1994). Strategies for the Discovery of Secondary Metabolites from Marine Bacteria: Ecological Perspectives. *Annual Review of Microbiology*, *48*(1), 559–584. https://doi.org/10.1146/annurev.mi.48.100194.003015

Jia, Y. P., Ma, B. Y., Wei, X. W., & Qian, Z. Y. (2017). The *in vitro* and *in vivo* toxicity of gold nanoparticles. *Chinese Chemical Letters*, *28*(4), 691–702. https://doi.org/10.1016/j.cclet.2017.01.021

Khademi-Azandehi, P., & Moghaddam, J. (2015). Green synthesis, characterization and physiological stability of gold nanoparticles from *Stachys lavandulifolia Vahl* extract. *Particuology*, *19*, 22–26. https://doi.org/10.1016/j.partic.2014.04.007

Koehler, J., Brandl, F. P., & Goepferich, A. M. (2018). Hydrogel wound dressings for bioactive treatment of acute and chronic wounds. *European Polymer Journal*, *100*, 1–11. https://doi.org/10.1016/j.eurpolymj.2017.12.046

Kumar, P., Singh, P., Kumari, K., Mozumdar, S., & Chandra, R. (2011). A green approach for the synthesis of gold nanotriangles using aqueous leaf extract of *Callistemon viminalis*. *Materials Letters*, *65*(4), 595–597. https://doi.org/10.1016/j.matlet.2010.11.025

Kumar, S. S. D., Rajendran, N. K., Houreld, N. N., & Abrahamse, H. (2018). Recent advances on silver nanoparticle and biopolymer-based biomaterials for wound healing applications. *International Journal of Biological Macromolecules*, *115*(2017), 165–175. https://doi.org/10.1016/j.ijbiomac.2018.04.003

Lau, P., Bidin, N., Islam, S., Shukri, W. N. B. W. M., Zakaria, N., Musa, N., & Krishnan, G. (2017). Influence of gold nanoparticles on wound healing treatment in rat model: Photobiomodulation therapy. *Lasers in Surgery and Medicine*, *49*(4), 380–386. https://doi.org/10.1002/lsm.22614

Leu, J., Chen, S., & Chen, H. (2012). The effects of gold nanoparticles in wound healing with antioxidant epigallocatechin gallate and α -lipoic acid. *Nanomedicine: Nanotechnology, Biology, and Medicine*, *8*(5), 767–775. https://doi.org/10.1016/j.nano.2011.08.013

Li, X., Wang, H., Rong, H., Li, W., Luo, Y., Tian, K., Quan, D., Wang, Y., & Jiang, L. (2015). Effect of composite SiO 2 @AuNPs on wound healing: *In vitro* and *vivo* studies. *Journal of Colloid and Interface Science*, *445*, 312–319. https://doi.org/10.1016/j.jcis.2014.12.084

Liu, X., Hao, W., Lok, C.-N., Wang, Y. C., Zhang, R., & Wong, K. K. Y. (2014). Dendrimer encapsulation enhances anti-inflammatory efficacy of silver nanoparticles. *Journal of Pediatric Surgery*, *49*(12), 1846–1851. https://doi.org/10.1016/j.jpedsurg.2014.09.033

Liu, Y., Zeng, S., Liu, Y., Wu, W., Shen, Y., Zhang, L., Li, C., Chen, H., Liu, A., Shen, L., Hu, B., & Wang, C. (2018). Synthesis and antidiabetic activity of selenium nanoparticles in the

presence of polysaccharides from *Catathelasma ventricosum. International Journal of Biological Macromolecules*, *114*, 632–639. https://doi.org/10.1016/j.ijbiomac.2018.03.161

Lo, C. M., Chen, R. T., Chang, Y. C., Yang, Y. W., Hung, M. J., Huang, C. S., & Chang, R. F. (2014). Multi-dimensional tumor detection in automated whole breast ultrasound using topographic watershed. *IEEE Transactions on Medical Imaging*, *33*(7), 1503–1511. https://doi.org/10.1109/TMI.2014.2315206

Logeart-Avramoglou, D., & Jozefonvicz, J. (1999). Carboxymethyl benzylamide sulfonate dextrans (CMDBS), a family of biospecific polymers endowed with numerous biological properties: A review. *Journal of Biomedical Materials Research*, *48*(4), 578–590. https://doi.org/10.1002/(SICI)1097-4636(1999)48:4<578::AID-JBM26>3.0.CO;2-8

Lu, B., Li, T., Zhao, H., Li, X., Gao, C., Zhang, S., & Xie, E. (2012). Graphene-based composite materials beneficial to wound healing. *Nanoscale*, *4*(9), 2978–2982. https://doi.org/10.1039/c2nr11958g

Martin-Pastor, M., Ferreira, A. S., Moppert, X., Nunes, C., Coimbra, M. A., Reis, R. L., Guezennec, J., & Novoa-Carballal, R. (2019). Structure, rheology, and copper-complexation of a hyaluronan-like exopolysaccharide from *Vibrio. Carbohydrate Polymers*, *222*(March), 114999. https://doi.org/10.1016/j.carbpol.2019.114999

Muthuvel, A., Adavallan, K., Balamurugan, K., & Krishnakumar, N. (2014). Biosynthesis of gold nanoparticles using *Solanum nigrum* leaf extract and screening their free radical scavenging and antibacterial properties. *Biomedicine & Preventive Nutrition*, *4*(2), 325–332. https://doi.org/10.1016/j.bionut.2014.03.004

Naderi, N., Karponis, D., Mosahebi, A., & Seifalian, A. M. (2018). Nanoparticles in wound healing; from hope to promise, from promise to routine. *Frontiers in Bioscience (Landmark Edition)*, *23*(3), 1038–1059. https://doi.org/10.2741/4632

Nanda, A., & Saravanan, M. (2009). Biosynthesis of silver nanoparticles from *Staphylococcus aureus* and its antimicrobial activity against MRSA and MRSE. *Nanomedicine: Nanotechnology, Biology, and Medicine*, *5*(4), 452–456. https://doi.org/10.1016/j.nano.2009.01.012

Narayan, N., Meiyazhagan, A., & Vajtai, R. (2019). Metal Nanoparticles as Green Catalysts. *Materials*, *12*(21), 3602. https://doi.org/10.3390/ma12213602

Navarro Gallón, S. M., Alpaslan, E., Wang, M., Larese-Casanova, P., Londoño, M. E., Atehortúa, L., Pavón, J. J., & Webster, T. J. (2019). Characterization and study of the antibacterial mechanisms of silver nanoparticles prepared with microalgal exopolysaccharides. *Materials Science and Engineering: C*, *99*, 685–695. https://doi.org/10.1016/j.msec.2019.01.134

Negut, I., Grumezescu, V., & Grumezescu, A. M. (2018). Treatment strategies for infected wounds. *Molecules*, *23*(9), 1–23. https://doi.org/10.3390/molecules23092392

Nethi, S. K., Mukherjee, S., Veeriah, V., Barui, A. K., Chatterjee, S., & Patra, C. R. (2014). Bioconjugated gold nanoparticles accelerate the growth of new blood vessels through redox signaling. *Chemical Communications (Cambridge, England)*, *50*(92), 14367–14370. https://doi.org/10.1039/c4cc06996j

Nichols, C. M., Lardière, S. G., Bowman, J. P., Nichols, P. D., A.E. Gibson, J., & Guézennec, J. (2005). Chemical Characterization of Exopolysaccharides from Antarctic Marine Bacteria. *Microbial Ecology*, *49*(4), 578–589. https://doi.org/10.1007/s00248-004-0093-8

Nowack, B., Krug, H. F., & Height, M. (2011). 120 years of nanosilver history: implications for policy makers. *Environmental Science & Technology*, *45*(4), 1177–1183. https://doi.org/10.1021/es103316q

Núñez, R. N., Veglia, A. V., & Pacioni, N. L. (2018). Improving reproducibility between

batches of silver nanoparticles using an experimental design approach. *Microchemical Journal*, *141*(May), 110–117. https://doi.org/10.1016/j.microc.2018.05.017

Nwodo, U. U., Green, E., & Okoh, A. I. (2012). Bacterial exopolysaccharides: functionality and prospects. *International Journal of Molecular Sciences*, *13*(11), 14002–14015. https://doi.org/10.3390/ijms131114002

Ousey, K., Cutting, K. F., Rogers, A. A., & Rippon, M. G. (2016). The importance of hydration in wound healing: reinvigorating the clinical perspective. *J. Wound Care*, *25*(3), 122–130. https://doi.org/10.12968/jowc.2016.25.3.122

Peña, C., Millán, M., & Galindo, E. (2008). Production of alginate by *Azotobacter vinelandii* in a stirred fermentor simulating the evolution of power input observed in shake flasks. *Process Biochemistry*, *43*(7), 775–778. https://doi.org/10.1016/j.procbio.2008.02.013

Philip, D. (2010). Green synthesis of gold and silver nanoparticles using *Hibiscus rosa sinensis*. *Physica E: Low-Dimensional Systems and Nanostructures*, *42*(5), 1417–1424. https://doi.org/10.1016/j.physe.2009.11.081

Philip, D., Unni, C., Aromal, S. A., & Vidhu, V. K. (2011). Murraya Koenigii leaf-assisted rapid green synthesis of silver and gold nanoparticles. *Spectrochimica Acta - Part A: Molecular and Biomolecular Spectroscopy*, *78*(2), 899–904. https://doi.org/10.1016/j.saa.2010.12.060

Pivodová, V., Franková, J., Galandáková, A., & Ulrichová, J. (2015). *In Vitro* AuNPs' Cytotoxicity and Their Effect on Wound Healing. *Nanobiomedicine*, *2*, 7. https://doi.org/10.5772/61132

Poli, A., Anzelmo, G., & Nicolaus, B. (2010). Bacterial Exopolysaccharides from Extreme Marine Habitats: Production, Characterization and Biological Activities. *Marine Drugs*, *8*(6), 1779–1802. https://doi.org/10.3390/md8061779

Punuri, J. B., Sharma, P., Sibyala, S., Tamuli, R., & Bora, U. (2012). Piper betle -mediated green synthesis of biocompatible gold nanoparticles. *International Nano Letters*, *2*(18), 1–9. https://doi.org/10.1186/2228-5326-2-18

Qiu, Y., Qiu, L., Cui, J., & Wei, Q. (2016). Bacterial cellulose and bacterial cellulose-vaccarin membranes for wound healing. *Materials Science & Engineering C*, *59*, 303–309. https://doi.org/10.1016/j.msec.2015.10.016

Rai, M. K., Deshmukh, S. D., Ingle, A. P., & Gade, A. K. (2012). Silver nanoparticles: The powerful nanoweapon against multidrug-resistant bacteria. *Journal of Applied Microbiology*, *112*(5), 841–852. https://doi.org/10.1111/j.1365-2672.2012.05253.x

Rajendran, N. K., Sundar, S., Kumar, D., Houreld, N. N., & Abrahamse, H. (2018). A review on nanoparticle based treatment for wound healing. *Journal of Drug Delivery Science and Technology*, *44*, 421–430. https://doi.org/10.1016/j.jddst.2018.01.009

Rasulov, B., Rustamova, N., Yili, A., Zhao, H. Q., & Aisa, H. A. (2016). Synthesis of silver nanoparticles on the basis of low and high molar mass exopolysaccharides of *Bradyrhizobium japonicum* 36 and its antimicrobial activity against some pathogens. *Folia Microbiologica*, *61*(4), 283–293. https://doi.org/10.1007/s12223-015-0436-5

Rigo, C., Ferroni, L., Tocco, I., Roman, M., Munivrana, I., Gardin, C., Cairns, W. R. L., Vindigni, V., Azzena, B., Barbante, C., & Zavan, B. (2013). Active silver nanoparticles for wound healing. *International Journal of Molecular Sciences*, *14*(3), 4817–4840. https://doi.org/10.3390/ijms14034817

Seo, D., Yoo, C. Il, Chung, I. S., Park, S. M., Ryu, S., & Song, H. (2008). Shape Adjustment between Multiply Twinned and Single-Crystalline Polyhedral Gold Nanocrystals: Decahedra, Icosahedra, and Truncated Tetrahedra. *The Journal of Physical Chemistry C*, *112*(7), 2469–2475. https://doi.org/10.1021/jp7109498

Sharma, V. K., Yngard, R. A., & Lin, Y. (2009). Silver nanoparticles: Green synthesis and their antimicrobial activities. *Advances in Colloid and Interface Science*, *145*(1–2), 83–96. https://doi.org/10.1016/j.cis.2008.09.002

Sheny, D. S., Mathew, J., & Philip, D. (2011). Phytosynthesis of Au, Ag and Au-Ag bimetallic nanoparticles using aqueous extract and dried leaf of Anacardium occidentale. *Spectrochimica Acta - Part A: Molecular and Biomolecular Spectroscopy*, *79*(1), 254–262. https://doi.org/10.1016/j.saa.2011.02.051

Sivakumar, A. S., Krishnaraj, C., Sheet, S., Rampa, D. R., Kang, D. R., Belal, S. A., Kumar, A., Hwang, I. H., Yun, S. Il, Lee, Y. S., & Shim, K. S. (2017). Interaction of silver and gold nanoparticles in mammalian cancer: as real topical bullet for wound healing— A comparative study. *In Vitro Cellular and Developmental Biology - Animal*, *53*(7), 632–645. https://doi.org/10.1007/s11626-017-0150-5

Smitha, S. L., Philip, D., & Gopchandran, K. G. (2009). Green synthesis of gold nanoparticles using *Cinnamomum zeylanicum* leaf broth. *Spectrochimica Acta - Part A: Molecular and Biomolecular Spectroscopy*, *74*(3), 735–739. https://doi.org/10.1016/j.saa.2009.08.007

Sorg, H., Tilkorn, D. J., Hager, S., Hauser, J., & Mirastschijski, U. (2017). Skin Wound Healing: An Update on the Current Knowledge and Concepts. *European Surgical Research*, *58*(1–2), 81–94. https://doi.org/10.1159/000454919

Stal, L. J., Grossberger, S., Krumbein, W. E., & Division, G. (1984). Nitrogen fixation associated with the cyanobacterial mat of a marine laminated microbial ecosystem. *Marine Biology*, *82*, 217–224. https://doi.org/10.1007/BF00392402

Stiolica, A. T., Popescu, M., Bubulica, M. V., Oancea, C. N., Nicolicescu, C., Croitoru, O., Neamtu, J., & Manda, C. V. (2017). Optimization of gold nanoparticles synthesis using design of experiments technique. *Revista de Chimie*, *68*(7), 1518–1523. https://doi.org/10.37358/rc.17.7.5707

Torres, C. A. V., Antunes, S., Ricardo, A. R., Grandfils, C., Alves, V. D., Freitas, F., & Reis, M. A. M. (2012). Study of the interactive effect of temperature and pH on exopolysaccharide production by *Enterobacter* A47 using multivariate statistical analysis. *Bioresource Technology*, *119*, 148–156. https://doi.org/10.1016/j.biortech.2012.05.106

Torres, C. A. V., Ferreira, A. R. V., Freitas, F., Reis, M. A. M., Coelhoso, I., Sousa, I., & Alves, V. D. (2015). Rheological studies of the fucose-rich exopolysaccharide FucoPol. *International Journal of Biological Macromolecules*, *79*, 611–617. https://doi.org/10.1016/j.ijbiomac.2015.05.029

Torres, C. A. V., Marques, R., Antunes, S., Alves, V. D., Sousa, I., Ramos, A. M., Oliveira, R., Freitas, F., & Reis, M. A. M. (2011). Kinetics of production and characterization of the fucose-containing exopolysaccharide from *Enterobacter* A47. *Journal of Biotechnology*, *156*(4), 261–267. https://doi.org/10.1016/j.jbiotec.2011.06.024

Torres, C. A. V., Marques, R., Ferreira, A. R. V., Antunes, S., Grandfils, C., Freitas, F., & Reis, M. A. M. (2014). Impact of glycerol and nitrogen concentration on *Enterobacter* A47 growth and exopolysaccharide production. *International Journal of Biological Macromolecules*, *71*, 81–86. https://doi.org/10.1016/j.ijbiomac.2014.04.012

Vanaja, M., Gnanajobitha, G., Paulkumar, K., Rajeshkumar, S., Malarkodi, C., & Annadurai, G. (2013). Phytosynthesis of silver nanoparticles by *Cissus quadrangularis*: influence of physicochemical factors. *Journal of Nanostructure in Chemistry*, *3*(1), 1–8. https://doi.org/10.1186/2193-8865-3-17

Velnar, T., Bailey, T., & Smrkolj, V. (2009). The Wound Healing Process: An Overview of the Cellular and Molecular Mechanisms. *Journal of International Medical Research*, *37*(5), 1528–1542. https://doi.org/10.1177/147323000903700531

Volkova, N., Yukhta, M., Pavlovich, O., & Goltsev, A. (2016). Application of Cryopreserved Fibroblast Culture with Au Nanoparticles to Treat Burns. *Nanoscale Research Letters*, *11*(1), 22. https://doi.org/10.1186/s11671-016-1242-y

Wai, S. N., Mizunoe, Y., & Yoshida, S. (1999). How *Vibrio cholerae* survive during starvation. *FEMS Microbiology Letters*, *180*(2), 123–131.https://doi.org/10.1111/j.1574-6968.1999.tb08786.x

Wojtowicz, A. M., Oliveira, S., Carlson, M. W., Zawadzka, A., Rousseau, C. F., & Baksh, D. (2014). The importance of both fibroblasts and keratinocytes in a bilayered living cellular construct used in wound healing. *Wound Repair Regen*, *22*(2), 246–255. https://doi.org/10.1111/wrr.12154

Xia, J., Li, T., Lu, C., & Xu, H. (2018). Selenium-Containing Polymers: Perspectives toward Diverse Applications in Both Adaptive and Biomedical Materials. *Macromolecules*, *51*(19), 7435–7455. https://doi.org/10.1021/acs.macromol.8b01597

Xue, M., & Jackson, C. J. (2015). Extracellular Matrix Reorganization During Wound Healing and Its Impact on Abnormal Scarring. *Advances in Wound Care*, *4*(3), 119–136. https://doi.org/10.1089/wound.2013.0485

Yan, J. K., Qiu, W. Y., Wang, Y. Y., Wang, W. H., Yang, Y., & Zhang, H. N. (2018). Fabrication and stabilization of biocompatible selenium nanoparticles by carboxylic curdlans with various molecular properties. *Carbohydrate Polymers*, *179*(August 2017), 19–27. https://doi.org/10.1016/j.carbpol.2017.09.063

Yang, X., Yang, J., Wang, L., Ran, B., Jia, Y., Zhang, L., Yang, G., Shao, H., & Jiang, X. (2017). Pharmaceutical Intermediate-Modified Gold Nanoparticles: Against Multidrug-Resistant Bacteria and Wound-Healing Application via an Electrospun Scaffold. *ACS Nano*, *11*(6), 5737–5745. https://doi.org/10.1021/acsnano.7b01240

Yu, Y., Shen, M., Song, Q., & Xie, J. (2018). Biological activities and pharmaceutical applications of polysaccharide from natural resources: A review. *Carbohydrate Polymers*, *183*(235), 91–101. https://doi.org/10.1016/j.carbpol.2017.12.009

Zanette, C., Pelin, M., Crosera, M., Adami, G., Bovenzi, M., Larese, F. F., & Florio, C. (2011). Silver nanoparticles exert a long-lasting antiproliferative effect on human keratinocyte HaCaT cell line. *Toxicology in Vitro*, *25*(5), 1053–1060. https://doi.org/10.1016/j.tiv.2011.04.005

Zhang, S. Y., Zhang, J., Wang, H. Y., & Chen, H. Y. (2004). Synthesis of selenium nanoparticles in the presence of polysaccharides. *Materials Letters*, *58*(21), 2590–2594. https://doi.org/10.1016/j.matlet.2004.03.031

Zhang, X.-F., Liu, Z.-G., Shen, W., & Gurunathan, S. (2016). Silver Nanoparticles: Synthesis, Characterization, Properties, Applications, and Therapeutic Approaches. *International Journal of Molecular Sciences*, *17*(9), 1534. https://doi.org/10.3390/ijms17091534

Zheng, Y., Monty, J., & Linhardt, R. J. (2014). Polysaccharide-based nanocomposites and their applications. In *CARBOHYDRATE RESEARCH* (Issue 405). Elsevier Ltd. https://doi.org/10.1016/j.carres.2014.07.016

Zhu, S., Hu, J., Liu, S., Guo, S., Jia, Y., Li, M., Kong, W., Liang, J., Zhang, J., & Wang, J. (2020). Synthesis of Se-polysaccharide mediated by selenium oxychloride: Structure features and antiproliferative activity. *Carbohydrate Polymers*, *246*(April), 116545. https://doi.org/10.1016/j.carbpol.2020.116545

7. Appendixes

Table S1. ANOVA statistical analysis for the EPS1/AuNP biocomposite.

Source	Sum of squares	df	Mean square	F-value	p-value	
Block	5.468×10^{-15}	1	5.468×10^{-15}			
Model	2.065×10^{-11}	7	2.949×10^{-12}	37.09	< 0.0001	significant
A-T	1.220×10^{-12}	1	1.220×10^{-12}	15.34	0.0016	
B-pH	5.255×10^{-12}	1	5.255×10^{-12}	66.09	< 0.0001	
C-Time	5.255×10^{-12}	1	5.255×10^{-12}	66.09	< 0.0001	
D-[Au]	1.220×10^{-12}	1	1.220×10^{-12}	15.34	0.0016	
AB	1.220×10^{-12}	1	1.220×10^{-12}	15.34	0.0016	
AC	1.220×10^{-12}	1	1.220×10^{-12}	15.34	0.0016	
AD	5.255×10^{-12}	1	5.255×10^{-12}	66.09	< 0.0001	
Curvature	7.144×10^{-11}	1	7.144×10^{-11}	898.43	< 0.0001	
Residual	1.113×10^{-12}	14	7.952×10^{-14}			
Lack of Fit	1.978×10^{-14}	8	2.472×10^{-15}	0.0136	1.0000	not significant
Pure Error	1.094×10^{-12}	6	1.823×10^{-13}			
Cor Total	9.321×10^{-11}	23	9.321×10^{-11}			

Table S1. ANOVA statistical analysis for the EPS2/AuNP biocomposite.

Source	Sum of squares	df	Mean square	F-value	p-value	
Block	2.331×10^{-14}	1	2.331×10^{-14}			
Model	1.888×10^{-11}	7	2.698×10^{-12}	22.63	< 0.0001	significant
A-T	4.979×10^{-13}	1	4.979×10^{-13}	4.18	0.0016	
B-pH	9.957×10^{-13}	1	9.957×10^{-13}	8.35	< 0.0001	
C-Time	1.084×10^{-11}	1	1.084×10^{-11}	90.96	< 0.0001	
D-[Au]	2.526×10^{-12}	1	2.526×10^{-12}	21.19	0.0016	
AB	2.526×10^{-12}	1	2.526×10^{-12}	21.19	0.0016	
AC	4.979×10^{-13}	1	4.979×10^{-13}	4.18	0.0016	
AD	9.957×10^{-13}	1	9.957×10^{-13}	8.35	< 0.0001	
Curvature	3.251×10^{-11}	1	3.251×10^{-11}	272.76	< 0.0001	
Residual	1.669×10^{-12}	14	1.192×10^{-13}			
Lack of Fit	6.807×10^{-13}	8	8.509×10^{-14}	0.5167	1.0000	not significant
Pure Error	9.881×10^{-13}	6	1.647×10^{-13}			
Cor Total	5.309×10^{-11}	23				

Table S2. ANOVA statistical analysis for the EPS3/AuNP biocomposite.

Source	Sum of squares	df	Mean square	F-value	p-value	
Block	5.466×10^{-14}	1	5.466×10^{-14}			
Model	1.978×10^{-10}	7	2.826×10^{-11}	538.08	< 0.0001	significant
A-T	5.660×10^{-12}	1	5.660×10^{-12}	107.78	< 0.0001	
B-pH	6.482×10^{-11}	1	6.482×10^{-11}	1234.25	< 0.0001	
C-Time	3.588×10^{-12}	1	3.588×10^{-12}	68.33	< 0.0001	
D-[Au]	5.724×10^{-11}	1	5.724×10^{-11}	1090.06	< 0.0001	
AB	5.660×10^{-12}	1	5.660×10^{-12}	107.78	< 0.0001	
AC	5.724×10^{-11}	1	5.724×10^{-11}	1090.06	< 0.0001	
AD	3.588×10^{-12}	1	3.588×10^{-12}	68.33	< 0.0001	
Curvature	2.171×10^{-11}	1	2.171×10^{-11}	413.37	< 0.0001	
Residual	7.352×10^{-13}	14	5.251×10^{-14}			
Lack of Fit	4.390×10^{-13}	8	5.488×10^{-14}	1.11	0.4616	not significant
Pure Error	2.962×10^{-13}	6	4.936×10^{-14}			
Cor Total	2.203×10^{-10}	23				

Table S3. ANOVA statistical analysis for the EPS4/AuNP biocomposite.

Source	Sum of squares	df	Mean square	F-value	p-value	
Block	4.309×10^{-13}	1	4.309×10^{-13}			
Model	2.028×10^{-10}	7	2.897×10^{-11}	39.18	< 0.0001	significant
A-T	2.461×10^{-13}	1	2.461×10^{-13}	0.3329	0.5731	
B-pH	1.945×10^{-12}	1	1.945×10^{-12}	2.63	0.1271	
C-Time	7.604×10^{-11}	1	7.604×10^{-11}	102.83	< 0.0001	
D-[Au]	6.118×10^{-11}	1	6.118×10^{-11}	82.73	< 0.0001	
AB	6.118×10^{-11}	1	6.118×10^{-11}	82.73	< 0.0001	
AC	2.461×10^{-13}	1	2.461×10^{-13}	0.3329	0.5731	
AD	1.945×10^{-12}	1	1.945×10^{-12}	2.63	0.1271	
Curvature	5.468×10^{-11}	1	5.468×10^{-11}	73.94	< 0.0001	
Residual	1.035×10^{-11}	14	7.395×10^{-13}			
Lack of Fit	9.924×10^{-12}	8	1.240×10^{-12}	17.36	0.0013	significant
Pure Error	4.288×10^{-13}	6	7.147×10^{-14}			
Cor Total	2.682×10^{-10}	23				

Table S4. ANOVA statistical analysis for the FucoPol/AuNP biocomposite.

Source	Sum of squares	df	Mean square	F-value	p-value	
Block	4.288×10^{-14}	1	4.288×10^{-14}			
Model	1.650×10^{-10}	7	2.358×10^{-11}	2303.90	< 0.0001	significant
A-T	1.408×10^{-11}	1	1.408×10^{-11}	1376.08	< 0.0001	
B-pH	3.624×10^{-11}	1	3.624×10^{-11}	3540.99	< 0.0001	
C-Time	1.408×10^{-11}	1	1.408×10^{-11}	1376.08	< 0.0001	
D-[Au]	3.624×10^{-11}	1	3.624×10^{-11}	3540.99	< 0.0001	
AB	1.408×10^{-11}	1	1.408×10^{-11}	1376.08	< 0.0001	
AC	3.624×10^{-11}	1	3.624×10^{-11}	3540.99	< 0.0001	
AD	1.408×10^{-11}	1	1.408×10^{-11}	1376.08	< 0.0001	
Curvature	1.712×10^{-12}	1	1.712×10^{-12}	167.32	< 0.0001	
Residual	1.433×10^{-13}	14	1.023×10^{-14}			
Lack of Fit	1.024×10^{-13}	8	1.280×10^{-14}	1.88	0.2289	not significant
Pure Error	4.087×10^{-14}	6	6.812×10^{-15}			
Cor Total	1.669×10^{-10}	23				

Table S5. ANOVA statistical analysis for the EPS1/SeNP biocomposite.

Source	Sum of squares	df	Mean square	F-value	p-value	
Block	1.504×10^{-11}	1	1.504×10^{-11}			
Model	6.976×10^{-07}	7	9.966×10^{-08}	265.93	< 0.0001	significant
A-T	1.690×10^{-10}	1	1.690×10^{-10}	0.4509	0.5128	
B-pH	2.323×10^{-07}	1	2.323×10^{-07}	619.90	< 0.0001	
C-Time	1.690×10^{-10}	1	1.690×10^{-10}	0.4509	0.5128	
D-[Au]	2.323×10^{-07}	1	2.323×10^{-07}	619.90	< 0.0001	
AB	1.690×10^{-10}	1	1.690×10^{-10}	0.4509	0.5128	
AC	2.323×10^{-07}	1	2.323×10^{-07}	619.90	< 0.0001	
AD	1.690×10^{-10}	1	1.690×10^{-10}	0.4509	0.5128	
Curvature	7.139×10^{-07}	1	7.139×10^{-07}	1905.00	< 0.0001	
Residual	5.247×10^{-09}	14	3.748×10^{-10}			
Lack of Fit	2.708×10^{-11}	8	3.385×10^{-12}	0.0039	1.0000	not significant
Pure Error	5.220×10^{-09}	6	8.700×10^{-10}			
Cor Total	1.417×10^{-06}	23				

Table S6. ANOVA statistical analysis for the EPS2/SeNP biocomposite.

Source	Sum of squares	df	Mean square	F-value	p-value	
Block	4.661×10^{-09}	1	4.661×10^{-09}			
Model	7.302×10^{-07}	7	1.043×10^{-07}	8.59	0.0004	significant
A-T	2.434×10^{-07}	1	2.434×10^{-07}	0.05	0.0005	
B-pH	6.912×10^{-12}	1	6.912×10^{-12}	0.0006	0.9813	
C-Time	6.912×10^{-12}	1	6.912×10^{-12}	0.0006	0.9813	
D-[Au]	2.434×10^{-07}	1	2.434×10^{-07}	20.05	0.0005	
AB	6.912×10^{-12}	1	6.912×10^{-12}	0.0006	0.9813	
AC	6.912×10^{-12}	1	6.912×10^{-12}	0.0006	0.9813	
AD	2.434×10^{-07}	1	2.434×10^{-07}	20.05	0.0005	
Curvature	5.353×10^{-07}	1	5.353×10^{-07}	44.10	< 0.0001	
Residual	1.699×10^{-07}	14	1.214×10^{-08}			
Lack of Fit	7.990×10^{-09}	8	9.988×10^{-10}	0.0370	0.9999	not significant
Pure Error	1.620×10^{-07}	6	2.699×10^{-08}			
Cor Total	1.440×10^{-06}	23				

Table S7. ANOVA statistical analysis for the EPS3/SeNP biocomposite.

Source	Sum of squares	df	Mean square	F-value	p-value	
Block	4.282×10^{-10}	1	4.282×10^{-10}			
Model	8.491×10^{-07}	7	1.213×10^{-07}	282.36	< 0.0001	significant
A-T	2.827×10^{-07}	1	2.827×10^{-07}	658.14	< 0.0001	
B-pH	2.271×10^{-10}	1	2.271×10^{-10}	0.5286	0.4792	
C-Time	2.271×10^{-10}	1	2.271×10^{-10}	0.5286	0.4792	
D-[Au]	2.827×10^{-07}	1	2.827×10^{-07}	658.14	< 0.0001	
AB	2.271×10^{-10}	1	2.271×10^{-10}	0.5286	0.4792	
AC	2.271×10^{-10}	1	2.271×10^{-10}	0.5286	0.4792	
AD	2.827×10^{-07}	1	2.827×10^{-07}	658.14	< 0.0001	
Curvature	6.929×10^{-07}	1	6.929×10^{-07}	1612.83	< 0.0001	
Residual	6.014×10^{-09}	14	4.296×10^{-10}			
Lack of Fit	3.172×10^{-09}	8	3.965×10^{-10}	0.8371	0.6035	not significant
Pure Error	2.842×10^{-09}	6	4.737×10^{-10}			
Cor Total	1.548×10^{-06}	23				

Table S8. ANOVA statistical analysis for the EPS4/SeNP biocomposite.

Source	Sum of squares	df	Mean square	F-value	p-value	
Block	1.569×10^{-10}	1	1.569×10^{-10}			
Model	4.479×10^{-07}	7	6.399×10^{-08}	519.09	< 0.0001	significant
A-T	6.399×10^{-08}	1	6.399×10^{-08}	519.09	< 0.0001	
B-pH	6.399×10^{-08}	1	6.399×10^{-08}	519.09	< 0.0001	
C-Time	6.399×10^{-08}	1	6.399×10^{-08}	519.09	< 0.0001	
D-[Au]	6.399×10^{-08}	1	6.399×10^{-08}	519.09	< 0.0001	
AB	6.399×10^{-08}	1	6.399×10^{-08}	519.09	< 0.0001	
AC	6.399×10^{-08}	1	6.399×10^{-08}	519.09	< 0.0001	
AD	6.399×10^{-08}	1	6.399×10^{-08}	519.09	< 0.0001	
Curvature	2.133×10^{-08}	1	2.133×10^{-08}	173.03	< 0.0001	
Residual	1.726×10^{-09}	14	1.233×10^{-10}			
Lack of Fit	1.726×10^{-09}	8	2.157×10^{-10}			
Pure Error	0.0000	6	0.0000			
Cor Total	4.711×10^{-07}	23				

Table S9. ANOVA statistical analysis for the FucoPol/SeNP biocomposite.

Source	Sum of squares	df	Mean square	F-value	p-value	
Block	9.997×10^{-09}	1	9.997×10^{-09}			
Model	4.832×10^{-07}	7	6.903×10^{-08}	2.88	0.0435	significant
A-T	1.642×10^{-09}	1	1.642×10^{-09}	0.0686	0.7972	
B-pH	6.609×10^{-08}	1	6.609×10^{-08}	2.76	0.1188	
C-Time	4.452×10^{-08}	1	4.452×10^{-08}	1.86	0.1942	
D-[Au]	2.587×10^{-07}	1	2.587×10^{-07}	10.80	0.0054	
AB	4.452×10^{-08}	1	4.452×10^{-08}	1.86	0.1942	
AC	6.609×10^{-08}	1	6.609×10^{-08}	2.76	0.1188	
AD	1.642×10^{-09}	1	1.642×10^{-09}	0.0686	0.7972	
Curvature	4.589×10^{-07}	1	4.589×10^{-07}	19.17	0.0006	
Residual	3.352×10^{-07}	14	2.394×10^{-08}			
Lack of Fit	6.179×10^{-08}	8	7.724×10^{-09}	0.1695	0.9874	not significant
Pure Error	2.734×10^{-07}	6	4.556×10^{-08}			
Cor Total	1.287×10^{-06}	23				

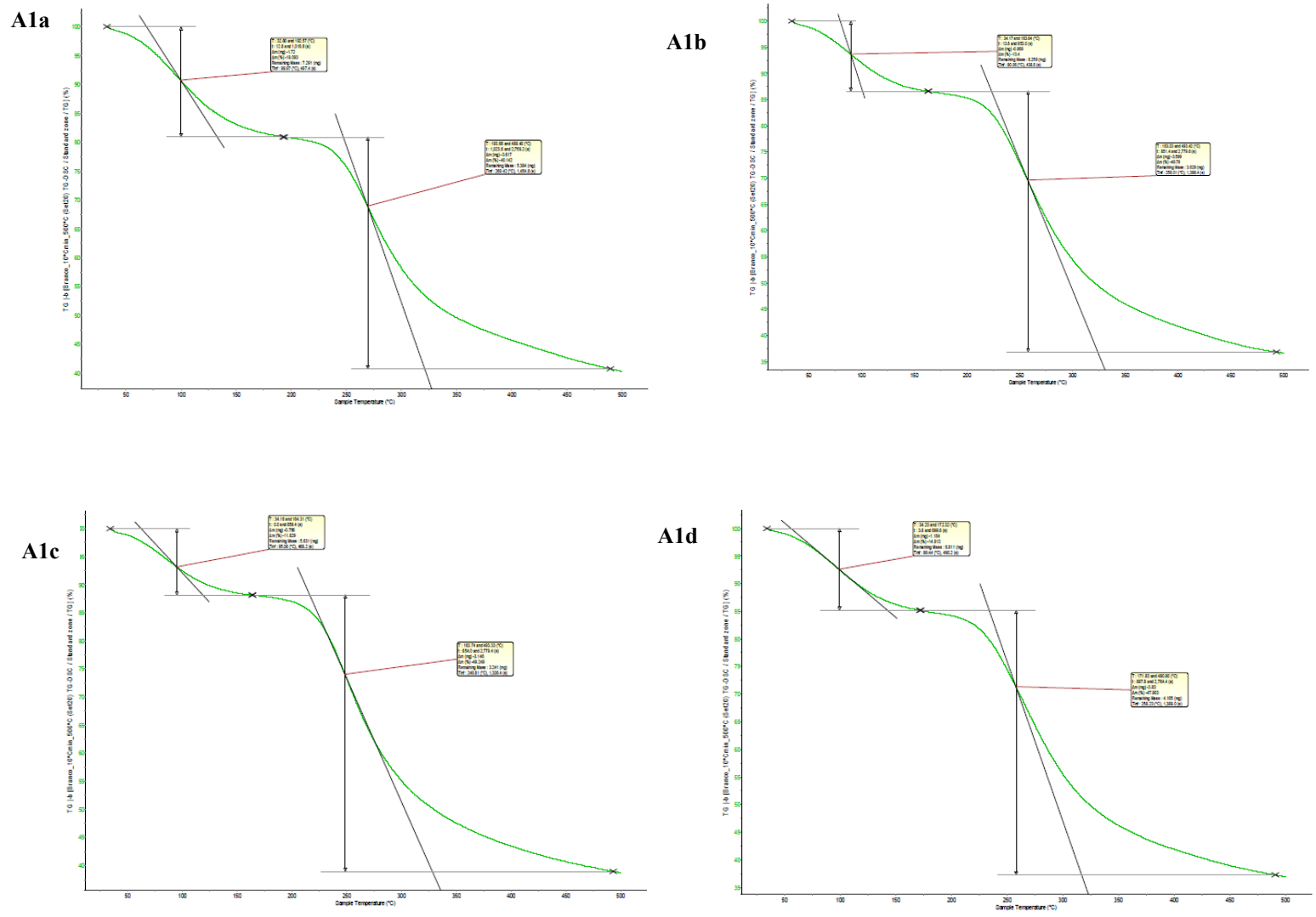

Figure A1. Thermogravimetric analysis (TGA) cuves of EPS1(A1a), EPS1/AgNP biocomposite (A1b), EPS1/AuNP biocomposite (A1c) and EPS1/SeNP biocomposite (A1d).

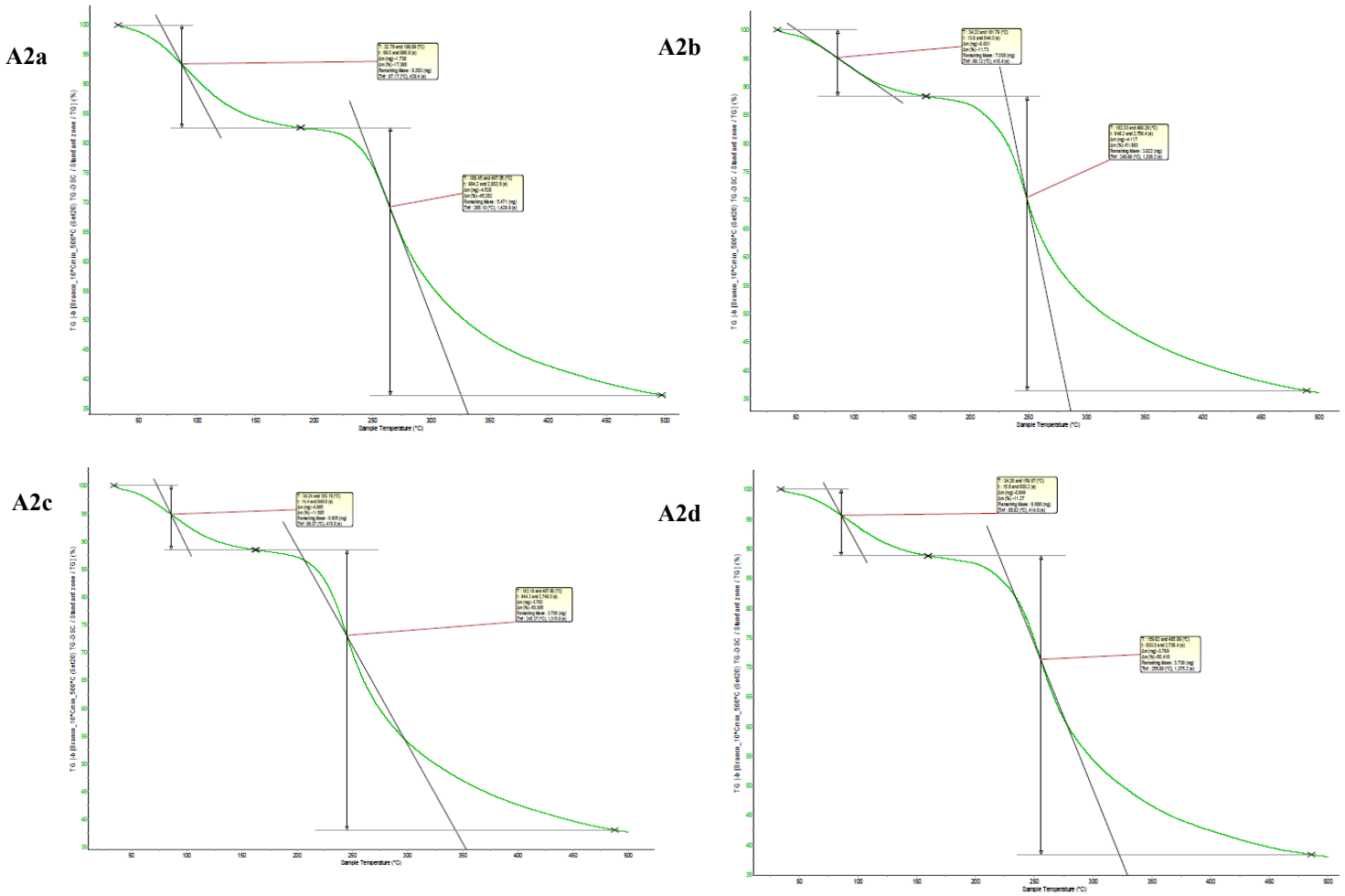

Figure A2. Thermogravimetric analysis (TGA) cuves of EPS2(A2a), EPS2/AgNP biocomposite (A2b), EPS2/AuNP biocomposite A2c) and EPS2/SeNP biocomposite (A2d).

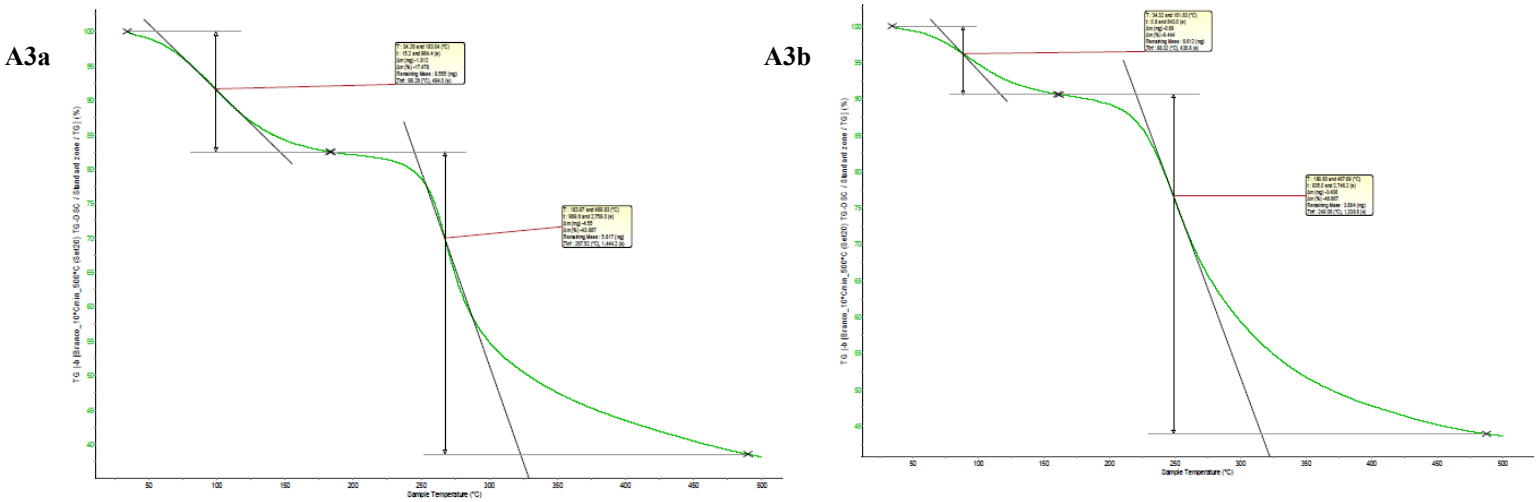

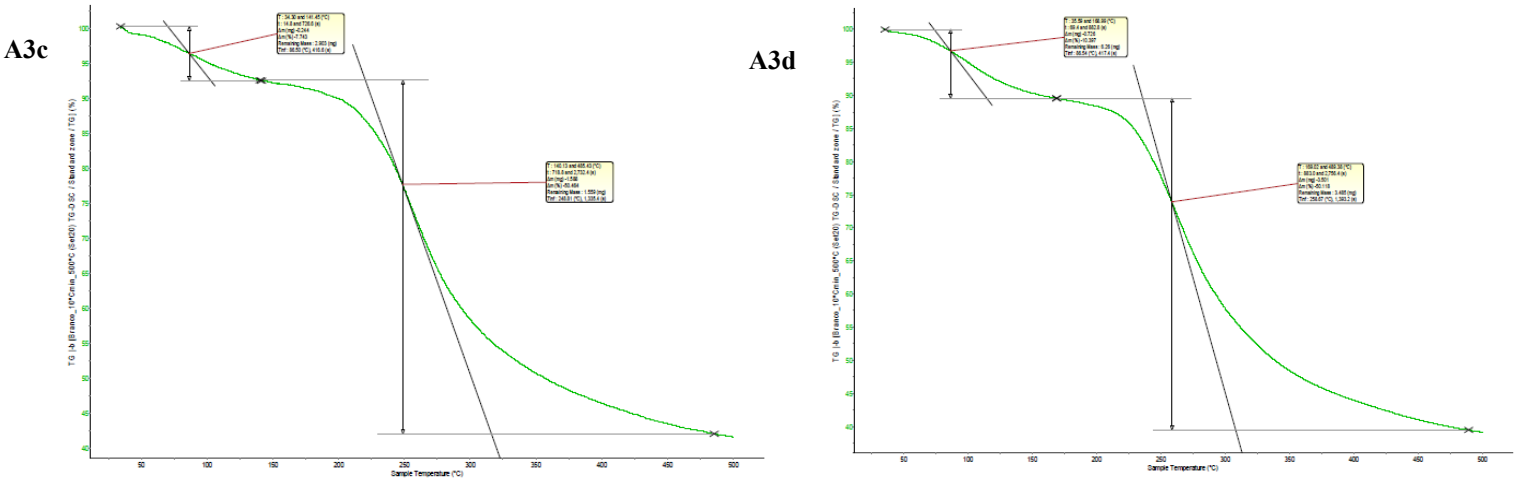

Figure A3. Thermogravimetric analysis (TGA) cuves of EPS3(A3a), EPS3/AgNP biocomposite (A3b), EPS3/AuNP biocomposite (A3c) and EPS3/SeNP biocomposite (A3d).

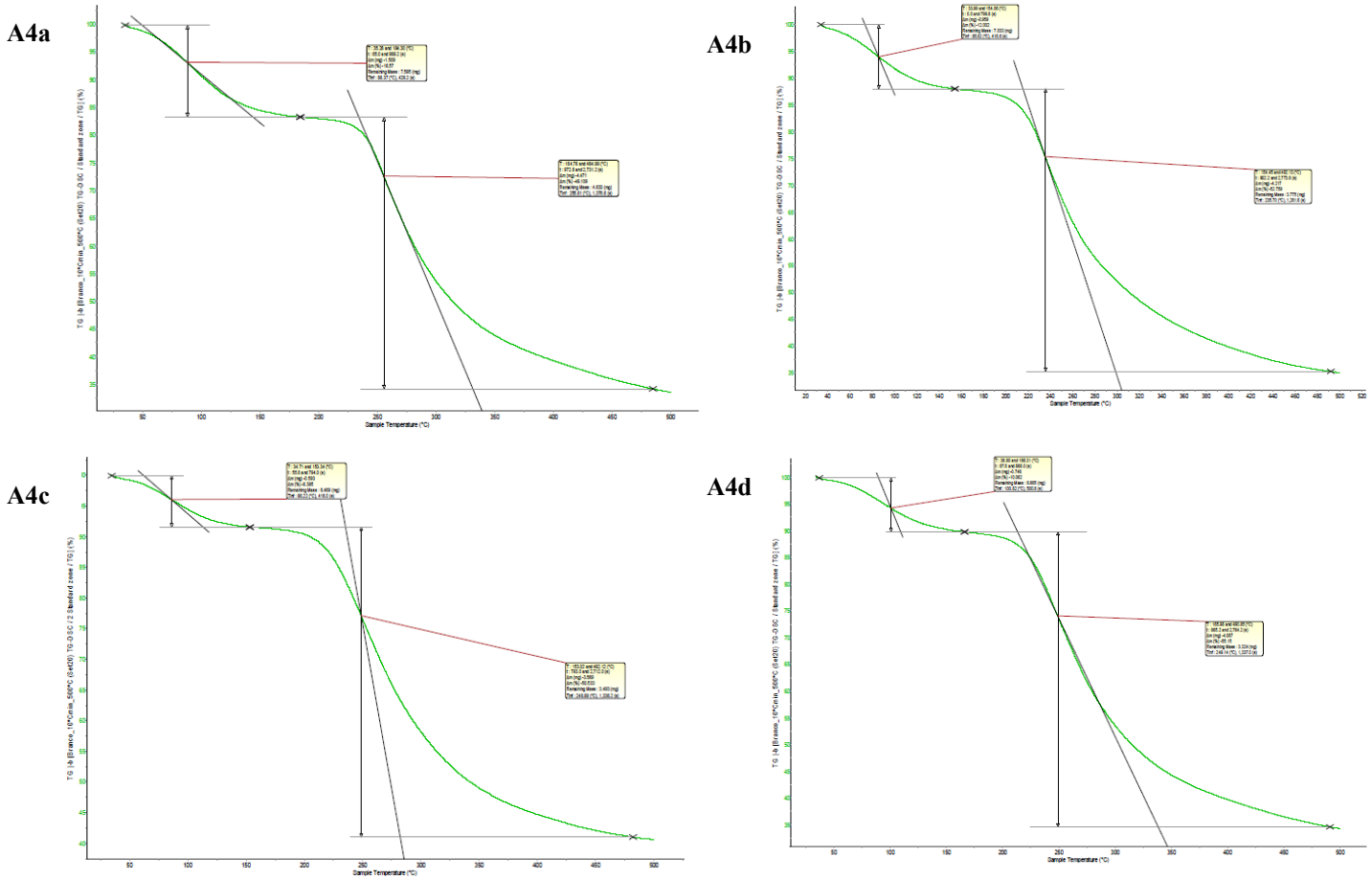

Figure A4. Thermogravimetric analysis (TGA) cuves of EPS4(A4a), EPS4/AgNP biocomposite (A4b), EPS4/AuNP biocomposite (A4c) and EPS4/SeNP biocomposite (A4d).

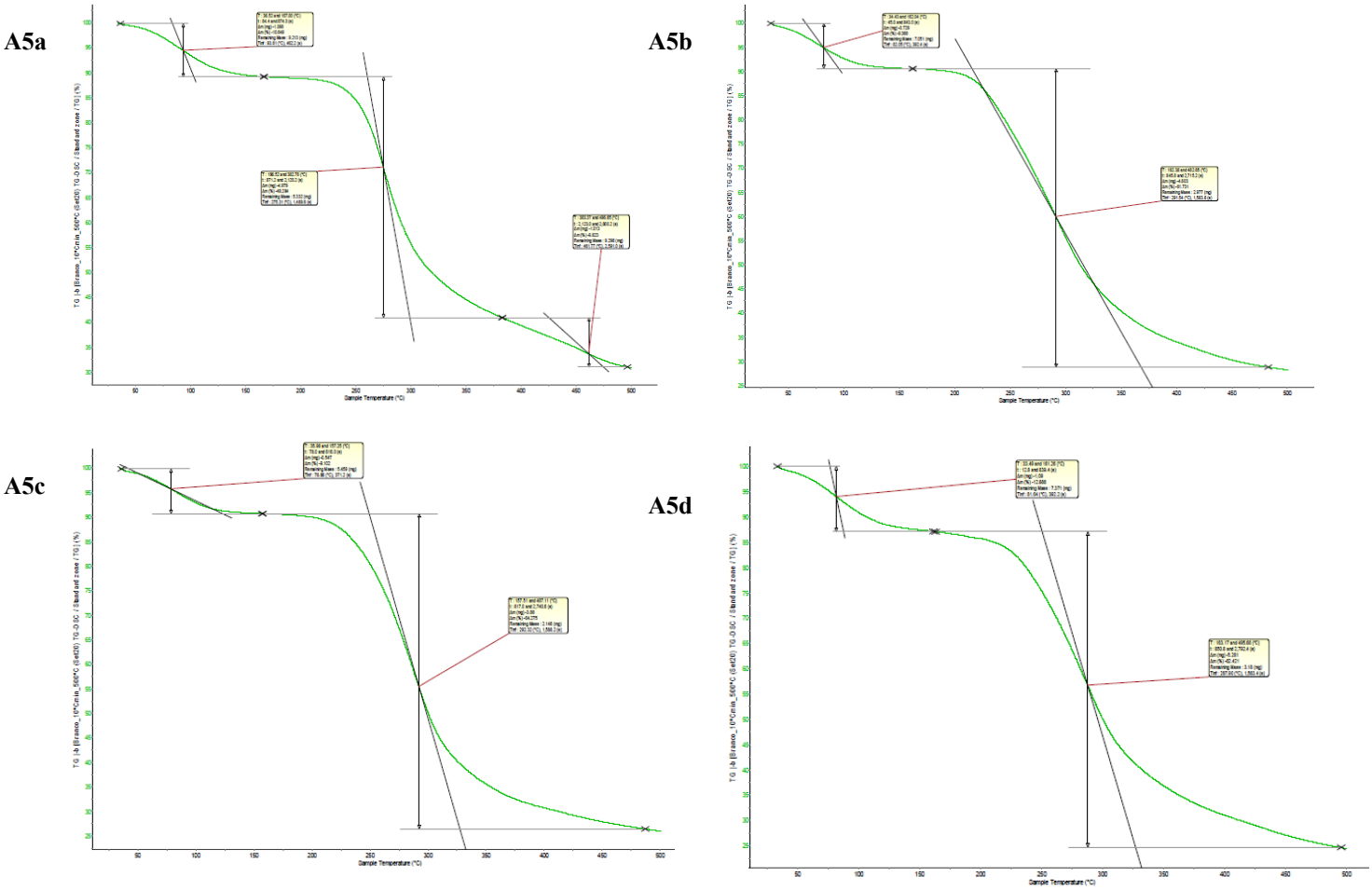

Figure A5. Thermogravimetric analysis (TGA) cuves of FucoPol(A5a), FucoPol/AgNP biocomposite (A5b), FucoPol/AuNP biocomposite (A5c) and FucoPol/SeNP biocomposite (A5d).